



LUND UNIVERSITY

Investigation of Iron-N-Heterocyclic Carbene Complexes for Photocatalytic Applications

Ilic, Aleksandra

2024

Document Version:
Publisher's PDF, also known as Version of record

[Link to publication](#)

Citation for published version (APA):
Ilic, A. (2024). *Investigation of Iron-N-Heterocyclic Carbene Complexes for Photocatalytic Applications*. Lund University.

Total number of authors:
1

General rights

Unless other specific re-use rights are stated the following general rights apply:
Copyright and moral rights for the publications made accessible in the public portal are retained by the authors and/or other copyright owners and it is a condition of accessing publications that users recognise and abide by the legal requirements associated with these rights.

- Users may download and print one copy of any publication from the public portal for the purpose of private study or research.
- You may not further distribute the material or use it for any profit-making activity or commercial gain
- You may freely distribute the URL identifying the publication in the public portal

Read more about Creative commons licenses: <https://creativecommons.org/licenses/>

Take down policy

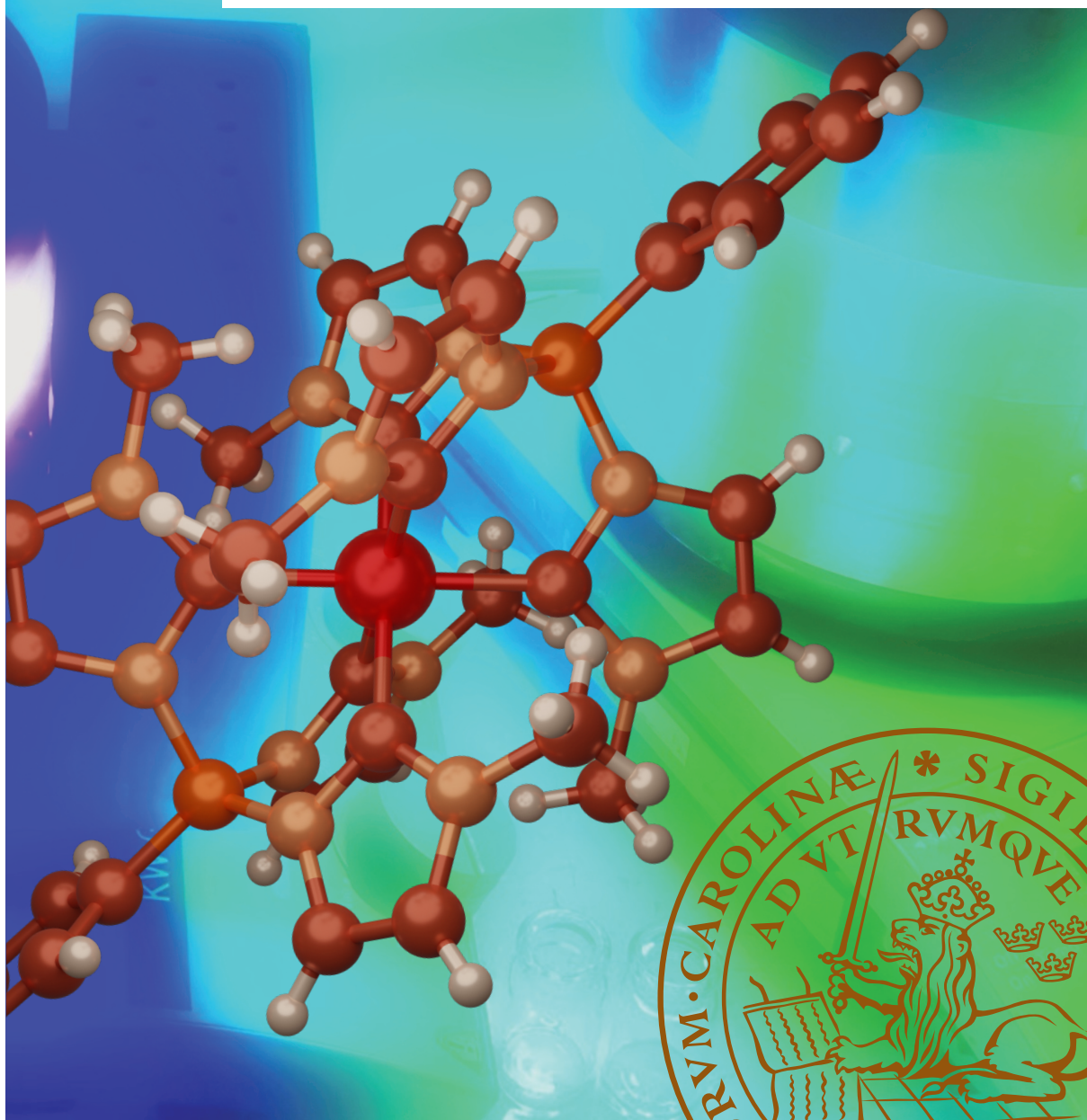
If you believe that this document breaches copyright please contact us providing details, and we will remove access to the work immediately and investigate your claim.

LUND UNIVERSITY

PO Box 117
221 00 Lund
+46 46-222 00 00

Investigation of Iron-*N*-Heterocyclic Carbene Complexes for Photocatalytic Applications

ALEKSANDRA ILIĆ | CENTRE FOR ANALYSIS AND SYNTHESIS | LUND UNIVERSITY



Investigation of Iron-*N*-Heterocyclic Carbene Complexes for
Photocatalytic Applications

Investigation of Iron-*N*-Heterocyclic Carbene Complexes for Photocatalytic Applications

Aleksandra Ilić



LUND
UNIVERSITY

DOCTORAL DISSERTATION

for the degree of Doctor of Philosophy (PhD) at the Faculty of Science at
Lund University to be publicly defended on Friday May 24th, 2024 at 09:00 in
Lecture Hall KC:A, Kemicentrum, Naturvetarvägen, 14, Lund.

Faculty opponent:

Prof. Oliver Wenger, University of Basel, Switzerland

Organization: LUND UNIVERSITY

Document name: Doctoral Dissertation

Date of issue: 2024-05-24

Author(s): Aleksandra Ilić

Sponsoring organization:

Title and subtitle: Investigation of Iron-*N*-Heterocyclic Carbene Complexes for Photocatalytic Applications

Abstract:

Humanity's ever-growing energy demands require the implementation of more sustainable ways to harvest and store energy. At the same time, the reduction of greenhouse gas emission and thus global warming remains of paramount importance. To this end, solar energy harvesting presents an attractive route towards satisfying these requirements—be that by conversion to thermal energy, electricity or to chemical energy. Molecular systems based on iron could prove particularly interesting in this area, due to their advantageous properties such as appreciable visible light-absorption as well as the high availability and low cost of iron. As of yet, they have not been extensively studied though, which can be attributed to the inherently poor photophysical and -chemical properties associated with these systems. However, well thought-out structural design can be used to combat said issues.

The ligand motif used in Fe-*N*-heterocyclic carbene (NHC) complexes aids in mitigating the formerly mentioned unfavourable properties, allowing for bimolecular quenching with electron donors and acceptors to occur, which is crucial for photocatalysis. In this thesis, the application of hexa-NHC complexes based on Earth-abundant iron as light-harvesters for solar-to-chemical energy conversion is demonstrated. The utility of Fe(III)-NHC complexes for sensitisation of artificial photosynthesis reactions as well as their performance as photoredox catalysts in organic transformations has been studied and the underlying mechanisms have been investigated, giving insight into the prospects and limitations associated with these systems. For the hydrogen evolution and aminomethylation reactions investigated here, conventional single-photon mechanisms were observed. Meanwhile, in the case of the atom transfer radical addition reactions, sequential photon absorption of two different oxidation states of the catalyst within the same catalytic turnover was shown to be operative. Furthermore, a study featuring the Fe(II)-congener of an Fe(III)-NHC complex with demonstrated photocatalytic activity revealed a less than favourable excited state lifetime compared to the Fe(III)-parent complex, showcasing that the preparation of Fe(II)-NHC complexes with synthetically useful photophysical and chemical properties is not necessarily facile. Early investigations of a photocatalytic reaction driven by heterogenisation of Fe(III)-NHC complexes are also shown. There the goal was to improve upon the sustainability of these catalysts by facilitating their recyclability. This thesis thus showcases the potential of Fe-NHC complexes for photocatalytic applications, whilst also revealing their shortcomings.

Key words: Photocatalysis, photoredox catalysis, photosensitisers, iron *N*-heterocyclic carbenes, visible light, artificial photosynthesis, Earth-abundant, iron

Language English

ISBN (print): 978-91-8096-040-3

ISBN (electronic): 978-91-8096-041-0

Number of pages: 286

I, the undersigned, being the copyright owner of the abstract of the above-mentioned dissertation, hereby grant to all reference sources permission to publish and disseminate the abstract of the above-mentioned dissertation.

Signature

Date 2024-04-05

Investigation of Iron-*N*-Heterocyclic Carbene Complexes for Photocatalytic Applications

Aleksandra Ilić



LUND
UNIVERSITY

Front Cover: Illustration by Aleksandra Ilić

Back Cover: Photo of Lunds Universitetsbiblioteket by Aleksandra Ilić

Copyright pp i-119 Aleksandra Ilić

Paper I © 2022 Royal Society of Chemistry

Paper II © 2022 Royal Society of Chemistry

Paper III © by the Authors (Manuscript unpublished)

Paper IV © by the Authors (Manuscript unpublished)

Faculty of Science

Department of Chemistry, Centre for Analysis and Synthesis

ISBN (print): 978-91-8096-040-3

ISBN (electronic): 978-91-8096-041-0

Printed in Sweden by Media-Tryck, Lund University

Lund 2024



Media-Tryck is a Nordic Swan Ecolabel certified provider of printed material. Read more about our environmental work at www.mediatryck.lu.se

MADE IN SWEDEN 

*“Don’t adventures ever have an end?
I guess not. Someone else always has to carry on the story.”*

*—J.R.R. Tolkien, *The Fellowship of the Ring**

Table of Contents

Abstract	xi
Popular Scientific Summary	xiii
Populärwissenschaftliche Zusammenfassung	xv
List of Publications	xvii
Abbreviations & Symbols	xxi
1 Background	1
2 Aim & Outline of this Thesis	3
3 Photocatalysis	5
3.1 Solar Energy Conversion	5
3.2 Fundamentals of Photocatalysis	6
3.2.1 Photocatalysis based on Single Electron Transfer (SET) Reactions	7
3.2.2 Energy Transfer (EnT)	10
3.3 Tools for Investigation of Photocatalytic Systems	12
3.3.1 Steady-State Spectroscopy & Stern–Volmer Quenching Studies	12
3.3.2 Time-Resolved Spectroscopy Techniques	15
3.3.3 Cyclic Voltammetry and Spectroelectrochemistry	16
3.3.4 Nuclear Magnetic Resonance Spectroscopy	18
3.3.5 Detection of Radicals	18
3.3.6 Chemical Actinometry	19
3.3.7 Cage Escape Yield Determination	19
4 Photophysics of Light-Harvesting Iron Complexes	21
5 Artificial Photosynthesis sensitised by an Fe(III)-NHC Complex	29
5.1 Analysis of Gaseous Reaction Products	31
5.2 High Turnover Hydrogen Evolution sensitised by an Fe(III)-NHC complex (Paper I)	33
5.3 CO ₂ -Reduction sensitised by an Fe(III)-NHC complex	38
5.4 Conclusions	41

6	Photoredox Catalysis of Organic Reactions driven by Fe-NHC Complexes	43
6.1	A Z-Scheme-type Mechanism as a Tool for Iron Photoredox Catalysis (Paper II).....	46
6.2	Visible Light-Induced Generation of α -Aminoalkyl Radicals as Reactive Intermediates (Paper III)	52
6.3	Conclusions	61
7	Excited state dynamics of an Fe(II) <i>Hexa</i>-NHC Complex (Paper IV)	63
8	Heterogenisation of Fe(III)-NHC Complexes for Photoredox Catalysis.....	71
8.1	Background and Motivation	71
8.2	Synthesis of Fe(III)-NHC complex (19)	72
8.3	Preparation of Al ₂ O ₃ -(18) and Al ₂ O ₃ -(19) and Solvent Stability Studies	74
8.4	Investigation of the Photocatalytic Activity & Reusability.....	77
8.5	Conclusion and Future Plans	80
9	Concluding Remarks & Outlook	81
10	Supporting Information.....	87
10.1	CO ₂ -Reduction sensitised by an Fe(III)-NHC complex	87
10.1.1	General Information	87
10.1.2	Experimental Details	87
10.1.3	Results	88
10.2	Heterogenisation of Fe(III)-NHC Complexes for Photoredox Catalysis	90
10.2.1	Materials & Methods.....	90
10.2.2	Synthesis of the Fe(III)-NHC complex (19)	91
10.2.3	Steady-State Emission Spectroscopy.....	94
10.2.4	Preparation of the sensitised Al ₂ O ₃ -Nanoparticles	94
10.2.5	Photocatalytic Dehalogenations	94
	Acknowledgements	95
	References	99

Abstract

Humanity's ever-growing energy demands require the implementation of more sustainable ways to harvest and store energy. At the same time, the reduction of greenhouse gas emission and thus global warming remains of paramount importance. To this end, solar energy harvesting presents an attractive route towards satisfying these requirements—be that by conversion to thermal energy, electricity or to chemical energy. Molecular systems based on iron could prove particularly interesting in this area, due to their advantageous properties such as appreciable visible light-absorption as well as the high availability and low cost of iron. As of yet, they have not been extensively studied though, which can be attributed to the inherently poor photophysical and -chemical properties associated with these systems. However, well thought-out structural design can be used to combat said issues.

The ligand motif used in Fe-*N*-heterocyclic carbene (NHC) complexes aids in mitigating the formerly mentioned unfavourable properties, allowing for bimolecular quenching with electron donors and acceptors to occur, which is crucial for photocatalysis. In this thesis, the application of *hexa*-NHC complexes based on Earth-abundant iron as light-harvesters for solar-to-chemical energy conversion is demonstrated. The utility of Fe(III)-NHC complexes for sensitisation of artificial photosynthesis reactions as well as their performance as photoredox catalysts in organic transformations has been studied and the underlying mechanisms have been investigated, giving insight into the prospects and limitations associated with these systems. For the hydrogen evolution and aminomethylation reactions investigated here, conventional single-photon mechanisms were observed. Meanwhile, in the case of the atom transfer radical addition reactions, sequential photon absorption of two different oxidation states of the catalyst within the same catalytic turnover was shown to be operative. Furthermore, a study featuring the Fe(II)-congener of an Fe(III)-NHC complex with demonstrated photocatalytic activity revealed a less than favourable excited state lifetime compared to the Fe(III)-parent complex, showcasing that the preparation of Fe(II)-NHC complexes with synthetically useful photophysical and -chemical properties is not necessarily facile. Early investigations of a photocatalytic reaction driven by heterogenisation of Fe(III)-NHC complexes are also shown. There the goal was to improve upon the sustainability of these catalysts by facilitating their recyclability. This thesis thus showcases the potential of Fe-NHC complexes for photocatalytic applications, whilst also revealing their shortcomings.

Popular Scientific Summary

“Climate change” and “global warming” are terms that frequently come up in the media and describe the changes in weather patterns and increasing global surface temperature during the last century, respectively. Both negatively affect agriculture—and consequently food security—general health, and biodiversity among other areas. Consequently, there is a need for action in combatting the climate crisis since humanity’s energy demands are still constantly on the rise. The use of traditional energy sources such as fossil fuels is highly problematic because they are not renewable and they generate greenhouse gases. Therefore, it becomes glaringly obvious that clean, abundant and renewable alternatives for energy conversion are needed. Here, solar energy is a very promising candidate and a well-known approach to harnessing this vast resource are photovoltaics. There, solar energy is converted directly into electrical energy. However, a larger variety of strategies is needed to make use of the practically inexhaustible resource that is the Sun. To this end, photocatalysis, which is used for the conversion of solar into chemical energy, is considered a promising avenue.

Similarly to solar cells, light—ideally from the Sun—is absorbed by bulk materials or molecular systems. Instead of converting the thereby afforded energy into electricity, it is used to drive chemical reactions. In this way, for example, solar fuels made from abundant substances such as water and carbon dioxide can be produced or transformations in organic chemistry can be achieved. When looking at molecular systems used in photocatalysis, very often rare and expensive metals such as ruthenium and iridium are used—not ideal when pursuing sustainable energy solutions. Iron, on the other hand, is one of the most abundant metals in the Earth’s crust. Despite of that, it has not been extensively used so far because of the inherent unfavourable properties of iron-based light-harvesting systems. However, through careful structural design, these problems have been mitigated, paving the way for their exploration in photocatalysis.

In this thesis, molecular light-harvesting systems based on Earth-abundant iron have been used in studies investigating the production of solar fuels as well as for organic synthesis and their potential for the future as well as their limitations are evaluated, giving insights that could aid future developments in this area.

Populärwissenschaftliche Zusammenfassung

“Klimawandel” und “globale Erwärmung” sind Begriffe, die ständig in den Medien aufscheinen. Diese Phänomene tragen unter anderem zum häufigeren Auftreten von Extremwetterereignissen bei und haben unbestreitbare negative Auswirkungen auf viele Bereiche unseres alltäglichen Lebens, sei das nun auf die Landwirtschaft—und folglich auf unsere Versorgung mit Nahrungsmitteln—die Gesundheit oder die Biodiversität auf unserem Planeten. Dementsprechend ist es mehr als an der Zeit tätig zu werden und Gegenschritte einzuleiten, da unser Energiebedarf nichtsdestotrotz stetig steigt. Herkömmliche Energieträger wie fossile Brennstoffe sind problematisch, da sie nicht-erneuerbar sind und zur globalen Erwärmung durch den Treibhaus-Effekt beitragen. In Anbetracht all dessen, ist die Entwicklung und Anwendung von leicht zugänglichen, erneuerbaren Energieträgern unabdingbar für das Fortbestehen unserer Gesellschaft. Solarenergie ist hier ein vielversprechender Anwärter und findet bereits durch Photovoltaik-Anlagen, in denen Sonnenlicht in elektrische Energie umgewandelt wird, breitere Verwendung. Die Sonne ist jedoch eine quasi unerschöpfliche Energiequelle und sollte als solche auf mehreren Wegen ausgenutzt werden.

Ein interessanter Ansatz könnte hier beispielsweise Photokatalyse sein—eine Methode um Sonnenlicht in chemische Energie umzuwandeln. Ähnlich wie bei Solarzellen wird Licht, idealerweise durch Sonneneinstrahlung, von einem geeigneten Halbleitermaterial oder durch molekulare Lichtfänger absorbiert und die gewonnene Energie genutzt um eine chemische Reaktion zu erwirken. Dadurch können unter anderem „solare Kraftstoffe“ aus Wasser und CO₂ hergestellt werden oder organische Reaktionen angetrieben werden. Im Falle der molekularen Lichtfänger werden oftmals Edelmetalle wie Ruthenium und Iridium verwendet. Diese sind jedoch selten und ausgesprochen teuer, und dementsprechend nicht besonders gut für nachhaltige Energiegewinnung geeignet. Eisen hingegen ist eines der häufigsten Metalle in der Erdkruste. Dennoch hat es bislang kaum Verwendung in photokatalytischen Reaktionen gefunden, was darauf zurückgeführt werden kann, dass bisherige Eisen-Photokatalysatoren mangelhafte photophysikalische und -chemische Eigenschaften hatten. Durch ausgeklügeltes strukturelles Design konnten diese Unzulänglichkeiten jedoch insoweit überwunden werden, als dass ihre effiziente Anwendung ermöglicht worden ist.

In dieser Dissertation wurde die Anwendbarkeit von Eisen-basierten Lichtfängern zur Herstellung von solaren Kraftstoffen sowie ihre Verwendung als Photokatalysatoren für organische Reaktionen erforscht. Die hier präsentierten Ergebnisse gewähren wertvolle Einblicke in die Möglichkeiten, die sie bieten, aber auch in die Limitationen, mit denen sie einhergehen, und können dadurch zur künftigen Weiterentwicklung dieses Forschungsgebietes beitragen.

List of Publications

This report is based on the following papers, which will be referred to by their roman numerals in the text.

‡ These authors contributed equally.

I **High turnover photocatalytic hydrogen formation with an Fe(III) *N*-heterocyclic carbene photosensitiser**

J. Schwarz,[‡] A. Ilic,[‡] C. Johnson,[‡] R. Lomoth, and K. Wärnmark
Chem. Commun. **2022**, 58, 5351–5354.

I contributed to planning the project and performed large parts of the initial testing and optimisation reactions, time trace-experiments, as well as control experiments for the photocatalytic reaction. I also conducted and analysed the results of mechanistic investigations, such as chemical actinometry and photostability studies. I contributed to the writing of the first draft and reviewing of the manuscript.

II **Photoredox catalysis *via* consecutive ²LMCT- and ³MLCT-excitation of an Fe(III)/(II)-*N*-heterocyclic carbene complex**

A. Ilic,[‡] J. Schwarz,[‡] C. Johnson,[‡] L. H. M. de Groot, S. Kaufhold, R. Lomoth, and K. Wärnmark
Chem. Sci. **2022**, 13, 9165–9175.

I performed large parts of the experimental work, including initial testing, optimisations and substrate scope for the reductive quenching route and planned and carried out mechanistic investigations such as radical trapping and wavelength-switching experiments as well as chemical actinometry. I substantially contributed to conceiving the proposed mechanisms, wrote major parts of the entire manuscript and coordinated the writing.

III **Aminomethylations of Electron-Deficient Compounds—Bringing Iron Photoredox Catalysis into Play**

A. Ilic, B. Strücker, C. Johnson, S. Hainz, R. Lomoth, K. Wärnmark
Submitted Manuscript

I conceived and planned the project and I performed initial testing, substrate syntheses as well as Stern–Volmer quenching studies. Furthermore, I supervised the synthetic experimental work including optimisations, control experiments, substrate scope and radical trapping experiments. I analysed the data, wrote major parts of the entire manuscript and coordinated the writing.

IV **³MLCT excited state dynamics of a Homoleptic Iron(II) Hexa-*N*-Heterocyclic Carbene Scorpionate Complex**

N. Kaul, M. Deegbay, A. Ilic, Catherine Johnson, O. Prakash, K. Wärnmark, E. Jakubikova, and R. Lomoth
In Manuscript

I synthesised the complex under investigation and performed the NMR-spectroscopic characterisation and photostability studies by in situ chemical reduction. I prepared and investigated the photostability of an additional *hexa*-NHC complex from literature that was used as a reference for computational calculations by collaborators in this study. I wrote parts of the first draft and contributed to the further writing as well as reviewing of the manuscript.

The following publications are not included since they are beyond the scope of this report. They are listed in chronological order.

‡ These authors contributed equally.

- V **Simultaneous non-invasive gas analysis in artificial photosynthesis reactions using rotational Raman spectroscopy**
J. Schwarz, ‡ A. Ilic, ‡ S. Kaufhold, J. Ahokas, P. Myllyperkiö, M. Pettersson, and K. Wärnmark
Sustainable Energy Fuels **2022**, 6, 4388–4392.
- VI **Photophysical Integrity of the Iron(III) Scorpionate Framework in Iron(III)-NHC Complexes with Long-lived ²LMCT Excited States**
O. Prakash, L. Lindh, N. Kaul, N. W. Rosemann, I. Bolaño Losada, C. Johnson, P. Chábera, A. Ilic, J. Schwarz, A. K. Gupta, J. Uhlig, T. Ericsson, L. Häggström, P. Huang, J. Bendix, D. Strand, A. Yartsev, R. Lomoth, P. Persson, and K. Wärnmark
Inorg. Chem. **2022**, 61, 44, 17515–17526.
- VII **Competing Dynamics of Intramolecular Deactivation and Bimolecular Charge Transfer Processes in Luminescent Fe(III) N-Heterocyclic Carbene Complexes**
N. W. Rosemann, L. Lindh, I. Bolaño Losada, S. Kaufhold, O. Prakash, A. Ilic, J. Schwarz, K. Wärnmark, P. Chábera, A. Yartsev, and P. Persson
Chem. Sci. **2023**, 14, 3569–3579.
- VIII **Iron Photoredox Catalysis – Exploring New Opportunities**
L. H. M. de Groot, ‡ A. Ilic, ‡ J. Schwarz, ‡ and K. Wärnmark
J. Am. Chem. Soc. **2023**, 145, 17, 9369–9388.
- IX **High-Efficiency Photoinduced Charge Separation in Fe(III)carbene Thin Films**
M. Zhang, C. E. Johnson, A. Ilic, J. Schwarz, M. B. Johansson, and R. Lomoth
J. Am. Chem. Soc. **2023**, 145, 35, 19171–19176.

Abbreviations & Key Symbols

A	Acceptor
<i>A</i>	Absorbance
ATRA	Atom Transfer Radical Addition
bpy	2,2'-Bipyridine
brphtmeimb	(4-Bromophenyl)tris(3-methylimidazol-2-ylidene)borate
btz	3,3'-Dimethyl-1,1'-bis(<i>p</i> -tolyl)-4,4'-bis(1,2,3-triazol-5-ylidene)
CEY	Cage Escape Yield (see η_{ce})
conPET	Consecutive Photo-induced Electron Transfer
coohphtmeimb	(4-Carboxyphenyl)tris(3-methylimidazol-2-ylidene)borate
CT	Charge-transfer
CV	Cyclic Voltammetry
D	Donor
dap	2,9-(<i>p</i> -Anisyl)-1,10-phenanthroline
DCM	Dichloromethane
dF(CF ₃)ppy	2-(2,4-Difluorophenyl)-5-(trifluoromethyl)pyridine
DMF	Dimethylformamide
dmgH	Dimethylglyoximate
DMSO	Dimethylsulfoxide
dtbpy	4,4'-Di- <i>tert</i> -butyl-2,2'-bipyridine
η_{ce}	Cage Escape Yield (see CEY)
η_q	Quenching Yield

ε	Extinction coefficient
E	Potential
$E_{1/2}$	Half-wave Potential
E_{0-0}	HOMO-LUMO Gap
EnT	Energy Transfer
EPR	Electron Paramagnetic Resonance
ES	Excited State
EWG	Electron-Withdrawing Group
Φ	Quantum Yield
Fc	Ferrocene
GC	Gas Chromatography
GS	Ground State
HER	Hydrogen Evolution Reaction
HOMO	Highest Occupied Molecular Orbital
HRMS	High Resolution Mass Spectrometry
I_0	Intensity of incident light
I_{em}	Emission intensity
I_{tr}	Intensity of transmitted light
IR	Infrared
ISC	Intersystem Crossing
k_{bc}	rate constant for geminate back-combination
k_{bd}	rate constant for backdonation
k_{ce}	rate constant for cage escape
k_{nr}	rate constant for non-radiative decay
k_q	rate constant for quenching
k_r	rate constant for radiative decay
k_s	rate constant for single electron transfer to a substrate S
K_{app}	Apparent Quenching constant

K_D	Dynamic quenching constant
K_{SV}	Stern–Volmer constant
K_S	Static quenching constant/association constant
λ	Reorganisation Energy
λ_{abs}	Absorption Wavelength
λ_{em}	Emission Wavelength
λ_{irr}	Irradiation Wavelength
LC	Ligand-Centred
LC–MS	Liquid Chromatography–Mass Spectrometry
LED	Light-Emitting Diode
LMCT	Ligand-to-Metal Charge-transfer
L^{N3}	1,4-bis(pyridin-2-ylmethyl)-1,4,7-triazonane
LUMO	Lowest Unoccupied Molecular Orbital
MC	Metal-Centred
MeCN	Acetonitrile
MLCT	Metal-to-Ligand Charge-transfer
MS	Mass Spectrometry
NHC	<i>N</i> -heterocyclic Carbene
NMR	Nuclear Magnetic Resonance
NP	Nanoparticle
OQ	Oxidative Quenching
OTf	Triflate
PC	Photoredox Catalyst
PCET	Proton-Coupled Electron Transfer
phtmeimb	Tris(3-methylimidazolin-2-ylidene)(phenyl)borate
ppy	2-Phenylpyridine
PRC	Proton Reduction Catalyst
PS	Photosensitiser

Q	Quencher
py	Pyridine
RQ	Reductive Quenching
SBCS	Symmetry-Breaking Charge-Separation
SCE	Standard Calomel Electrode
SET	Single Electron Transfer
SHE	Standard Hydrogen Electrode
τ_0	Excited State Lifetime
TA	Transient Absorption
TCSPC	Time-correlated Single Photon Counting
TD-DFT	Time-dependant Density Functional Theory
TEA	Triethylamine
TEOA	Triethanolamine
THF	Tetrahydrofuran
TIM	2,3,9,10-Tetramethyl-1,4,8,11-tetraazacyclotetradeca-1,3,8,10-tetraene
TM	Transition Metal
TMS	Trimethylsilyl
TOF	Turnover Frequency
TON	Turnover Number
UV	Ultraviolet
VIS	Visible
VLIH	Visible Light-Induced Homolysis

1 Background

Climate change and the threat of an energy crisis are ever-present concerns of modern society. Our energy requirements are constantly increasing and fossil fuel reserves are likely to remain our primary global energy source in the future [1]. However, beside the fact that they are not renewable [1-3], the use of fossil fuels contributes to air pollution, greenhouse gas emission and the consequent environmental deterioration—and ultimately climate change and global warming [4]. In order to combat these issues and limit the usage of energy sources that have detrimental effects on the environment [5], alternative ways of harvesting energy are needed. One approach to renewable energy production that has been the focus of many studies, is the conversion of solar energy to electric or chemical energy. The interest in this area arises from the fact that the Sun presents an essentially limitless energy source, with slightly more than one hour of irradiation being sufficient to supply Earth with enough energy to cover humanity's annual requirements [6].

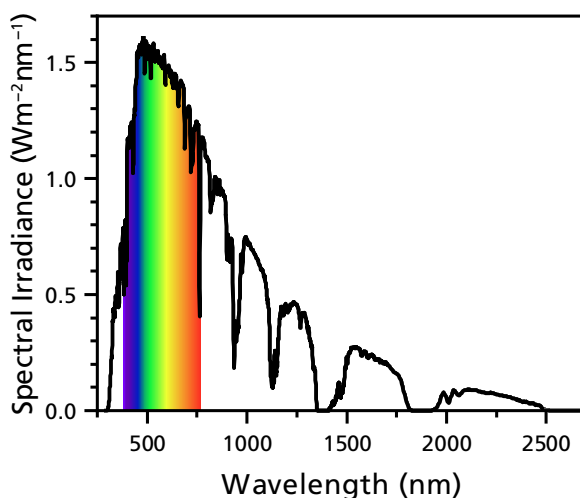


Figure 1.1: Spectral irradiance by the Sun. Adapted from [7]

Besides photovoltaic applications, photocatalysis constitutes an alternative way of harvesting and converting sunlight. Figure 1.1 depicts the spectral irradiance over the electromagnetic spectrum, ranging from the ultraviolet (UV) region over the part of the spectrum that is visible to the human eye, up to the infrared (IR). From there, it is

quite apparent that visible light should be of particular interest, as the Sun's spectral irradiance is highest in that region [8]. Additionally, using low energy visible light for irradiation leads to fewer undesired side reactions, caused by unwanted excitation of organic additives, substrates and products, whilst still providing sufficient amounts of energy to drive these processes. This is particularly important for organic transformations mediated by light [9].

2 Aim & Outline of this Thesis

In this thesis, complexes based on Earth-abundant iron are investigated with respect to their applicability in photocatalysis to reveal their potential but also their limitations. This has been made possible by the emergence of new Fe-*N*-heterocyclic carbene (NHC) complexes with significantly prolonged excited state (ES) lifetimes of their charge-transfer (CT) states in recent years [10-12]. Their exploration in photocatalysis and the elucidation of the operative mechanisms can lead to new insights for future design strategies, allowing for them to become reasonable alternatives to already existing systems and providing a better understanding of the field at large. Said developments could include both the prolongation of ES lifetimes and improvement of redox potentials of the complexes, but also fine-tuning of reaction conditions to effect better charge-separation, which in turn increases the efficiency of the bimolecular quenching necessary to drive photocatalytic reactions. Here, particular focus has been given to the application of Fe-NHC complexes as photoredox catalysts (PC) in organic transformations as well as their use as photosensitisers (PS) for solar fuel generation.

To establish the context for this thesis work some fundamental concepts and tools utilised in the field of photocatalysis are touched upon in Chapter 3. Thereafter, a brief discussion of the photophysical properties of light-harvesting iron complexes, focusing on Fe-NHC complexes, is given in Chapter 4.

Chapter 5 describes the use of an iron-based PS, [Fe(III)(phtmeimb)₂]PF₆ (**11**) (phtmeimb = tris(3-methylimidazolin-2-ylidene)(phenyl)borate)), in artificial photosynthesis reactions, which gave rise to the first example of high-turnover photocatalytic hydrogen evolution reactions sensitised by such systems (Paper I). Furthermore, first attempts towards the photocatalytic reduction of CO₂ to CO, using the same PS, are discussed.

In Chapter 6, the major findings of Paper II and III are relayed, where outer-sphere single electron transfer (SET) from CT states of Fe-NHC complexes was exploited for visible-light mediated photoredox catalysis of organic reactions. In Paper II, [Fe(III/II)(btz)₃]^{3+/2+} (**9**)/(**10**) (btz = 3,3'-dimethyl-1,1'-bis(*p*-tolyl)-4,4'-bis(1,2,3-triazol-5-ylidene)), was applied as PC in the well-explored atom transfer radical addition (ATRA) reaction. These reactions were driven via reductive quenching (RQ) by utilising excitation of the two photoactive oxidation states (**9**) and (**10**) within the same catalytic turnover—an underexplored mechanism in synthetic photoredox

catlysis. Additionally, oxidative quenching (OQ) of (9) could be employed to effect the same chemical transformations. In Paper III, the use of (11) as PC in visible light-mediated aminomethylation reactions by in situ generation of α -aminoalkyl radicals is described.

Based on the findings of Paper I–III demonstrating that the Fe-NHC complexes under investigation can be successfully employed in photocatalytic applications and showcasing the possibility for sequential multi-photon excitation of different photoactive oxidation states of the same complex, Chapter 7 details the preparation and investigation of the ES properties of the Fe(II)-congener of (11) (Paper IV).

Finally, initial results towards the heterogenisation of Fe(III)-NHC complexes with the goal of improving their overall sustainability as PCs are presented in Chapter 8. There, a known homoleptic as well as a newly synthesised heteroleptic structural analogue of complex (11) were anchored to Al_2O_3 -nanoparticles and investigated with respect to their photocatalytic activity and reusability.

3 Photocatalysis

3.1 Solar Energy Conversion

Solar energy has been widely recognised as the potentially most attractive source of renewable, clean and abundant energy. Different strategies to its utilisation have been pursued, such as photothermal, photovoltaic as well as photocatalytic methods. The conversion of solar energy into chemical energy within the context of photocatalytic chemical synthesis and artificial photosynthesis of fuels to afford storable products, is of particular interest [13]. Advances such as the already in 1972 reported use of TiO_2 as a photoelectrode for water splitting demonstrated by Fujishima and Honda have led to photocatalysis being viewed as a promising technology for solar-to-chemical energy conversion [14]. The therefrom resulting research efforts have given rise to the development of many different types of systems, both molecular and bulk material-based—all with the goal of harvesting light and driving various photoreactions [15].

Generally, light is harvested by a photocatalyst and the energy is either transferred to a substrate or converted into an electrical potential which can subsequently be used to effect an electron transfer between the excited photocatalyst and a substrate [16]. Due to the previously mentioned abundance of light, it is generally considered to be a low-cost resource [17]. However, solar energy conversion poses several challenges, such as lack of broad-spectrum absorption of the photocatalytic system, undesired side reactions due to UV irradiation and wavelength mismatch leading to inefficient energy conversion due to low quantum yields and losses via thermalisation [15, 16]. As a result, studies of photocatalytic systems oftentimes incorporate artificial light sources in the form of lamps or light-emitting diodes (LEDs) to allow for more targeted and reproducible irradiation [18]. The cost of the energy input into the reaction system should therefore also be taken into consideration when developing light-harvesting systems for larger scale applications [16, 17].

3.2 Fundamentals of Photocatalysis

In photocatalysis, the energy difference between the ground state (GS) and the excited state (ES) of a molecule, based on the gap E_{0-0} between its highest occupied molecular orbital (HOMO) and lowest unoccupied molecular orbital (LUMO), is utilised to access high-energy intermediates that can drive chemical reactions, by providing a thermodynamic driving force. The ES can act as a strong photoreductant and/or -oxidant, due to the altered electronic structure as a result of the excitation, being quenched by a suitable reaction partner—a so-called quencher (Q)—in the process [19]. This is illustrated in Figure 3.1.

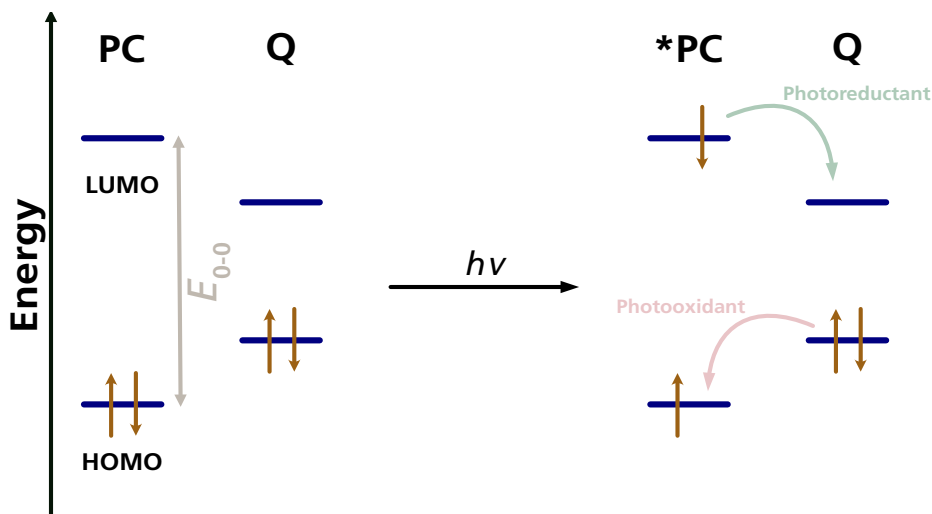


Figure 3.1: Photoexcitation leading to the generation of a strong photoreductant/-oxidant (PC = photoredox catalyst, Q = quencher, E_{0-0} = HOMO–LUMO energy gap).

Within the published literature in this field, the term photochemical sensitisation and photo(redox) catalysis are considered to be closely related and occasionally used interchangeably [20]. Throughout this thesis, a distinction between photosensitisers (PSs) and photoredox catalysts (PCs) is made based on whether an additional catalytic unit is involved in the reaction system. In the herein investigated artificial photosynthesis reactions, the light-harvesting unit is not directly involved in the product formation step and is consequently referred to as PS, whereas in the case of photoredox catalysis of organic reactions, the term PC is used as the light-absorbing unit engages in electron transfer processes with the product-forming reactants. However, the fundamental photochemical reaction pathways for both PS or PC as used herein follow the same principles and will thus be discussed in conjunction in this chapter.

3.2.1 Photocatalysis based on Single Electron Transfer (SET) Reactions

For a molecule to be successfully employed as a PC or PS, certain requirements need to be met. In general, strong light absorption—preferably in the visible region of the electromagnetic spectrum—along with a sufficiently long ES lifetime τ_0 (commonly ns– μ s) to allow for participation in diffusion-controlled bimolecular quenching processes are considered crucial [19, 21]. Additionally, it is highly desirable for PCs and PSs to exhibit considerable photostability [21].

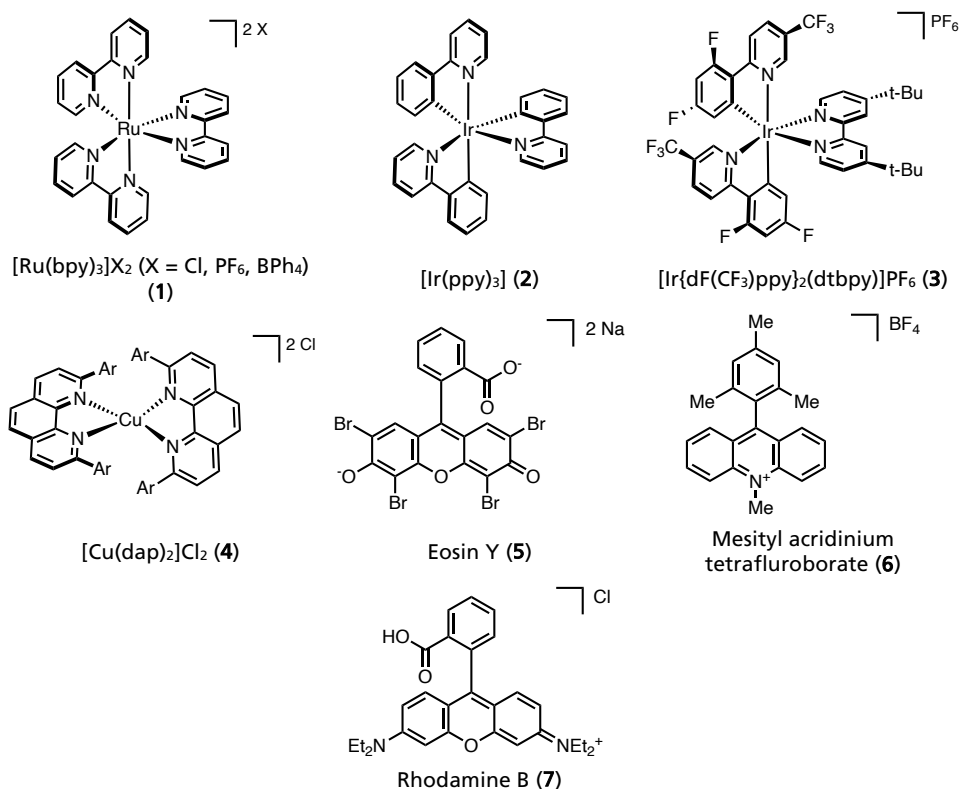


Figure 3.2: Selected examples of compounds used as photocatalysts and photosensitizers (bpy = 2,2'-bipyridine, ppy = 2-phenylpyridine, dF(CF₃)ppy = 2-(2,4-difluorophenyl)-5-(trifluoromethyl)pyridine, dtbbpy = 4,4'-di-*tert*-butyl-2,2'-bipyridine, dap = 2,9-(*p*-anisyl)-1,10-phenanthroline) [22-24].

A range of both organic and transition metal (TM)-based PCs/PSs fulfil the requirements discussed above. As a result, they have been used to catalyse/sensitise a wide variety of reactions, with TM complexes being particularly heavily featured [19, 25-34]. Their extensive application can be attributed to their more facile tunability, which, e.g., can be achieved by careful ligand modification or by changing the counter-ion [35-37]. Moreover, such metal complexes have the advantage of giving access to different oxidation states. These can be exploited to provide a stronger thermodynamic driving force for the target reaction to take place [35]. Some

photoactive compounds frequently featured in photocatalytic applications are shown in Figure 3.2.

Figure 3.3A depicts different reaction pathways a PC or PS can undergo following light absorption shown on the example of a TM complex [38]. Upon excitation of the PC, the resulting ES, denoted as *PC, can decay back to the GS either by radiative decay with a rate constant k_r by emitting light or non-radiatively via thermalisation (k_{nr}). Such pathways are generally considered non-productive in the context of photocatalysis and are thus undesirable. In the presence of the quencher Q, *PC can engage in single electron transfer (SET) or energy transfer (EnT), the latter of which will be touched upon in Chapter 3.2.2. In the case of SET, reductive quenching (RQ) by an electron donor or oxidative quenching (OQ) by an electron acceptor, gives access to the reduced or oxidised GS, respectively—states of higher reactivity than the original GS. Electron acceptors and donors can be sacrificial in nature, a substrate or an intermediate of the reaction. Most commonly, following another electron transfer to/from a suitable acceptor/donor molecule or intermediate, the original GS can be restored, making the reaction catalytic in nature. The efficiency of the SET event that proceeds from *PC is governed by different factors and can be quantified by the rate of quenching (k_q) and the corresponding quenching yield (η_q). Following the quenching event, a RQ here, the reaction partners remain in close proximity to each other within the same solvent cage, providing the opportunity for undesired geminate back-combination (k_{bc}), a spontaneous thermal process [38, 39].

For the photocatalytic reaction to proceed, cage escape of the photoproducts from the solvent cage to afford the charge-separated species is essential. A schematic illustration of the cage escape of a PC following SET from an electron donor is shown in Figure 3.3B. The cage escape yield (CEY, η_{ce}) thus gives a measure of how many of the quenched ESs result in charge-separated photoproducts that have left the solvent cage and are available to engage in diffusion-controlled reactions. The rate constant for the cage escape is given by k_{ce} . Because of this, CEYs can govern the rate of photoredox catalytic reactions, despite the interplay of several different steps involved in the overall reaction [40, 41]. Consequently, CEY is a fundamental aspect of photoredox catalysis that has not been afforded widespread attention for many years, but has been identified as a key element to the efficiency of photocatalytic processes more recently [40-46]. The factors affecting cage escape can be manifold and are to date still not entirely known or understood [38, 39, 47-53]—and thus hard to predict. Different aspects such as solvent polarity and viscosity [40, 51, 53-55], electrostatic interactions [56], ion-pairing effects [39, 54, 55] as well as spin and heavy-atom effects [38-40, 51, 57, 58] among a number of others have however been stated to play a key role in the cage escape of electron-transfer products. Following cage escape, unproductive backdonation between the charge-separated products can still occur, recovering the original PC and Q (k_{bd}).

However, ideally the, in this case, reduced PC^- will partake in a SET to a substrate (S) with a rate constant k_s .

As a consequence of the differing pathways the excited PC or PS can undergo, not every absorbed photon leads to formation of the desired photoproduct, be that the reduced or the oxidised GS [59]. The quantum yield $\Phi = \eta_q \eta_{ce}$ essentially describes the ratio between photoproducts generated and photons absorbed. While within this context the quantum yield solely pertains to the quenching step, such a quantification can also be expressed in more general terms, as number of events per number of photons absorbed [60].

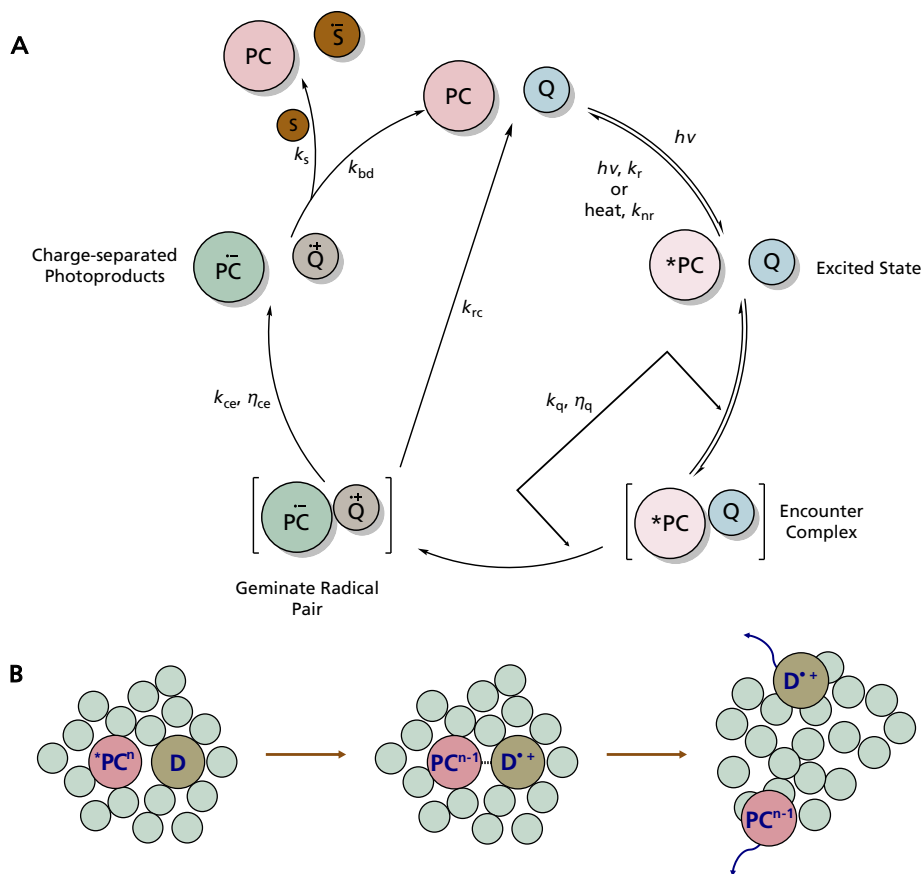


Figure 3.3: A) Schematic overview of the different steps and pathways involved in a photocatalytic reaction shown on the example of reductive quenching. PC = photoredox catalyst, Q = quencher, S = substrate, k_r = rate of radiative decay, k_{nr} = rate of non-radiative decay, k_q = rate of quenching, η_q = quenching yield, k_{ce} = rate of cage escape, η_{ce} = cage escape yield, k_{bd} = rate of backdonation, k_s = rate of SET to S. Adapted with permission from [61] © 2023, John Wiley & Sons, Inc. B) Illustration of cage escape of charge-separated photoproduct following reductive quenching using an electron donor D.

A further prerequisite for a photocatalytic reaction to take place via SET, are favourable and reversible redox potentials of the involved GSs/ESs of the PC as well as the reactants and intermediates (Figure 3.4) [62].

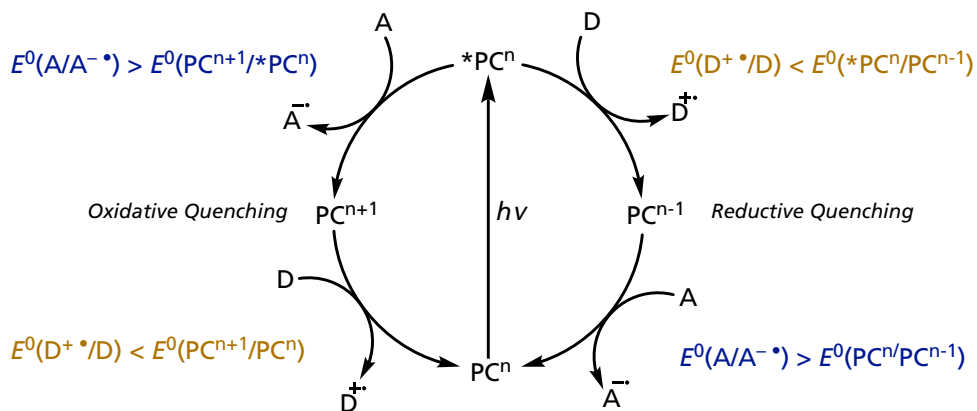


Figure 3.4: Thermodynamic requirements for SET in a photoredox reaction. (PC = photoredox catalyst, D = electron donor, A = electron acceptor).

While GS redox potentials can be determined by methods such as cyclic voltammetry (CV), ES redox potentials are estimated from the GS reduction and oxidation potentials in combination with the ES energy of the PC (E_{0-0}) using the simplified Rehm–Weller equation (Eq. (3.1) for oxidative quenching, Eq. (3.2) for reductive quenching) [63].

$$E^0(\text{PC}^{n+1}/^*\text{PC}^n) = E^0(\text{PC}^{n+1}/\text{PC}^n) - E_{0-0}(^*\text{PC}^n/\text{PC}^n) \quad (3.1)$$

$$E^0(^*\text{PC}^n/\text{PC}^{n-1}) = E^0(\text{PC}^n/\text{PC}^{n-1}) - E_{0-0}(^*\text{PC}^n/\text{PC}^n) \quad (3.2)$$

3.2.2 Energy Transfer (EnT)

Another way of exploiting ES reactivity that has been pursued in the field of photocatalysis is the previously mentioned EnT, where excess energy of a donor molecule (D) is transferred to an acceptor molecule (A) (Figure 3.5) [62, 64]. This gives access to ESs that would otherwise be less or not at all available via direct light-induced excitation. Dexter EnT, follows an exchange mechanism that necessitates orbital overlap between D and A, which is a spin-conserved process [65, 66]. The triplet-ES energy of the *PC is transferred to an A via intermolecular exchange of GS- and ES-electrons (Figure 3.5, left) [65-67].

In the Förster EnT (Figure 3.5, right), also referred to as coulombic EnT, the energy is transferred through-space between transition dipole moments over distances of 10 to 100 Å [68], thus not requiring physical D–A contact [65, 66, 69]. In this case, the electronic absorption spectrum of the A and the emission spectrum of the D need to exhibit an overlap [62]. Consequently, this mechanism is of importance in fluorescence labelling and bioimaging, but not widely applicable to photocatalytic systems, due to the lack of visible light absorption of most organic substrates [67].

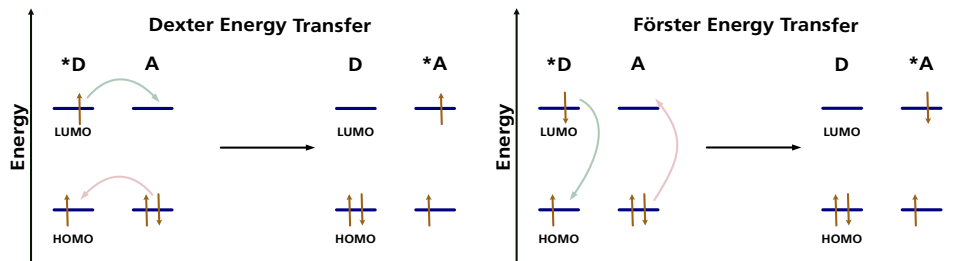


Figure 3.5: Dexter and Förster Energy Transfer (D = donor, A = acceptor). Adapted from [70] with permission from the Royal Society of Chemistry. © 2015 Royal Society of Chemistry.

3.3 Tools for Investigation of Photocatalytic Systems

While advancements in the area of (organic) photoredox catalysis have been heavily reliant on empirical reaction optimisation, an improved understanding of the underlying mechanisms of existing reaction systems can facilitate and accelerate progress—not just in specific cases—but rather for the field of photocatalysis at large [61, 71, 72].

In light of the requirements for conducting photocatalysis mentioned in the previous section, methods of predicting whether these prerequisites are fulfilled are essential to planning and designing new photocatalytic systems and reactions. To this end, a range of different tools can be used to investigate both photophysical and -chemical properties of potential reaction components [61, 73, 74].

3.3.1 Steady-State Spectroscopy & Stern–Volmer Quenching Studies

Steady-state spectroscopy can be utilised to obtain fundamental information on both the PS and reactants for a photocatalytic reaction. Absorbance A gives a measure of the intensity of the transmitted light I_{tr} through the sample compared to the intensity of the incident light I_0 and is expressed in Eq. (3.3) in the form of the Beer-Lambert law. The absorbance is linearly dependant on the extinction coefficient ε , the concentration c of the sample and the pathlength l [75].

$$A = -\log\left(\frac{I_{\text{tr}}}{I_0}\right) = \varepsilon cl \quad (3.3)$$

UV–VIS absorption spectroscopy can for instance afford insights into aspects such as ideal irradiation wavelength for excitation based on the absorption maxima (λ_{abs}) of the PS. The extinction coefficient ε of the latter can also be determined by utilising the aforementioned linear dependence. Furthermore, additional properties of the reaction system that could impact reactivity or give mechanistic insights, such as the possible formation of ground state complexes between different reactants, can be determined. The photostability of the PS or PC can also be investigated using this technique by tracking the change in absorption features—a point of large interest for photocatalytic applications, as the degradation of the light-harvesting unit within the reaction can be detrimental to the formation of product [62, 74].

Oftentimes, PCs can also exhibit room-temperature emission of a photon upon relaxation from their ESs back to the GSs. Determining the emission wavelength of photoactive compounds by steady-state emission spectroscopy makes it possible to calculate the energy difference between the GS and ES (E_{0-0}). Additionally, monitoring changes of the emission intensity in the presence of reactants and additives can give

valuable information on possible interactions occurring between the ES of the PC (*PC) and other reaction components, such as SET or EnT. Both of these phenomena can lead to a decrease in emission intensity, signifying quenching of the ES [61, 74].

A simplified illustration of the measurement principle behind steady-state absorption and emission spectroscopy as well as examples for the appearance of the resulting spectra are shown in Figure 3.6.

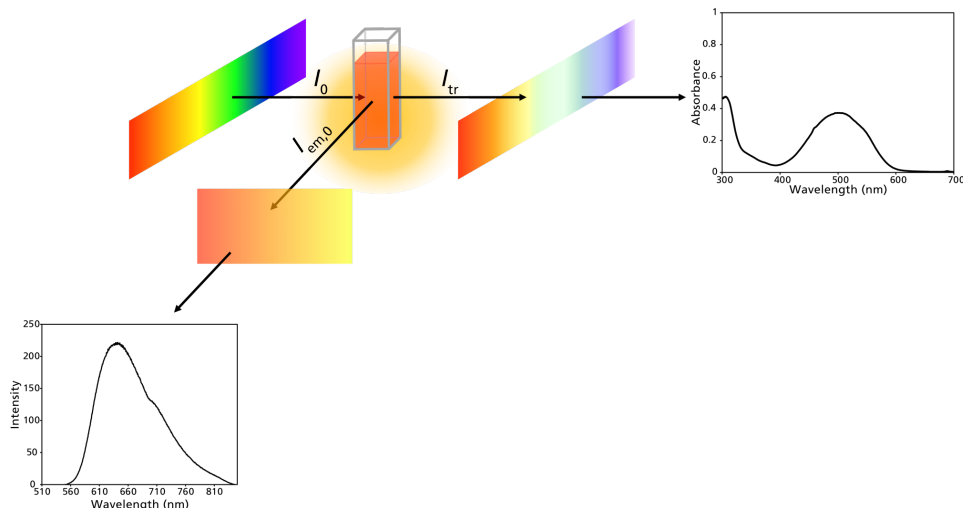
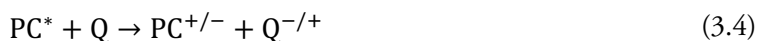


Figure 3.6: Schematic drawing of the measurement principle behind steady-state absorption and emission spectroscopy. I_0 = incident light, I_{tr} = transmitted light, $I_{em,0}$ = emitted light.

Through Stern–Volmer quenching experiments the change between emission intensity in the absence of quencher, $I_{em,0}$, and the emission intensity I_{em} in the presence of different quencher concentrations $[Q]$ can be utilised to obtain insights into the kinetics of the quenching process [61, 62].

For the case of purely collisional bimolecular quenching, the decrease in intensity is described by Eq. (3.5) for a reaction as shown in Eq. (3.4). By plotting $I_{em,0}/I_{em}$ vs $[Q]$ and performing a linear fit, the Stern–Volmer constant K_{SV} (in M^{-1}), which corresponds to the slope of the function, and thus k_q (in $M^{-1} s^{-1}$) can be obtained. Consequently, the rate of the activation step in a photocatalytic reaction can be determined using this rather simple method, provided that the ES lifetime τ_0 in the respective solvent is known [61, 62, 76].



$$\frac{I_{em,0}}{I_{em}} = 1 + K_{SV}[Q] = 1 + k_q\tau_0[Q] \quad (3.5)$$

ES quenching can also originate from the formation of a non-emissive GS adduct between the PS and Q. Such an adduct returns to the GS without emission of a photon upon irradiation and only PS molecules that are not complexed will exhibit detectable emission. $I_{em,0}$ versus I_{em} will in this case also exhibit linear behaviour (Eq. (3.6)). However, the constant K_S (in M^{-1}) now corresponds to the association constant for the formation of the adduct [76].

$$\frac{I_{em,0}}{I_{em}} = 1 + K_S[Q] \quad (3.6)$$

Deviations of said linear behaviour can also occur, indicative of a static quenching component in combination with diffusion-controlled collisional quenching. In such a case, a quadratic dependence on the concentration of Q (Eq. (3.7)) can be used to model the obtained data. K_D corresponds to the dynamic quenching constant in this case and describes the collisional component of the reaction. The dynamic component of the quenching can be extracted from lifetime measurements, using the linear relationship given in Eq. (3.8), where τ corresponds to the lifetime in presence of the quencher. By introducing the apparent quenching constant K_{app} , as defined in Eq. (3.9), this quadratic expression can be simplified and utilised to graphically separate K_S and K_D , by constructing a plot of $K_{app}/[Q]$ versus $[Q]$ and extracting the values for the slope ($K_D K_S$) and intercept ($K_D + K_S$) [62, 76, 77].

$$\frac{I_{em,0}}{I_{em}} = 1 + (K_D + K_S)[Q] + K_D K_S [Q]^2 = 1 + K_{app}[Q] \quad (3.7)$$

$$\frac{\tau_0}{\tau} = 1 + K_D[Q] \quad (3.8)$$

$$K_{app} = (K_D + K_S) + K_D K_S [Q] \quad (3.9)$$

Figure 3.7 illustrates the typical appearance of steady-state ($I_{em,0}/I_{em}$) and time-resolved emission data (τ_0/τ) resulting from dynamic quenching, static quenching and a combination of both [62, 76].

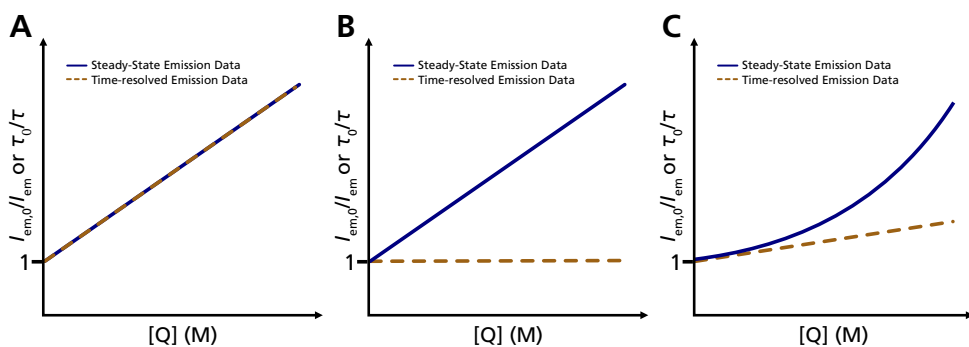


Figure 3.7: Schematic Stern–Volmer plots obtained from systems exhibiting A) dynamic quenching, B) static quenching and C) both dynamic and static quenching. Adapted from [62] with permission from the Royal Society of Chemistry. © 2016 Royal Society of Chemistry.

3.3.2 Time-Resolved Spectroscopy Techniques

Time-resolved spectroscopy techniques are a powerful tool for the investigation of photophysical and -chemical properties of the components and intermediates in photocatalytic systems as well as of the dynamic processes taking place in those reactions. Transient absorption (TA) spectroscopy constitutes the most frequently used of these techniques, allowing for the determination of the ES lifetime of a non-emissive PC in solution as well as giving insights into the formation of reaction intermediates, reaction kinetics and other mechanistic features [61, 73, 74, 78]. During TA spectroscopy, a sample is irradiated by a laser pulse—referred to as pump—generating the ES, the absorption spectrum of which is then recorded as a function of time (fs–s range) using a broad-band spectrum lamp—the probe. A differential spectrum of the absorption following the pump and the absorption prior to excitation can then reveal changes that occur. Figure 3.8 shows a schematic TA spectrum, illustrating what kind of qualitative information can be obtained. There, the difference in the extinction coefficient ε of the GS and ES depending on the wavelength can be seen. Positive features originate from the ES absorbing more strongly than the GS and vice versa for negative features, also referred to as bleach. If the absorbance of the GS and ES is equal at a certain wavelength, an isosbestic point is observed [62].

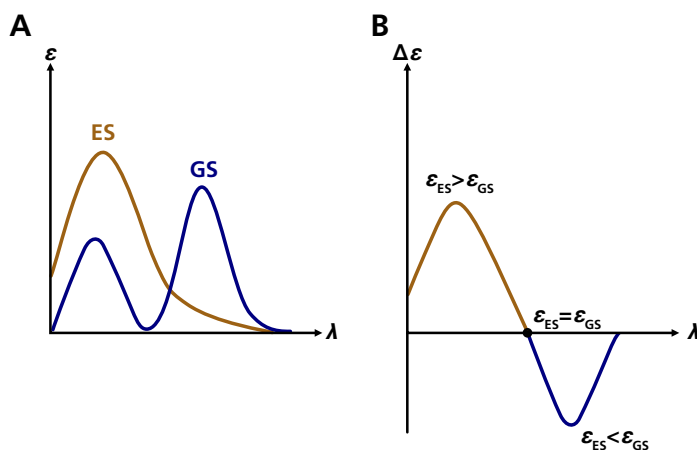


Figure 3.8: A) Schematic spectra showing the absorption of the ground state (GS) and excited state (ES). B) Schematic illustration of a transient absorption spectrum exhibiting a positive feature (brown) and a negative feature (blue) corresponding to the bleach. Adapted from [62] with permission from the Royal Society of Chemistry. © 2016 Royal Society of Chemistry.

Additionally, in a reaction of *PC with a Q, it is possible to elucidate whether the ES reaction is an SET. If so, a change in the spectral features corresponding to what would be the resulting oxidation state of the respective RQ or OQ event is observed. Consequently, provided that the absorption features of the resulting reduced or oxidised GS are known and the quenching does indeed result in a detectable amount of charge-separated photoproducts, a reasonable assignment of the nature of the ES reaction can be made. The tracing of these processes at specific wavelengths can furthermore provide data from which kinetic rate constants can be extracted [79, 80].

Time-resolved emission spectroscopy—used to determine the ES lifetimes of emissive PCs—time-resolved IR spectroscopy, time-resolved Raman spectroscopy and X-ray TA spectroscopy constitute further examples of techniques that have found application in the investigation of photocatalytic mechanisms [61].

3.3.3 Cyclic Voltammetry and Spectroelectrochemistry

With SET processes at the core of many photocatalytic reactions, knowledge of the electrochemical behaviour of the components in a photocatalytic reaction system—PC, sacrificial electron donors or acceptors, substrates and additives—is crucial both to predicting but also to rationalising reactivity patterns [62, 73]. CV constitutes a comparatively simple but powerful method towards investigating reversible and irreversible reduction and oxidation processes of molecular reactants [81].

CV measurements are performed in an electrochemical cell featuring a working electrode, a reference electrode as well as a counter electrode, which are immersed in an

electrolyte solution containing the analyte-sample S. Through the working electrode, a potential E is applied as a function of the reference electrode and gradually changed until reaching a set potential, upon which the direction of the “sweep” is reversed. The thereby induced current I is monitored and corresponds to the flow of electrons between the working and counter electrode [82]. Figure 3.9 depicts a schematic illustration of a cyclic voltammogram, from which the desired information on the electrochemical properties of a compound can be obtained. There, the values on the abscissa denote the applied potential E , while the ordinate shows the current I that is passed. It ought to be noted that in this particular case the US convention of reporting CV data was used, as indicated by the abscissa, where the values for the applied voltage go from high potentials to low potentials. The sweep thus occurs from high to low potentials, from the initial potential 1 to the switching potential 4. The scan direction is then reversed and the potential is increased again until the end potential 7 is reached. Point 2 and 5 indicate where the concentration of S and S^+ is equal, corresponding to the value of interest, the half-wave potential $E_{1/2}$ —the halfway point between the peak cathodic current 3 and the peak anodic current 6 [81].

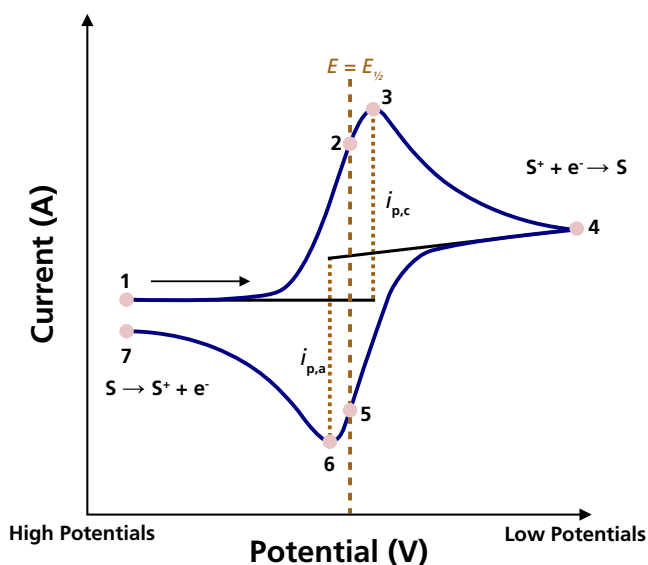


Figure 3.9: Schematic depiction of a cyclic voltammogram showcasing a reversible reduction of a sample S. 1: initial potential, 2 & 5: points of equal concentration between S and S^+ , 3: peak cathodic current, 4: switching potential, 6: peak anodic current, 7: end potential. Adapted with permission from [81]. © 2017 American Chemical Society.

The thereby obtained potentials are reported in relation to the previously mentioned reference electrode. There are several commonly used reference electrode materials, such as the saturated calomel electrode (SCE), standard hydrogen electrode (SHE) and different Ag/Ag⁺ electrodes, the latter of which are also used in non-aqueous media [81]. Tables can be utilised for the conversion between the most common reference electrodes [83], but the use of an internal reference such as ferrocene, if possible, enables the most reliable comparison between different set-ups [84].

The combination of electrochemical measurements and steady-state spectroscopy (UV–VIS, IR, Raman, etc.)—spectroelectrochemistry—enables the simultaneous determination of redox potentials and characterisation of the accompanying changes in spectroscopic features. This allows for the identification of reaction intermediates as well as reduced or oxidised GSs of the PC. A prerequisite for this technique is the electrochemical stability of the investigated components as well as them exhibiting absorption features in the investigated spectral range [12, 85–88].

3.3.4 Nuclear Magnetic Resonance Spectroscopy

Nuclear Magnetic Resonance (NMR) spectroscopy presents one of the most commonplace analytical techniques in synthetic chemistry and is thus also extensively used for the investigation of photocatalytic systems. Beyond its usage to identify and quantify reaction products, NMR spectroscopy is a powerful, non-invasive and non-destructive method that can be employed to detect and identify sufficiently long-lived reaction intermediates with high-sensitivity, determine photodegradation of reaction components, obtain information on intermolecular interactions as well as diffusion-coefficients of reaction components, which can for instance be used to estimate the pathlength an excited PC can diffuse during its ES lifetime. A built-in LED irradiation source can even allow for in situ tracing of photoreactions over time [59, 89].

3.3.5 Detection of Radicals

Electron paramagnetic resonance (EPR) spectroscopy is a technique that allows for the detection and analysis of paramagnetic samples, such as open-shell intermediates which are often generated during photocatalytic reactions. It is an analogous technique to NMR spectroscopy, albeit based on electron spin excitation rather than nuclear spin excitation. To induce the transitions between electron spin energy levels, an external magnetic field and microwave radiation are applied [90]. EPR can also be performed with time resolution to enable tracing of the change in electron spin over time, providing information on the sample's dynamic behaviour. Both static and time-resolved EPR require appropriate instrumental setup and are thus not as wide-spread as NMR spectroscopy [61, 91].

Alternatively, radical traps—compounds which bind radicals hampering product formation and are often based on persistent radicals—can be utilised in the investigation of the participation of radicals in a reaction. The resulting closed-shell adducts can then be detected and analysed by commonplace analytical methods (NMR, mass spectrometry (MS), etc.). Employing this method for the detection of radical reaction intermediates furthermore allows for analysis of short-lived radicals or intermediates that form in too low concentrations for detection via EPR [92].

3.3.6 Chemical Actinometry

As previously mentioned, an essential metric for evaluating the efficiency of photo-induced process—be that a photocatalytic reaction or a specific step of the photocatalytic cycle—is the quantum yield Φ . Quantum yields can be determined using chemical actinometers—systems containing a light-harvesting unit that can participate in a light-induced reaction at a specified wavelength and that have a known quantum yield, among other prerequisites [93]. They can for instance be employed to determine the number of product molecules formed per absorbed photon [94]. By measuring the reaction rate for the chemical actinometer in a reaction set-up, the photon flux in that specific set-up can be determined. Chemical actinometry can thus also provide indication for the presence of a radical chain propagation mechanism in a photocatalytic reaction. In an ideal case, a non-chain mechanism would exhibit a quantum yield of 1, but due to not all photons being absorbed productively, a number smaller than unity is often obtained. Conversely, $\Phi \gg 1$ gives strong support for chain propagation being operative, as more product molecules are being generated than photons absorbed. However, $\Phi < 1$ does not evidence the absence of a chain propagation as the chain reaction might just be very inefficient [95]. While providing good indication of a possible underlying chain propagation mechanism or lack thereof, chemical actinometry itself can be prone to experimental errors due to undesired background reaction caused by e.g., ambient light, leading to inaccurate quantum yields being obtained [59].

3.3.7 Cage Escape Yield Determination

CEYs, as previously discussed, give a measure of the number of charge-separated photoproducts that escape the solvent cage following the quenching event and can be determined by comparative actinometry techniques [61, 96]. There, absorption changes that originate from the reduction or oxidation of the PS are compared to the absorption changes of the ES of a reference actinometer, often $[\text{Ru}(\text{bpy})_3]^{2+}$ (1) (bpy = 2,2'-bipyridine), and normalised by their relative absorbances at the excitation wavelength, giving rise to the relative yield of reduced PS (PS^-) or oxidised PS (PS^+) [61]. The CEY

is then obtained by the ratio of relative yield of PS^- or PS^+ to the percentage of quenched photoluminescence, with the latter usually being determined by time-resolved or steady-state emission measurements. Photostability of both PS and Q for the duration of the experiment is essential for these measurements to give reliable results. Additionally, the actinometer and PS must absorb at the same excitation wavelength [96].

4 Photophysics of Light-Harvesting Iron Complexes

As previously mentioned in Chapter 3.2.1, TM-based complexes have been particularly heavily utilised for photocatalytic applications. Most of them are *hexa*-coordinated, meaning that they form six metal–ligand bonds, with the ligands being arranged in an octahedron around the metal centre. Although in reality, actual complex geometries tend to deviate to varying degrees from that geometry. The five d-orbitals (d_{xy} , d_{xz} , d_{yz} , $d_{x^2-y^2}$ and d_z^2) that are the frontier orbitals of TMs and thus partake in the bond formation are depicted in Figure 4.1 along with the splitting they undergo if the resulting complex exhibits perfect octahedral geometry, giving rise to two sets of degenerate orbitals (t_{2g} and e_g). The e_g -set, corresponding to the $d_{x^2-y^2}$ - and d_z^2 -orbitals, is strongly destabilised as these orbitals have the strongest interaction with the ligands as a result of their σ -symmetry, whereas the π -symmetric t_{2g} -set, consisting of the d_{xy} -, d_{xz} - and d_{yz} -orbitals, is lower in energy due to the comparatively lesser destabilisation as a result of lesser interaction with the ligands.

Particularly organometallic complexes based on noble metals, such as $[\text{Ru}(\text{II})(\text{bpy})_3]^{2+}$ (**1**), *fac*- $[\text{Ir}(\text{III})(\text{ppy})_3]$ (ppy = 2-phenylpyridine) (**2**) and $[\text{Ir}(\text{III})(\text{dF}(\text{CF}_3)\text{ppy})_2(\text{dtbpy})]^+$ (dF(CF₃)ppy = 2-(2,4-difluorophenyl)-5-(trifluoromethyl)pyridine, dtbpy = 4,4'-di-*tert*-butyl-2,2'-bipyridine) (**3**) are frequently used in photocatalysis. However, the scarcity of those metals along with their comparatively blue-shifted absorption and the lack of long-term photostability of their organometallic complexes pose a distinct disadvantage to their usage [97-100].

Consequently, complexes based on Earth-abundant metals have been given increasingly more consideration as light-harvesters, both for photoredox catalysis of organic transformations and artificial photosynthesis, as a means of generating solar fuels [101-106]. Such complexes can exhibit comparatively long-lived CT ESs, favourable reversible redox chemistry and strong visible light absorption. In addition to that, they offer the advantage of higher abundance and more facile production of the metals compared to their already established noble metal counterparts [102]. Among others, complexes of Cu(I) [107-112], Mn(I) [113], Cr(0) and Cr(III) [114-117], Co(III) [118] as well as Mo(0) [119] have been investigated and have shown promise as Earth-abundant PSs.

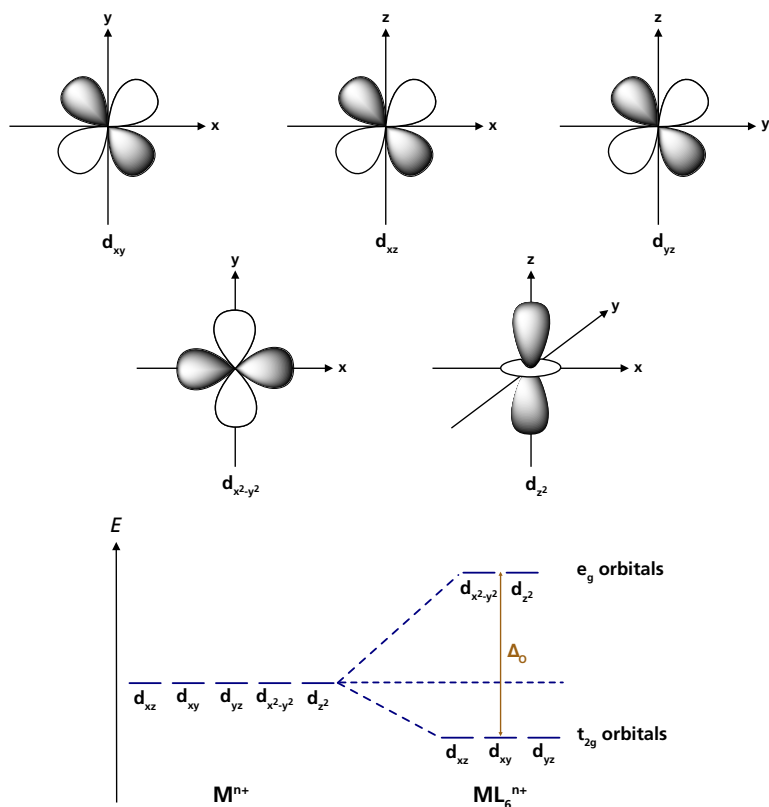
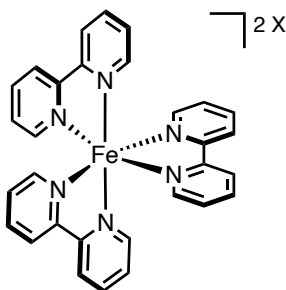


Figure 4.1: Schematic overview of d-orbitals in a TM and their splitting in an octahedral complex [120].

However, in terms of relative abundance of TMs, iron in particular stands out, due to its high availability, low cost and comparatively small environmental impact [121]. Unfortunately, finding efficient iron-based PSs poses a great challenge. Fe(II)-polypyridyl complexes such as $[\text{Fe}(\text{II})(\text{bpy})_3]^{2+}$ (**8**) are isoelectronic with regard to their valence electrons when comparing to similar Ru(II) complexes, resulting in the presence of the same electronic states, albeit in differing relative order of charge transfer (CT) and metal-centred (MC) states [122]. Said difference can be ascribed to the so-called “primogenic effect”, which describes the phenomenon of electronic repulsion between valence and core electrons or lack thereof depending on the presence of radial nodes in the wave functions of the d-orbitals [123, 124]. The 3d-orbitals of first row-metals such as iron are contracted as a consequence of poor shielding of the nuclear charge by the core electrons, which can primarily be attributed to there being no radial node away from the nucleus. As a result, electrostatic repulsion between the metal and ligand is increased, leading to less efficient orbital-overlap and thus weaker binding. On the other hand, the 4d-orbitals of second row-metals such as ruthenium extend further than the 4s- and 4p-orbitals, allowing for stronger metal–ligand bonds [122].



[Fe(II)(bpy)₃]₂X₂ (X = Cl or PF₆) (**8**)

The different electronic states and transitions in Ru(II)- and Fe(II)-polypyridyl complexes are illustrated in Figure 4.2 [125]. Assuming a near-octahedral geometry imposed by the *hexa*-coordinate ligand environment surrounding the metal centre, the d-orbitals are split into t_{2g} and e_g , as previously discussed, with the field strength of the ligands leading to a low-spin d^6 -configuration. The better orbital–overlap between the 4d-orbitals in Ru(II) complexes and the ligand orbitals, leads to stronger ligand field splitting and thus an increase in energy of the t_{2g} -orbitals, the HOMO, pushing them above the π^* -orbitals of the ligands, making the latter the LUMO [122]. Due to the prevalent metal-character of the HOMO and ligand-character of the LUMO, the lowest energy transition of an electron upon light-excitation is a metal-to-ligand charge-transfer (MLCT). The GS \rightarrow ES transition occurs under conservation of the spin multiplicity ($^1\text{GS} \rightarrow ^1\text{MLCT}$), but intersystem crossing (ISC)—an isoenergetic radiationless transition between two electronic states with different spin multiplicity—results in the population of the more stable $^3\text{MLCT}$, the lowest energy ES of such a complex. Consequently, the ES lifetime of the $^3\text{MLCT}$ governs the photochemical reactivity [21]. Owing to the strong ligand-field splitting in second- and third-row metals, the MC states (^3MC and ^5MC) have the same or higher energy compared to the MLCT states in the case of [Ru(bpy)₃]²⁺ (**1**)—precluding rapid, radiationless decay to the GS via these MC states—giving rise to long-lived CT states of 930 ± 40 ns in deaerated acetonitrile [62].

On the other hand, in Fe(II)-polypyridyl systems, the e_g^* -orbitals are lower in energy than the π^* -orbitals. Subsequently, complexes such as (**8**) notoriously suffer from short excited state lifetimes due to ultrafast deactivation of $^3\text{MLCT}$ ESs via low lying $^3/5\text{MC}$ states [122, 126, 127]. The resulting sub ps-lifetimes therefore limit their applicability significantly [128-130].

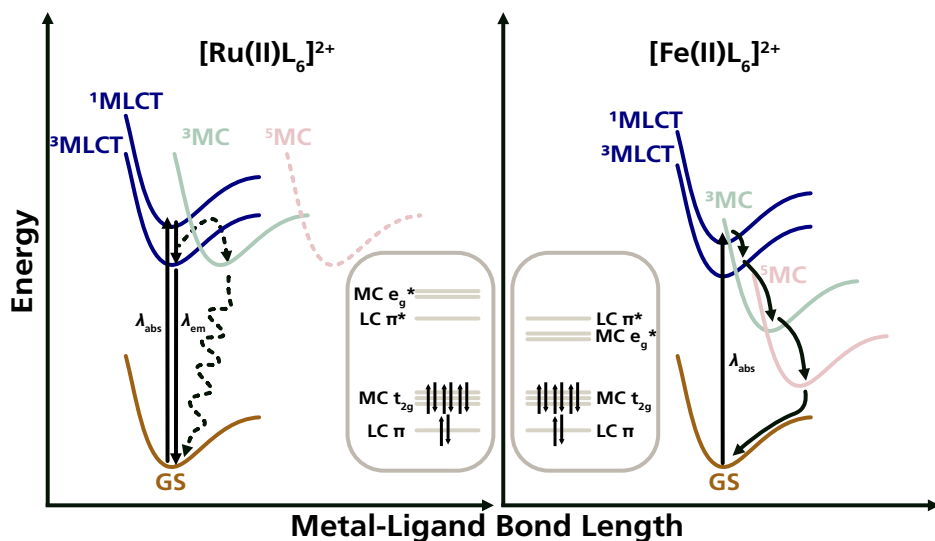


Figure 4.2: Energy levels and excited state deactivation pathways of $[\text{Ru}(\text{II})\text{L}_6]^{2+}$ (left) and $[\text{Fe}(\text{II})\text{L}_6]^{2+}$ (right) complexes. (dashed arrows: competing non-radiative deactivation pathway for which an activation barrier must be overcome) Adapted from [125] with permission. © 2016 American Chemical Society.

As a way of mitigating said issues that arise from the deactivation through low-lying MC states in Fe(II)-polypyridyl complexes, different strategies with the goal of switching the relative ordering of MC and MLCT states have been pursued [131-134]. One such approach that has led to a substantial increase in ES lifetimes for photoactive iron-complexes is based on the introduction of strongly σ -donating *N*-heterocyclic carbene (NHC) ligands [135, 136]. These prevalently destabilise the MC e_g -orbitals, which exhibit σ -symmetry, thus leading to a significant extension of $^3\text{MLCT}$ ES lifetimes [21, 125, 137]. An additional benefit of incorporating these specific NHC-motifs is the optimised geometry of the resulting complexes, more closely resembling an ideal octahedron, which further promotes ligand field splitting. For *hexa*-NHC ligands, the Fe(III/II)-redox couple is shifted to more negative values, affording the Fe(III) oxidation state under ambient conditions. With the MC states being raised in energy to lie above the ligand-centred (LC) state, these d^5 -systems are consequently excited via ligand-to-metal charge-transfer (LMCT) upon visible light absorption, corresponding to their lowest energy transition. The electronic states and transitions in Fe(II)-NHC and Fe(III)-NHC complexes are depicted in Figure 4.3.

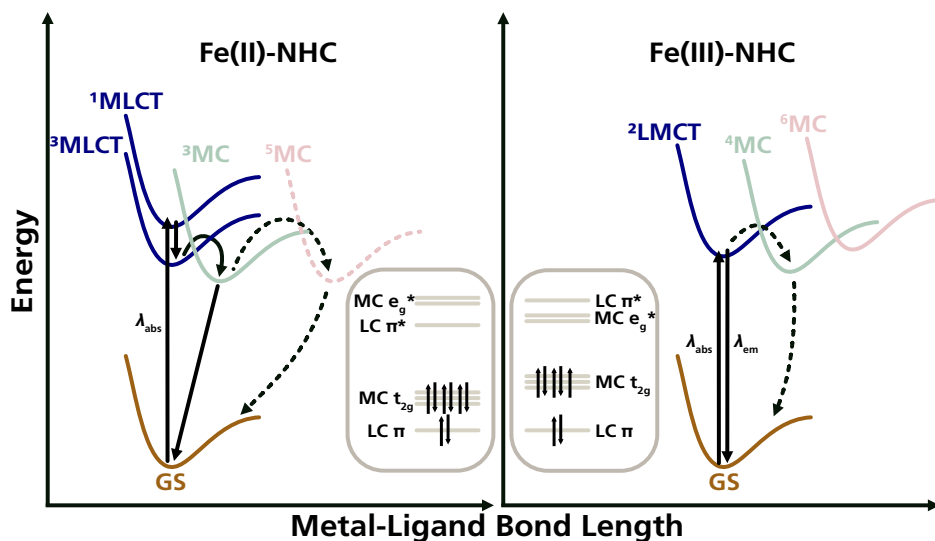
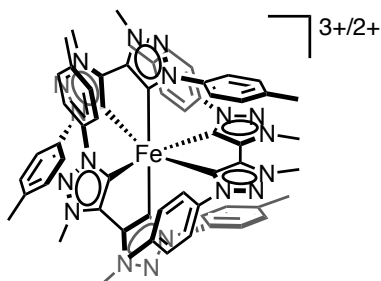
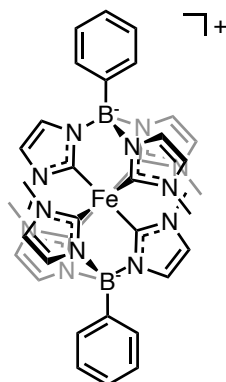


Figure 4.3: Energy levels and excited state deactivation pathways of Fe(II)-NHC (left) and Fe(III)-NHC (right) complexes (dashed arrows: competing non-radiative deactivation pathway for which an activation barrier must be overcome). Adapted from [21] and [125] with permission. © 2016 American Chemical Society.

From the series of photoactive complexes harbouring NHC-moieties that have come forth in recent years, two air-stable Fe(III) *hexa*-NHC-complexes, $[\text{Fe(III)(btz)}_3]^+$ (**9**) (btz = 3,3'-dimethyl-1,1'-bis(*p*-tolyl)-4,4'-bis(1,2,3-triazol-5-ylidene)) in 2017 [10] and $[\text{Fe(III)(phtmeimb)}_2]^+$ (phtmeimb = tris(3-methylimidazolin-2-ylidene)(phenyl)borate) (**11**) in 2019 [12], have emerged. Both had at the time of their publication unprecedented lifetimes of their respective $^2\text{LMCT}$ states—100 ps for the former and 2 ns for the latter—and exhibited room temperature photoluminescence with quantum yields of 0.03 % for (**9**) and 2 % for (**11**). Concurrently, by reduction of complex (**9**) to its Fe(II)-congener, $[\text{Fe(II)(btz)}_3]^{2+}$ (**10**), an iron-complex with a non-emissive $^3\text{MLCT}$ state featuring a lifetime of 528 ps was prepared in 2018, which was however prone to oxidation under prolonged exposure to air [11].



[Fe(III/II)(btz)₃]^{3+/2+} (**9**)/(**10**)



[Fe(III)(phtmeimb)₂]⁺ (**11**)

$\lambda_{\text{abs}}(\mathbf{9})/(\mathbf{10}) = 558 \text{ nm}/540 \text{ \& } 730 \text{ nm}$ $(\epsilon_{\text{max}} = 1.5 \times 10^3 \text{ M}^{-1}\text{cm}^{-1}/$ $5.5 \times 10^3 \text{ \& } 2.5 \times 10^3 \text{ M}^{-1}\text{cm}^{-1})$ $\lambda_{\text{em}}(\mathbf{9})/(\mathbf{10}) = 600 \text{ nm}/-$ $\tau_0(^2\text{LMCT } \mathbf{9})/^3\text{MLCT}(\mathbf{10})) = 100 \text{ ps}/528 \text{ ps}$	$\lambda_{\text{abs}} = 502 \text{ nm } (\epsilon_{\text{max}} = 3.0 \times 10^3 \text{ M}^{-1}\text{cm}^{-1})$ $\lambda_{\text{em}} = 655 \text{ nm}$ $\tau_0(^2\text{LMCT}) = 2 \text{ ns}$
--	---

The introduction of a *hexa*-NHC framework not only significantly improved photophysical but also redox properties, ultimately giving rise to the first examples of bimolecular quenching of CT states in iron complex [12, 44, 138, 139], enabling their use as photoredox catalysts [40, 44, 45, 139, 140], as well as photosensitisers in artificial photosynthesis [43]. In addition, (**11**) has been used for organic LEDs recently [141], which further highlights the more general applicability of these complexes.

An overview of the redox potentials of the different relevant states for the *hexa*-Fe-NHC complexes utilised for photocatalytic reactions in this thesis—(**9**), (**10**) as well as (**11**)—is illustrated in Figure 4.4. A more detailed discussion of the redox chemistry of the respective compounds will be given in the pertinent sections discussing their application in the following chapters.

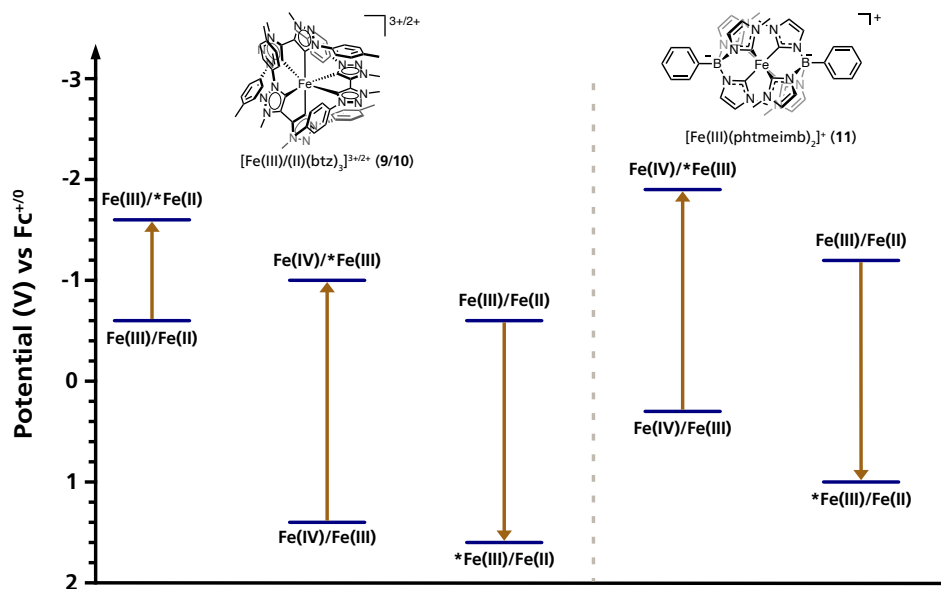


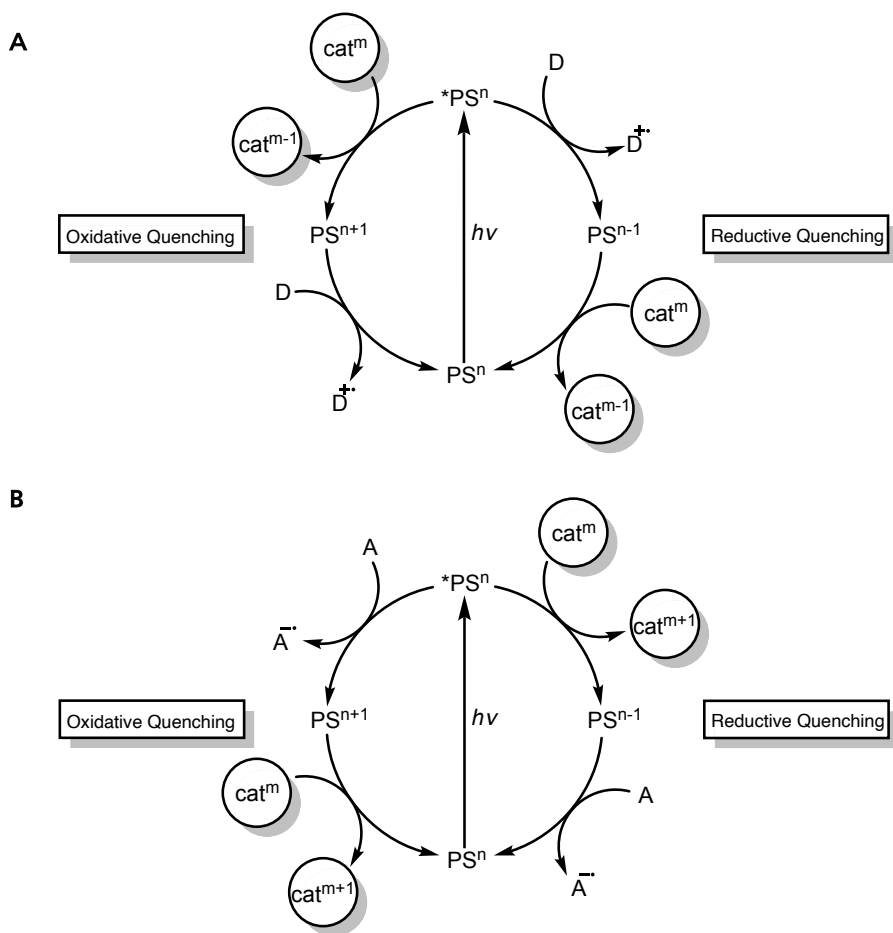
Figure 4.4: Ground and excited state potentials of $[Fe(III/II)(btz)_3]^{3+/2+}$ (**9**)/(**10**) and $[Fe(III)(phtmeimb)_2]^+$ (**11**) versus $Fc^{+/0}$. Potentials from [10-12].

5 Artificial Photosynthesis sensitised by an Fe(III)-NHC Complex

The field of artificial photosynthesis is inspired by natural photosynthesis, where sunlight is harvested and converted into chemical energy [142]. The transformation of solar energy into biomass via natural photosynthesis produces significantly more energy than humanity's annual energy consumption. While the overall efficiency of energy conversion in plants is very low (below 1%)—mainly due to the inherent energy demands related to processes such as growth—the actual photosynthesis, meaning light capture, charge-separation and water-splitting reaction, is very efficient [143-145]. Consequently, inspired by these natural processes, artificial photosynthesis has the goal of direct production of solar fuels, necessitating the efficient absorption of photons, electron transfer reactions from the ES to afford highly reactive charge-separated species as well as the storage of the captured energy by multi-electron catalysis [143, 146].

Hydrogen production is of particular interest for industrial applications, as a potential fuel source, in fertiliser production as well as oil refining [147, 148]. However, most hydrogen gas is currently being generated from natural gas, which is commonly referred to as “grey”-hydrogen [149]. The major issue with this method is the emission of substantial amounts of carbon dioxide [32]. Generating hydrogen, ideally from water, in a green and sustainable manner requires the development of carbon-free, efficient, robust and inexpensive methods is thus the focus of extensive research [32, 150-154].

Beside water splitting reactions, where hydrogen and oxygen can be produced [155], the reduction of carbon dioxide to carbon monoxide for syngas—a mixture of hydrogen and carbon monoxide used for industrial synthetic processes—as well as fuels such as formic acid, methanol, methane or low molecular weight hydrocarbons, even extending to bulk chemicals such as formaldehyde and CO₂-based polymers, is another energy-demanding process that could be driven photocatalytically, as shown by several reports [156-161].



Scheme 5.1: Photosensitisation of A) a reduction reaction and B) an oxidation reaction in artificial photosynthesis (D = (sacrificial) electron donor, A = (sacrificial) electron acceptor, cat = reduction or oxidation catalyst driving product formation in a dark reaction).

Some more general prerequisites for successful artificial photosynthesis have been discussed in Chapter 3.2 and include efficient photon absorption to access the ES of a PS and subsequent SET to obtain the charge-separated species. Part of the photocatalytic system, oftentimes an additional catalytic unit, furthermore needs to provide means of multi-electron storage to deliver the energy necessary for the desired reaction [145]. Molecular systems for artificial photosynthesis—as previously discussed—feature a PS in combination with a catalytic unit that performs the actual reduction or oxidation reaction. There, the excited PS can donate to (Scheme 5.1A) or accept an electron from (Scheme 5.1B) the catalyst, either reducing or oxidising the latter. The catalyst then goes on to effect the desired reaction in a multi-electron process that is not light-mediated, such as hydrogen or oxygen evolution from water or CO₂ reductions [33, 36, 145].

Many research efforts in this field are focused on gaining a more profound understanding of the processes of natural photosynthesis on a fundamental level by utilising simplified model systems, with their larger scale application being the long-term goal. However, to date solar fuel technologies based on artificial photosynthesis systems have not found practical application yet, partially due to their lack of efficiency and reliance on sacrificial reagents among other issues [162, 163].

5.1 Analysis of Gaseous Reaction Products

The products of artificial photosynthesis reactions are often gases, which requires the usage of appropriate analysis methods for their identification and quantification. Commonly employed techniques include gas chromatography (GC) [164], MS [165], and electrode sensors among others [166-168]. However, these methods necessitate penetration of the reaction system and sometimes removal of a sample aliquot, increasing the risk of leakage or introducing impurities. This can interfere both with the reaction progress as well as the analysis results. Additionally, bringing sensitive equipment such as electrode sensors or GC columns into direct contact with reaction components can lead to their faster deterioration.

To mitigate these issues, we employed a custom-built instrument based on rotational Raman spectroscopy for the analysis of our artificial photosynthesis reactions in a non-invasive way, while enabling the simultaneous quantification of gases such as H₂, O₂, N₂, CO₂, and CO. Raman-based gas analysis has undergone many developments in recent years [169-172] and we have been able to demonstrate the applicability of our custom-built set-up for the analysis of artificial photosynthesis [173]. The set-up used herein allows for the quantification of gases based on their back-scattering geometry and rotational Raman spectrum. The optical layout is illustrated in Figure 5.1.

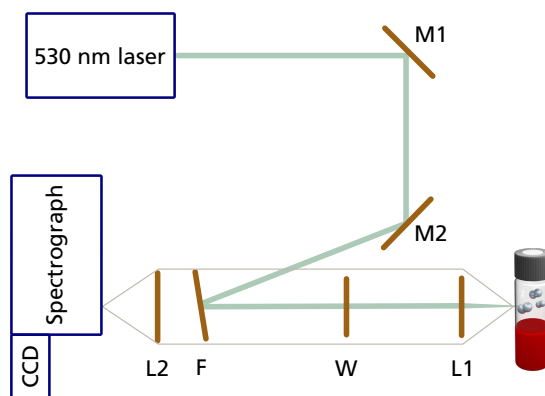


Figure 5.1: Schematic overview of the optical layout for the Raman-based gas analyser. M = mirror, L = lens, F = edge filter, W = CaF₂ window, CCD = charge couple device camera. Adapted from [173] with permission from the Royal Society of Chemistry.

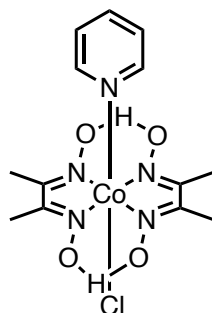
Generally, the gas content in the headspace of the vial is measured and the signal intensity of the Raman band is compared to the signal intensity of the appropriate library spectrum of the analyte gas(es), the latter of which corresponds to a nominal concentration of “100 %”. By assuming near-ideal behaviour of the analysed gases, the ideal gas law (Eq. (5.1), where p is the absolute pressure (Pa or N m⁻²), V is the volume (m³), n is the amount of substance (mol), R is the ideal gas constant (8.31441 J K⁻¹ mol⁻¹) and T is the temperature (K)) can be applied to calculate the amount of substance that was detected in the library spectrum and consequently also the amount of analyte in the investigated sample.

$$pV = nRT \quad (5.1)$$

5.2 High Turnover Hydrogen Evolution sensitised by an Fe(III)-NHC complex (Paper I)

With the growing need for increasing amounts of hydrogen, different strategies for its green production are being pursued. One such approach is based on using molecular systems for driving hydrogen evolution reactions (HERs). While a number of proton reduction catalysts (PRCs) are based on Earth-abundant metals, most PSs used for HERs feature noble metals, such as ruthenium (1) and iridium (2)/(3) [25, 27, 31, 32].

In this study, we sought to replace such complexes with a PS based on Earth-abundant iron. $[\text{Fe}(\text{III})(\text{phtmeimb})_2]^+$ (11) was chosen due to its 2 ns-lifetime, green light absorption and ability to engage in bimolecular quenching reactions of its CT state. Additionally, due to the relatively strong oxidation power (+0.97 V vs $\text{Fc}^{+/0}$, +1.37 V vs SCE) [12] of its ES, reduction to the Fe(II)-state is facile in the presence of a variety of electron donors. The resulting Fe(II)-complex (-1.16 V vs $\text{Fc}^{+/0}$, -0.77 V vs SCE) [12] can then go on to transfer an electron to a PRC to promote the HER. To this end, we investigated the photocatalytic formation of hydrogen using colloidal Pt or the cobaloxime $[\text{Co}(\text{dmgH})_2\text{pyCl}]$ (12) (dmgH = dimethylglyoximato, py = pyridine).



$[\text{Co}(\text{dmgH})_2\text{pyCl}]$ (12)

Following initial testing and optimisations, we were able to demonstrate that photocatalytic hydrogen production using Pt colloids (Table 5.1) and the Earth-abundant, homogenous PRC (12) (Table 5.2) could successfully be sensitised by the Fe(III)-NHC complex (11) at an irradiation wavelength λ_{irr} of 530 nm. The reactions were performed with a PS-concentration of 1 mM and 0.5 mM using 0.5 M Et_3N (triethylamine) and 0.377 M TEOA (triethanolamine), respectively. In all reactions, $[\text{HNEt}_3][\text{BF}_4]$ was used as a proton source.

Using these two systems, turnover numbers (TONs) of 1176 with the Pt-PRC and 1311 with (12) were obtained, constituting the first high-turnover photocatalytic HERs sensitised by an Earth-abundant iron-NHC complex under green light irradiation [174, 175].

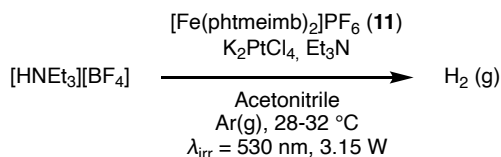


Table 5.1: HER using (11) as PS, Pt-colloids as PRC, [HNEt₃][BF₄] as proton source, and Et₃N as sacrificial reductant. (^aTON = mol H₂ / mol PRC, ^baverage of 2 replicates). Reproduced from Paper I with permission from the Royal Society of Chemistry.

Entry	[PRC] (mM)	Time (h)	H ₂ (μmol)	TON ^a	Initial TOF (h ⁻¹)
1 ^b	0.45	21	48.0	53.3	-
2	0.9	21	5.79	3.22	-
3	0.05	22	117.6	1176	129
4	0.01	20	12.2	612	68
5 ^b	0.005	17	7.12	712	-

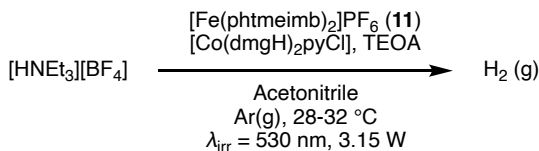


Table 5.2: HER using (11) as PS, [Co(dmgH)₂pyCl] (12) as PRC, [HNEt₃][BF₄] as proton source, and TEOA as sacrificial reductant. (^aTON = mol H₂ / mol PRC, ^baverage of 2 replicates, ^c3 mM of free dmgH₂-ligand added. ^d66 mM [HNEt₃][BF₄]. ^eDCM used as reaction solvent. ^fn.d. = no hydrogen detected.). Reproduced from Paper I with permission from the Royal Society of Chemistry.

Entry	[PRC] (mM)	Time (h)	H ₂ (μmol)	TON ^a	Initial TOF (h ⁻¹)
1	0.1	4	9	45	-
2 ^{b,c,d}	0.1	17	100	498	-
3 ^c	0.01	21	21	1024	152
4 ^c	0.005	21	13	1311	152
5 ^e	0.1	18	n.d. ^f	-	-

The comparable rates of hydrogen formation observed for the two different PRCs (6.5 μmol h⁻¹, based on Figure 5.2A & B at 3.15 W) indicated that the turnover frequencies (TOFs) were not limited by the catalysts but rather the generation of charge-separated species following excitation and quenching of the PS. This was further probed by investigating the rate of hydrogen evolution at different irradiation

intensities, revealing that the changes in TOF were approximately proportional to intensity of the illumination (Figure 5.2A & B).

Interestingly, comparison to the archetypal Ru-PS (**1**) furthermore showed that initial TOFs for this noble metal complex were significantly higher than for our Fe-NHC complex (**11**) (Figure 5.2D). However, already after one hour, hydrogen evolution had reached a plateau, presumably due to photodecomposition of the PS. Direct comparison of the photostability of (**1**) and (**11**) demonstrated that while the Ru-based complex had decomposed significantly after 14 h of irradiation, the absorption features for the Fe-complex under investigation in this study remained essentially unchanged even after 22 h (Figure 5.2C).

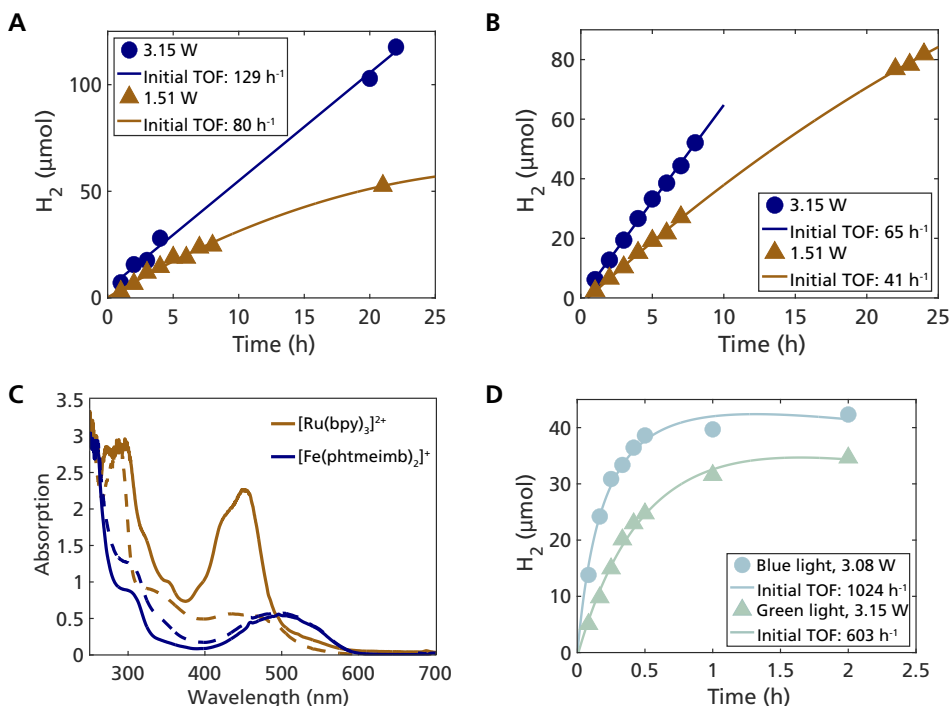
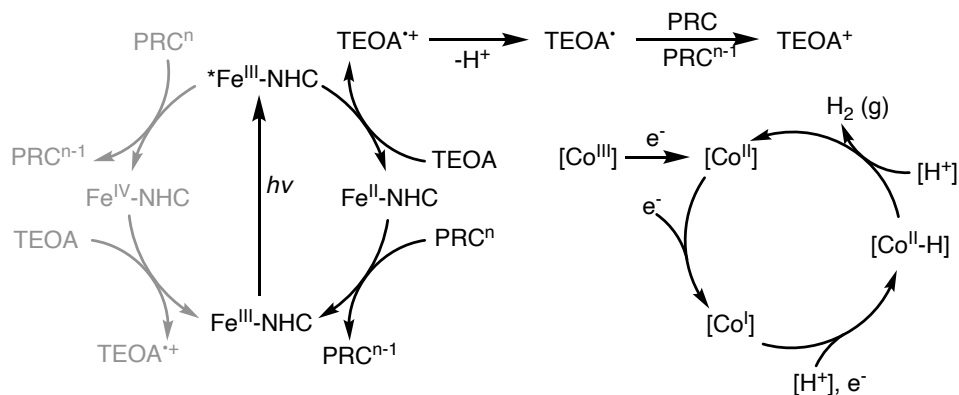


Figure 5.2: A) Time trace of the HER using PS (**11**) (1 mM), K₂PtCl₄ (0.05 mM), [HNET₃][BF₄] (165 mM), Et₃N (500 mM) in acetonitrile at 3.15 W (blue) and 1.51 W (brown) light intensity ($\lambda_{\text{irr}} = 530$ nm). B) Time trace of the HER using PS (**11**) (0.5 mM), PRC (**12**) (0.1 mM), free ligand dmgH₂ (3 mM), [HNET₃][BF₄] (165 mM), TEOA (377 mM) in acetonitrile at 3.15 W (blue) and 1.51 W (brown) light intensity ($\lambda_{\text{irr}} = 530$ nm). C) Absorption spectra of the reaction solutions for the HER with Ru-PS (**1**) (brown) and the Fe-PS (**11**) (blue), before (solid line) and after irradiation (dashed line, 14 h and 22 h respectively). D) Time trace of the HER with the Ru-PS (**1**) using green ($\lambda_{\text{irr}} = 530$ nm) and blue irradiation ($\lambda_{\text{irr}} = 455$ nm), using the same conditions as for **B**. Adapted from Paper I with permission from the Royal Society of Chemistry.

Based on the reduction potentials of the involved species, as well as Stern–Volmer quenching studies, we proposed a reaction mechanism for the Co-catalysed HER reaction sensitised by (**11**) (Scheme 5.2). There, the ²LMCT state of the Fe(III)-complex is reductively quenched by TEOA giving rise to the more reducing Fe(II)-

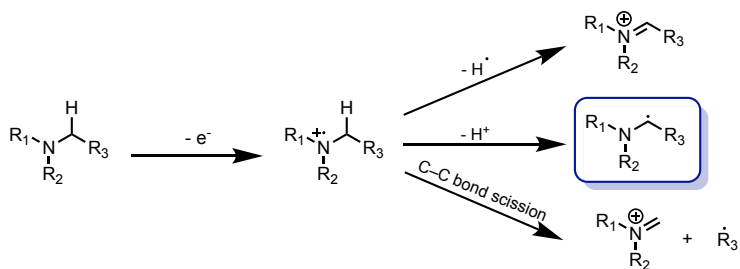
species, which can in turn transfer an electron to the PRC ($\text{Co(III)} \rightarrow \text{Co(II)}$, $E_{1/2} = -1.07 \text{ V vs Fc}^{+/0}$) [176]. Further reduction of the Co(II) - to the Co(I) -species ($E_{1/2} = -1.52 \text{ V vs Fc}^{+/0}$, -1.12 V vs SCE) [176] is however unlikely to be effected by the reduced PS ($-1.16 \text{ V vs Fc}^{+/0}$), albeit electron transfer from the Fe(II) -intermediate to regenerate the Fe(III) -GS is still required for catalytic turnover. Instead, the α -aminoalkyl radical ($E^0 = -1.4 \text{ V}$ [177] to -2.1 V [178, 179] vs $\text{Fc}^{+/0}$) generated by rapid deprotonation of the oxidised sacrificial reductant could promote the further reduction of the PRC, thus enabling the formation of hydrogen.



Scheme 5.2: Proposed mechanism of hydrogen formation using the Fe-PS (11) and PRC (12). Adapted from Paper I with permission from the Royal Society of Chemistry.

An alternative mechanism involving OQ of the ²LMCT state (Scheme 5.2, grey) is also thermodynamically feasible. In fact, oxidative quenching of the ²LMCT of (11) by (12) was observed (Table 5.3), albeit the low PRC concentration precludes a major contribution of this pathway to the overall reaction. Furthermore, no spectroscopic evidence for the formation of the resulting quenching products was obtained.

Interestingly, for PRC (12), superior results were obtained in the HER when using TEOA rather than TEA, even though k_q for the former was lower (Table 5.3). This can likely be attributed to its lower pK_a (TEOA-H^+ : 15.9, Et_3NH^+ : 18.7) [180]. CEYs for both amine quenchers were similarly low (2–3 %). The apparent necessity for α -aminoalkyl radicals to drive the $\text{Co(II)} \rightarrow \text{Co(I)}$ -reduction furthermore imposes some limitations on the HERs performed using our Fe-PS (11). Trialkylamine radical cations, such as the ones formed upon SET to the excited PS, are highly reactive intermediates and show a propensity for rapid further reaction (Scheme 5.3), including the formerly mentioned and herein desired deprotonation to yield C-centred neutral radicals, hydrogen abstraction affording an iminium ion or C–C bond scission [181–183]. The reason for these reactivity pathways is the significant weakening of the $\text{C}(\alpha)\text{-H}$ bond adjacent to the N -atom [181].



Scheme 5.3: Examples for further amine reactivity following single electron oxidation [181-183].

While it is prevalently stated in the literature that the acidity of the α -H significantly increases as a consequence of said weakening of the C–H bond, there are reports showing that the deprotonation might not be as facile as commonly assumed [184-185]. α -Aminoalkyl radicals can furthermore also undergo oxidation not just by reaction with the PRC but also other reaction components such as the Fe(III)-PS to give the corresponding iminium ion and the reduced GS of the PS, since the PS is present in higher concentrations than the PRC. This would effectively result in the strongly reducing species needed for the Co(II) \rightarrow Co(I)-step undergoing what could essentially be viewed as a side reaction. In addition, the comparatively low CEYs for the quenching of (11) by NEt₃ and TEOA in acetonitrile lead to rather inefficient formation of the amine radical cations and the subsequent α -aminoalkyl radicals. With these low efficiencies for the formation of this strong reductant needed in the reaction, aforementioned alternative reaction pathways for the amine radical cations could be of further detriment.

Table 5.3: ES Quenching data for (11) and quantum yields of the HER for Pt-colloids and Co-PRC (12) in acetonitrile solution. ^aStern–Volmer constant, ^bbimolecular quenching constant, ^cQuenching yield at given quencher concentration used for HER. ^dCEY, ^eQuantum yield for the hydrogen formation. ^fPRC: colloidal Pt, ^gPRC: (12), ^hpredominantly static quenching with a minor dynamic component ($5.4 \times 10^9 \text{ M}^{-1} \text{ s}^{-1}$). ⁱno detectable quenching products. ^jNo hydrogen formation via OQ with (12). Reproduced from Paper I with permission from the Royal Society of Chemistry.

Quencher	K_{SV} (M ⁻¹) ^a	k_q (10 ⁹ M ⁻¹ s ⁻¹) ^b	η_q ([Q]/(M)) ^c	η_{ce} ^d	ϕ_{H_2} ^e
NEt ₃	15.6	7.8	0.88 (500)	0.02	0.011 ^f
TEOA	2.62	1.3	0.51 (377)	0.03	0.013 ^g
Co-PRC (12)	114.2	– ^h	<0.01 (0.1)	– ^j	– ^j

Ideally, water would act as a proton source in the HER instead of an organic acid. However, in our case, use of water as opposed to [HNEt₃][BF₄] resulted in a significant decrease of the amount of hydrogen being produced. The obtained results essentially corresponded to hydrogen evolution in absence of any additional proton source, with protons likely originating from the amine radical cation generated by single electron

oxidation of the trialkylamine quencher. Investigation of the photostability of the PS (11) in the presence of water showed no notable degradation, but nevertheless it can be concluded that water is not a suitable proton source in the given reaction system. The reasons for this lack of reactivity might be manifold and are as of yet not fully understood, especially since cobaloxime (12) has been used for efficient hydrogen evolution from partially aqueous solutions using different PSs [186]. However, it ought to be noted that the solubility of our PS (11), featuring a PF₆-counterion, in water is poor and that upon addition of water, some precipitation of the compound can be observed, which might be a contributing factor.

5.3 CO₂-Reduction sensitised by an Fe(III)-NHC complex

Having demonstrated that Fe(III)-NHC complexes can sensitise HERs with high TONs, we set out to investigate the possibility of driving another artificial photosynthesis reaction—the reduction of carbon dioxide to carbon monoxide and other fuels—with these complexes as PS.

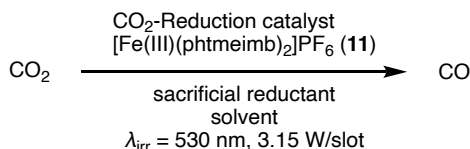
The one-electron reduction of CO₂ to CO₂^{•-} is a highly endergonic reaction (−2.14 V vs SCE) with limited product control and an overpotential of 0.1–0.6 V vs SCE being required for rapid reduction. However, proton-assisted multi-electron reduction of CO₂ has been shown to be a more attainable process ((5.2)–(5.7)) in the context of low-energy light application [156, 158, 187].



Similarly to HERs, the conversion of CO₂ imposes certain requirements on the reaction system to enable the accumulation and intermediary storage of multiple electrons. Many reported systems consist of a PS, a (sacrificial) reductant and a reduction catalyst [158, 188].

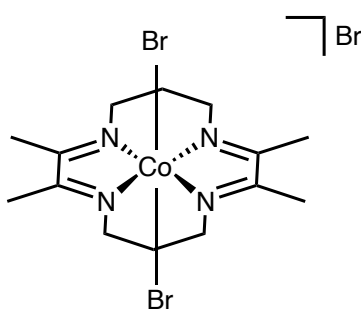
Complex (11) with its redox potentials of $E_{1/2}(\text{III/II}) = -0.53 \text{ V vs SCE}$ ($-1.16 \text{ V vs Fc}^{+/0}$), 2 ns-lifetime and demonstrated applicability in HERs, was therefore chosen as a potential Fe-NHC-based PS to sensitise a photocatalytic carbon dioxide reduction. Due

to the limited reducing power of this complex, a small range of potential catalysts can be used—particularly when not taking contributions to the reactivity from reducing degradation products of the utilised sacrificial electron donors into consideration.



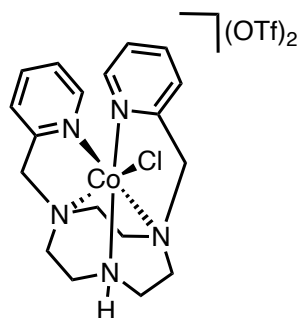
Scheme 5.4: Overview scheme for the photocatalytic CO₂-reduction sensitised by Fe(III)-NHC complex (11).

When taking into account the strong reducing power of the α -aminoalkyl radicals that are generated upon electron transfer to the PS and subsequent deprotonation, the scope of potential CO₂-reduction catalysts could potentially be broadened, akin to the HER demonstrated in Paper I. However, the catalytic efficiencies would still be expected to be rather low as CEYs for trialkylamines in acetonitrile and DMF, solvents often used for CO₂-reductions, are quite low for Fe-PS (11) [40]. However, the cobalt complexes [Co(III)(TIM)Br₂]Br (13) (TIM = 2,3,9,10-tetramethyl-1,4,8,11-tetraazacyclotetradeca-1,3,8,10-tetraene) [189] and [Co(III)L^{N3}Cl](OTf)₂ (14) (L^{N3} = 1,4-bis(pyridin-2-ylmethyl)-1,4,7-triazonane, OTf = triflate) [190] as well as the rhenium complexes *fac*-[Re(I)(bpy)(CO)₃(MeCN)]PF₆ (15) [191, 192] and *fac*-[Re(I)(bpy)(CO)₃Cl] (16) [193, 194] were tested for CO₂ reduction to CO sensitised by Fe-PS (11). These reduction catalysts exhibit demonstrated activity in conjunction with other PSs and their redox chemistry appears suited to the comparatively low reducing power of the Fe(II)-GS of complex (11) or alternatively reduction via oxidative quenching of the ES of (11) (-1.5 V vs SCE, -1.9 V vs Fc⁺⁰).



[Co(TIM)Br₂]Br (13)

($E_{1/2}(\text{III/I}) = -0.34 \text{ V vs SCE}, -0.74 \text{ V vs Fc}^{+/0}$) [189]

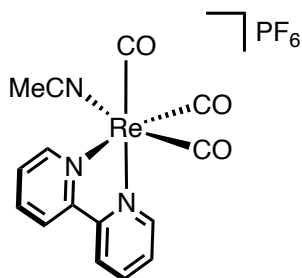


[Co(L^{N3})Cl](OTf)₂ (14)

($E_{1/2}(\text{III/II}) = -0.19 \text{ V vs SCE}, -0.59 \text{ V vs Fc}^{+/0}$) [190]

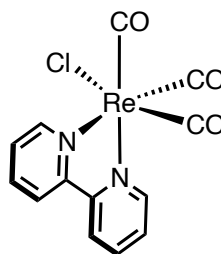
Screening of the photocatalytic activity of the Co-based reduction catalysts (13) and (14) at different concentrations using Fe(III)-NHC complex (11) as PS led to low amounts of CO being produced resulting in TONs < 1. TEA and TEOA were used as sacrificial reductants in DMF or a binary acetonitrile:methanol mixture as reaction

solvent (Table S1 & Table S2, Supporting Information). However, even with PSs that are known to produce the charge-separated photoproducts more efficiently than (11), systems featuring (13) and (14) as catalysts inherently suffer from rather low TONs. Nevertheless, they were explored here due to their redox potentials that should allow for reduction by the Fe(II)-GS of (11).



fac-[Re(bpy)(CO)₃(MeCN)]PF₆ (15)

($E_{1/2}(L/L^+) = -1.25$ V vs SCE, -1.65 V vs $Fc^{+/0}$) [195]



fac-[Re(bpy)(CO)₃Cl] (16)

($E_{1/2}(L/L^+) = -1.35$ V vs SCE, -1.75 V vs $Fc^{+/0}$) [193]

Subsequently, the Re-based catalyst (15) (Table S3, Supporting Information) was also investigated, due to its reported higher catalytic activity than the cobalt reduction catalysts used herein. An initial attempt at using (15) in the CO₂ reduction sensitised by (11) afforded a TON of 19 (Table S3, Supporting Information). However, a control experiment in the absence of the Fe-PS revealed a strong background reaction, resulting in an even higher TON of 30 (Table S3, Supporting Information). Said background reaction might originate from light-absorption of the rhenium complex, which is known to act as a photocatalyst in CO₂-reductions at lower wavelengths (<400 nm), albeit its absorptivity at the irradiation wavelength of 530 nm is very low [195]. Upon lowering the light intensity from 3.15 W per slot to 1.51 W per slot, catalytic activity was still maintained without the Fe-PS (11) present. For the CO₂ reduction catalyst (16) a similar situation was observed at 1.51 W, where the TONs in presence and in absence of the Fe(III)-NHC complex (11) were 34 and 52 respectively (Table S4, Supporting Information). Therefrom, it could be concluded that the sensitisation of the CO₂-reduction by (11) using (16) and (15) is very inefficient.

Based on the data obtained at different light intensities, it is likely that in these particular reactions, addition of Fe-PS (11) leads to absorption of photons by the PS and subsequent reductive quenching but rather ineffective further reaction with the reduction catalysts, the ESs of which can be quenched by trialkylamines themselves. Thus, while incorporating lower energy light to sensitise CO₂-reduction would be desirable, use of Fe-PS (11) provides a less efficient competitive reaction compared to direct excitation of (15) and (16), which is optimised by irradiation with higher energy wavelengths.

Consequently, our Fe(III)-NHC complex (11) has so far not been successfully employed as PS in photocatalytic CO₂-reduction reactions. In the case of the Co-based reduction catalysts (13) and (14), the overall reactivity of the system was too low, while an attempt to drive such reactions with Re-complexes (15) and (16) upon irradiation with lower energy light by sensitisation with (11) appeared to be rather inefficient as indicated by the strong background reaction in absence of the PS.

Overall, numerous other CO₂-reduction catalysts exhibiting better catalytic activity for the production of CO have been reported in literature, however their use with (11) as PS is likely precluded by the comparatively low reducing power of the associated Fe(II)-GS of our Fe(III)-NHC complex.

5.4 Conclusions

Generally, photosensitisation of artificial photosynthesis reactions is a thermodynamically challenging process due to the need for transferring and storing multiple electrons for product formation to occur. With the study presented in Paper I, we were able to show that [Fe(III)(phtmeimb)₂]⁺ (11) can be employed as a stable PS for hydrogen evolution using heterogenous, colloidal Pt-particles as well as a molecular Co-PRC (12), affording high TONs in both cases. However, the overall efficiencies of the reactions, while vastly improved from earlier reports using PSs based on Fe-NHC complexes [174, 175], were still limited by the comparatively low CEYs, resulting in inefficient formation of charge-separated species following the quenching event. While attempts at efficient photocatalytic CO₂-reduction sensitised by Fe-PS (11) have so far not been successful, with further exploration a suitable reaction system might be found to enable CO₂-reduction using an Fe-NHC-based PS as a proof-of-principle.

Improvement of the CEYs could consequently result in a more effective system, while still using an Earth-abundant PS with high photostability. To this end, different solvents and additives could be screened. However, for example the use of DCM, a solvent known to result in significantly improved CEYs for the quenching of (11) with trialkylamines [40], resulted in no hydrogen being produced. This exemplifies that the improvement of existing photocatalytic systems can pose a rather complex issue even if the limiting factors are known. Optimisation of the efficiency of a specific step does not necessarily result in higher overall efficiencies for the target reaction, as other steps leading to product formation might be negatively impacted by the changes in reaction conditions. The use of different sacrificial reductants could also be explored. For instance, oxalates have been found to rapidly decompose to CO₂^{•-} ($E^0 \approx -2.2$ V vs SCE, -2.6 V vs Fc⁺⁰), providing access to an even more reducing intermediate than α -aminoalkyl radicals, while not being prone to side reactions [183]. This might allow for

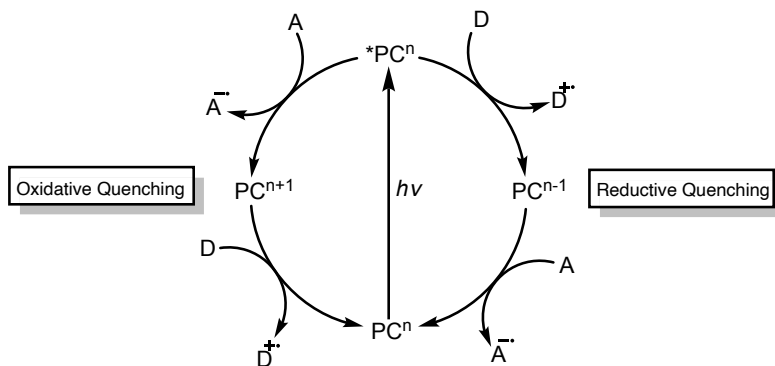
conducting reactions with even higher energy demands or using reduction catalysts that require higher reducing power thus improving the overall catalytic efficiencies.

Another approach that could prove beneficial in this case is the use of molecular dyads—system where the light-harvesting unit and the reduction catalyst are covalently linked—or catalysts consisting of a PS anchored to suitable semiconductor materials, both of which could help improve the transfer of charge carriers by mitigating some of the issues associated with diffusion-controlled electron transfer processes [196, 197].

6 Photoredox Catalysis of Organic Reactions driven by Fe-NHC Complexes

Photoredox catalysis has been widely recognised as a valuable tool for synthetic organic chemistry, thus attracting much attention and undergoing rapid growth in recent decades. It provides access to high-energy reactive intermediates that facilitate known chemical transformations and more importantly enable the development of new reactions [74]. A significant advantage of driving reactions in this way is that photons are capable of providing sufficient amounts of energy to effect the desired reactivities, whilst avoiding high temperature or other harsh conditions [198]. This results in an efficient and useful method for conducting a wide range of organic reactions [19]. Consequently, this type of chemistry has been used to accomplish and improve many reactions in organic chemistry [199-201].

Some fundamental aspects of photoredox catalysis have already been discussed in Chapter 3.2. As previously mentioned, photoredox catalysis driven by TM-based PCs is very widespread and one of the main focal points of the work presented in this thesis. It is commonly reliant on the RQ or OQ of MLCT and, albeit less frequently featured, LMCT states by donor or acceptor molecules, which can be sacrificial in nature as well as substrates or reactants. This provides an increased thermodynamic driving force for the reaction to proceed by giving access to a GS in a different oxidation state [19]. An overview of the general steps of a photoredox catalytic reaction is again given in Scheme 6.1.



Scheme 6.1: General mechanism of photoredox catalysis via outer-sphere SET (D = (sacrificial) electron donor, A = (sacrificial) electron acceptor).

Both organic dyes and TM complexes have been used for organic transformations, albeit the latter have been more prevalent [19, 28, 35, 202]. Photoredox catalysis driven by iron-PCs has gained increasing amounts of interest, particularly in recent years [72, 203]. As a result of the inherent limitations photoactive complexes based on iron generally exhibit, different strategies for conducting photoredox catalysis using iron have been pursued—namely outer-sphere electron transfer from MC states, inner-sphere electron transfer and outer-sphere electron transfer from CT states (Figure 6.1).

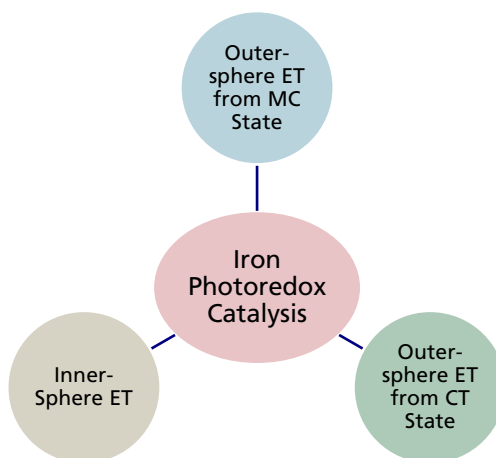


Figure 6.1: Three general approaches to iron photoredox catalysis.

As mentioned in Chapter 4, Fe(II)-polypyridyl complexes for instance, which constitute structural analogues of the prolific Ru(II)-polypyridyl PCs, harbouring the same number of valence electrons as the latter, suffer from rapid decay of the $^3\text{MLCT}$ state to lower-lying MC states. Consequently, electron transfer from Fe(II)-polypyridyl complexes is proposed to occur from the ^5MC state as opposed to the CT state, due to

the significantly longer lifetime of the former [204]. Examples of photocatalytic reactions proposed to be driven by electron transfer from aforementioned MC states include a small range of synthetically useful reactions [205-207]. This type of reactivity is however still limited by the less favourable redox chemistry of the MC states compared to the CT states.

A strategy to mitigate issues originating from short ES lifetimes is to use inner-sphere SET between an iron centre and a substrate that coordinates to the metal in situ during the reaction [208-210]. The resulting complex is excited upon irradiation and the SET leads to cleavage of the Fe–substrate bond generating a highly reactive radical intermediate—a process commonly referred to as visible light-induced homolysis (VLIH) [209, 211]. While harbouring advantages such as the inexpensiveness of the utilised iron compounds, usually iron salts, as well as proposed chemo- and site selectivity, this strategy exhibits limitations in terms of reaction types that can be performed.

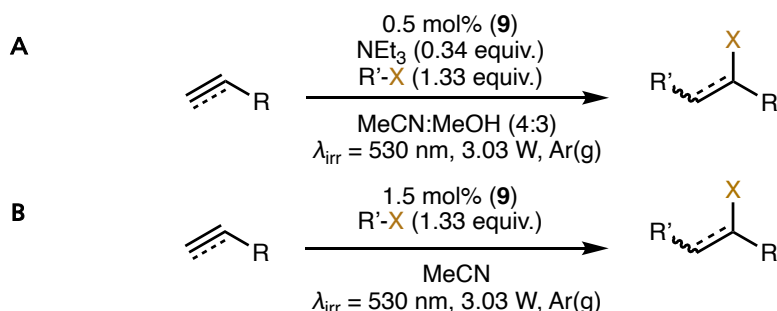
Therefore, outer-sphere SET from CT states in iron complexes to drive photoredox catalysis in a fashion akin to traditional PCs based on noble metals remains desirable and can be achieved by extending the ES lifetime of the CT state [106, 134, 137]. However, to date there are few examples of photoredox catalysis driven by complexes based on Earth-abundant iron, utilising bimolecular quenching of their CT states [40, 44, 45, 139, 140]. As a result, iron complexes harbouring strongly σ -donating NHC-ligands and thus prolonged lifetimes of their CT (Chapter 4), have been subject to investigations into their applicability, not just as PSs for artificial photosynthesis reactions as described in Chapter 5, but also PCs for organic reactions. Troian-Gautier and co-workers investigated the use of $[\text{Fe(III)(phtmeimb)}_2]^+$ (**11**) as PC for a dehalogenation reaction, which was published in 2021 [40], where they highlighted the impact of solvent variation on the CEY of the charge-separated photoproducts generated upon reductive quenching of (**11**) with different amines. Further examples for the use of (**11**) in photoredox catalysis have emerged since [45, 140].

In addition to that, concomitantly with our own study on the visible light-mediated Atom Transfer Radical Addition (ATRA) reaction catalysed by $[\text{Fe(III)(btz)}_3]^{3+}$ (**9**) (Paper II, see below), Kang and co-workers demonstrated radical cationic [4+2]-cycloaddition reactions catalysed by the same PC in 2022 [139].

6.1 A Z-Scheme-type Mechanism as a Tool for Iron Photoredox Catalysis (Paper II)

Atom transfer radical addition (ATRA) reactions are considered a rather simple and versatile tool in synthetic organic chemistry and are often used for the 1,2-bifunctionalisation of alkenes and alkynes by cleavage and subsequent addition of alkyl halides [212]. Photoredox catalysis provides a method of conducting ATRA reactions under comparatively mild conditions resulting in them becoming the subject of numerous studies, and to be regarded as benchmark reactions in the field [19, 213-216].

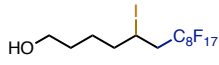
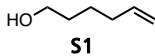
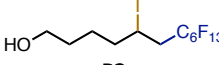
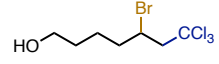
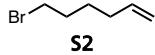
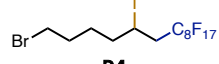
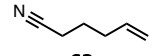
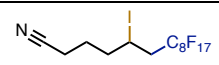
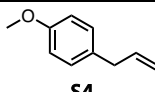
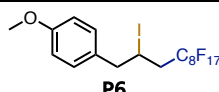
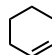
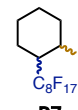
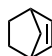
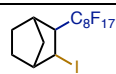
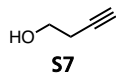
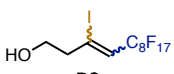
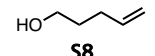
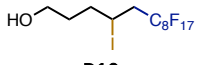
Here, we investigated the possibility of using $[\text{Fe}(\text{III})(\text{btz})_3](\text{PF}_6)_3$ (**9**) as photoredox catalyst in an organic reaction, due to its previously reported $^2\text{LMCT}$ state lifetime of 100 ps in acetonitrile and relatively strong absorption of visible light [10]. Interestingly, the Fe(II)-congener of this complex, $[\text{Fe}(\text{II})(\text{btz})_3](\text{PF}_6)_2$ (**10**), also has a long-lived CT state, a $^3\text{MLCT}$ of 528 ps in acetonitrile, and exhibits an absorption band in the green light region [11]. The potential photocatalytic activity of (**9**) was explored in ATRA reactions, where we were able to effect the desired transformation—the addition of (perfluoro)alkyl halides to alkenes and alkynes—both via reductive as well as oxidative quenching of the ES of (**9**) using green light irradiation ($\lambda_{\text{irr}} = 530 \text{ nm}$). Following optimisations, reliable procedures for both routes were found (Scheme 6.2A & B). In the case of the RQ route, NEt_3 was used as sacrificial reductant.

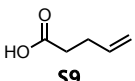
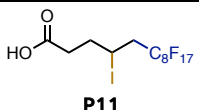
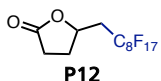
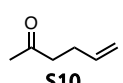
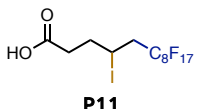
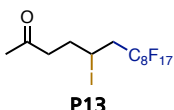
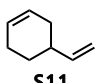
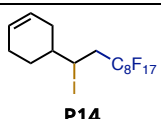
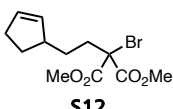
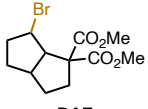
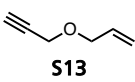
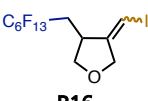


Scheme 6.2: Optimised reaction conditions for the visible light-mediated ATRA reaction via A) reductive and B) oxidative quenching of PC (**9**). Adapted from Paper II with permission from the Royal Society of Chemistry.

The wider applicability of our protocols was then demonstrated on a range of alkene/alkyne substrates to which perfluoroalkyl iodides and CBrCl_3 (Table 6.1) were added. For both the RQ and the OQ route, prevalently good to excellent yields were obtained, with catalytic efficiencies being comparable to reactions driven by $[\text{Ru}(\text{II})(\text{bpy})_3]^{2+}$ (**1**) [214], here under green light irradiation.

Table 6.1: Scope of the visible light-mediated ATRA reaction through reductive (RQ) and oxidative (OQ) quenching of (**9**). ^aRQ: 0.5 mol% (**9**), NEt₃ (0.34 equiv.), R-X (1.33 equiv.), 4:3 MeCN:MeOH. OQ: 1.5 mol% (**9**), R-X (1.33 equiv.), MeCN. ^bIsolated Yield after silica column chromatography. ^cIntramolecular reaction without an external halide source. Adapted from Paper II with permission from the Royal Society of Chemistry.

Entry	Substrate	Route ^a	Time (min)	Product	Yield (%) ^b
1		RQ	10		91
		OQ	40	P1	92
2		RQ	10		93
		OQ	40	P2	93
3		RQ	60		43
		OQ	40	P3	35
4		RQ	10		90
		OQ	40	P4	94
5		RQ	40		76
		OQ	40	P5	57
6		RQ	40		58
		OQ	80	P6	74
7		RQ	15		22 (<i>cis:trans</i> 17:5)
		OQ	40	P7	32 (<i>cis:trans</i> 25:7)
8		RQ	15		80
		OQ	40	P8	91
9		RQ	20		62 (<i>E:Z</i> 42:20)
		OQ	80	P9	81 (<i>E:Z</i> 65:16)
10		RQ	10		93
		OQ	40	P10	89

11	 S9	RQ	30	 P11	43
				 P12	26
12	 S10	OQ	40	 P11	87
		RQ	15	 P13	98
		OQ	40		97
13	 S11	RQ	30	 P14	63
14 ^c	 S12	RQ	45	 P15	49
		OQ	40		31
15	 S13	RQ	150	 P16	51 (<i>E:Z</i> 25:26)
		OQ	150		49 (<i>E:Z</i> 25:24)

The scope of substrates was chosen to feature terminal and internal double bonds as well as a range of functional groups, including carbonyl- and nitrile-functionalities, halides and hydroxy groups, all of which could gratifyingly be transformed. Furthermore, an intramolecular ATRA reaction featuring a C–Br- instead of a C–I-bond cleavage was demonstrated. However, using the given protocol, the addition of perfluorooctyl iodide, C₈F₁₇I, to Michael acceptors was not possible, highlighting also the limitations of our system.

Following the successful use of (9) as PC despite its comparatively short ES lifetime, we sought to elucidate the mechanisms operating in the two different reaction routes. As the ground state of the Fe(II)-complex (10), generated by reductive quenching of the ²LMCT state, is a relatively weak reductant, we hypothesised that (10) is in turn also excited, upon which its ³MLCT state can be oxidatively quenched by the (perfluoro)alkyl halide, ultimately leading to product formation (Scheme 6.3). In order to probe for the involvement of two consecutive ESs rather than conventional single photon excitation, two solutions containing (9), NEt₃ and 5-hexen-1-ol (S1) in

acetonitrile:methanol (4:3) were irradiated at 525 nm, leading to the in situ formation of (10), as indicated by the change in colour and the absorption spectra of the solutions (Figure 6.2, A → B). C₈F₁₇I was added to both samples after which one was stored in the dark for one hour, while the other was irradiated at 700 nm—a wavelength where (10) exhibits an absorption band, but (9) does not, therefore precluding formation of the ES state (*9)—for the same amount of time. In the case of single photon excitation, the GS of (10) would reduce the perfluoroalkyl halide. However, no conversion to the desired product was observed for the sample stored in the dark, due to (10) not being sufficiently reducing (−0.58 V vs Fc⁺⁰) (Figure 6.2, B → D). Meanwhile, upon irradiation of the solution containing (10) and the other reaction components, product formation was observed (Figure 6.2, B → C) along with restoration of the GS of (9). This strongly suggested that consecutive photo-induced electron transfer (conPET) is required for the ATRA reactions investigated herein to be driven via RQ of (9), meaning that two sequential ESs partake in SET reactions within one catalytic turnover [217-220]. Since no further reaction could subsequently take place under irradiation at 700 nm due to the lack of absorptivity of (9) at that wavelength, the observed product formation of 5 % obtained during a “single turnover” indicated that an underlying chain propagation mechanism is likely to be operative. Further support for this was provided by determining the quantum yield of the overall reaction ($\Phi = 6$) via chemical actinometry using a method by Pitre et al. [221].

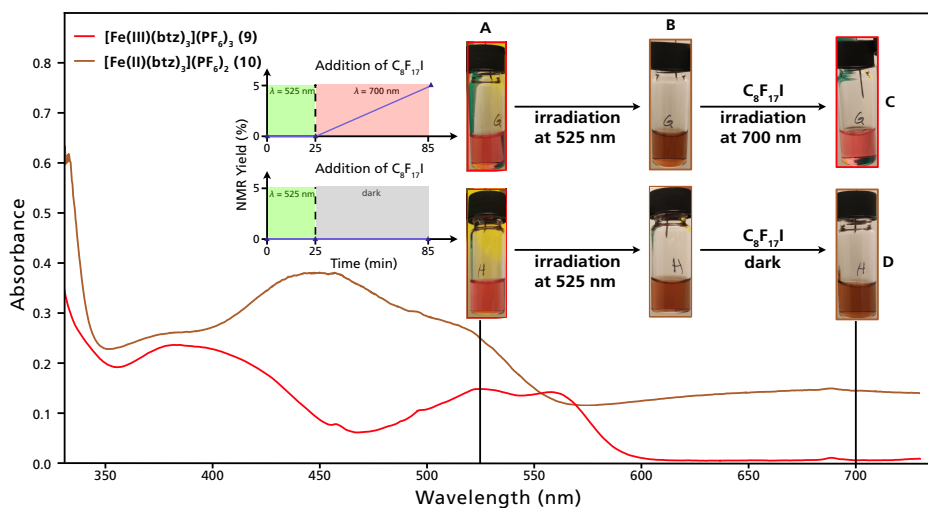
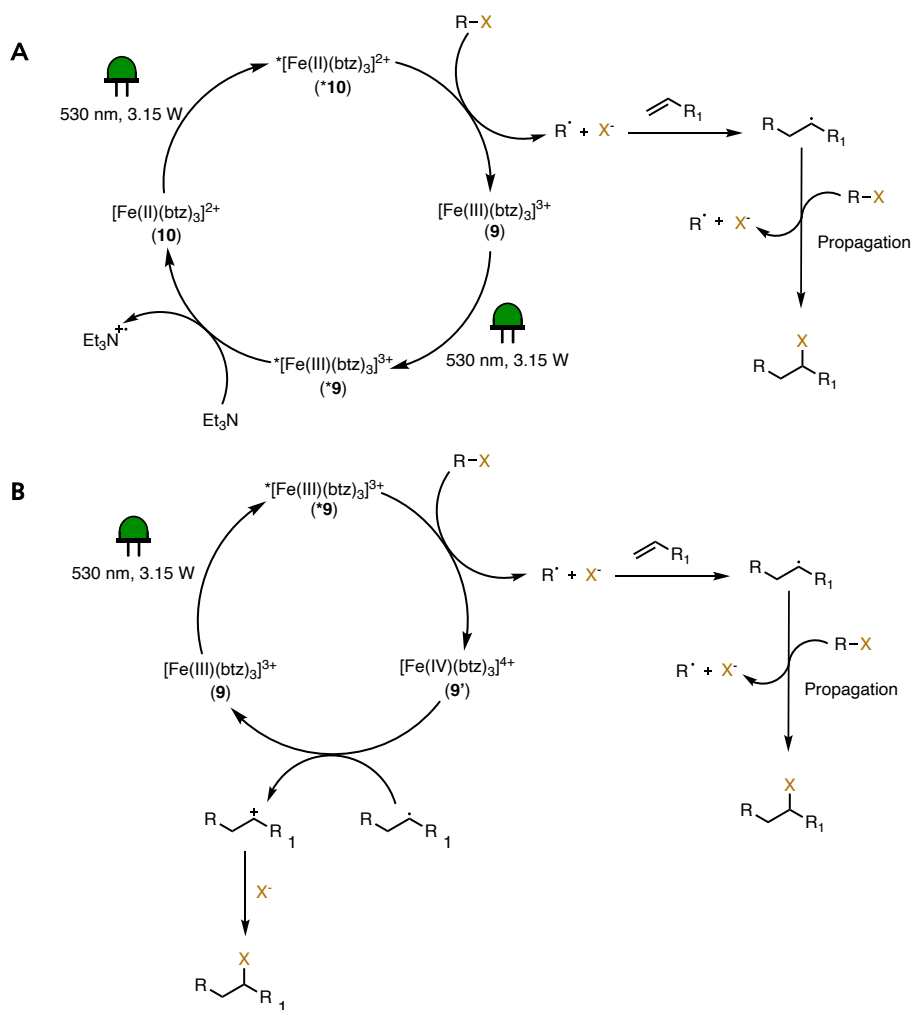


Figure 6.2: Wavelength-switching experiment to probe for the involvement of consecutive photo-induced electron transfer (conPET) in the ATRA reaction via RQ of (9). (A) A solution containing (9) (0.357 mM), 5-hexen-1-ol (S1) (71.4 mM), NEt₃ (23.6 mM) & mesitylene (15 μL, internal standard) in acetonitrile:methanol (4:3) was irradiated at 525 nm for 25 min; absorption spectrum of the reaction solution prior to irradiation (red line). (B) Absorption spectrum of the reaction solution containing in situ generated (10) (brown line). (C) Reaction solution after addition of C₈F₁₇I (95 mM) and irradiation at 700 nm for 60 min; 5 % NMR yield of product (P1). (D) Reaction solution after addition of C₈F₁₇I (95 mM) and storing in the dark for 1 h; no formation of (P1). Adapted from Paper II with permission from the Royal Society of Chemistry.



Scheme 6.3: A) Proposed reaction mechanism for the visible light-mediated ATRA reaction via reductive quenching of the excited state of (9). B) Proposed reaction mechanism for the visible light-mediated ATRA reaction via oxidative quenching of the excited state of (9). Adapted from Paper II with permission from the Royal Society of Chemistry.

Based on these insights, we proposed the mechanism shown in Scheme 6.3A for the visible light-mediated ATRA reaction driven by RQ of Fe(III)-complex (9). This mechanistic proposal was further supported by Stern–Volmer quenching studies and TA spectroscopy showing that RQ of the excited Fe(III)-complex (*9) by the sacrificial reductant NEt_3 and oxidative quenching of its excited Fe(II)-congener (*10) by $\text{C}_8\text{F}_{17}\text{I}$ occur with CEYs of 29 % and above 30 % respectively.

Alternatively, for the proposed OQ route driven by single photon excitation (Scheme 6.3B), SET from the ES of (9) to C₈F₁₇I is possible in acetonitrile as solvent if the use of a sacrificial reductant is omitted, although with a CEY of below 15 %. The thusly formed oxidised PS, formally denoted as [Fe(IV)(btz)₃]⁴⁺ (9^o), could not be spectroscopically identified and could also correspond to [Fe(III)(btz)₂(btz⁺)]⁴⁺, which is the product of single electron oxidation of one of the ligands instead [10]. In this route, chain propagation is also proposed to be operative based on the quantum yield Φ of 5 for the formation of ATRA product per absorbed photon.

With this study, we were able to demonstrate that even Fe-NHC complexes with sub-ns lifetimes of their CT ESs—and as such significantly shorter than conventional lifetimes in the ns– μ s range—can be utilised for efficient photoredox catalysis of organic transformations as long as the rates of bimolecular quenching and CEYs are high enough to generate sufficient amounts of charge-separated species to effect the desired reaction. Interestingly, compared to CEYs obtained for RQ of [Fe(III)(phtmeimb)₂]⁺ (11) by NEt₃ in acetonitrile [40, 43], cage escape of [Fe(II)(btz)₃]²⁺ (10) and the oxidised amine following RQ is significantly more efficient.

In the RQ route, the energy of two photons was utilised within the same catalytic cycle—a mechanism that somewhat resembles the Z-scheme in natural and artificial photosynthesis—thus achieving higher reactivity and enabling a reaction that would not be attainable under traditional single photon excitation-based photoredox catalysis using (9) as PC. Previous examples of applications of such a two-photon mechanism in photoredox catalysis of organic reactions using metal complexes are very scarce [222, 223]. Additionally, OQ could be employed to drive the same scope of ATRA reactions in a conventional single photon excitation mechanism whilst omitting the use of a sacrificial reagent—albeit, slightly higher catalyst loading and longer reaction times were required.

6.2 Visible Light-Induced Generation of α -Aminoalkyl Radicals as Reactive Intermediates (Paper III)

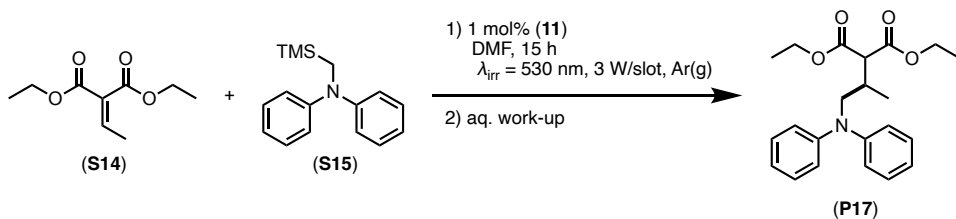
As previously touched upon, alkylamines are widely used as sacrificial electron donors for photocatalytic applications [162]. However beyond this, they can serve as precursors to valuable synthetic building blocks, due to the reaction intermediates formed from the amine radical cations afforded upon their photo-induced single electron oxidation, something which has already been discussed in Chapter 5.2.

These intermediates—namely iminium ions and α -aminoalkyl radicals—can be utilised for the formation of C–C bonds, enabling the rapid functionalisation and thus generation of structurally complex amines in a single step-reaction. However, α -aminoalkyl radicals in particular remain somewhat underexplored as building blocks in organic synthesis, which can be attributed to their proneness towards undergoing further oxidation to iminium ions when generated under thermal conditions [181, 224, 225]. Photoredox catalysis provides a method of generating α -aminoalkyl radicals under milder conditions, mitigating issues of undesired side reactions occurring. The formation of said radicals usually occurs through deprotonation of an α -C(sp³) in the amine radical cation, but can also be obtained via homolytic cleavage of the α -C–H bond by a hydrogen atom transfer catalyst [226, 227].

However, the deprotonation of the amine radical cation might not be as facile as generally assumed and issues due to potential lack of regioselectivity in presence of multiple α -C(sp³) atoms might arise. Therefore, the incorporation of substituents that would lead to more selective bond fragmentation, such as trialkylsilyl-moieties, has been explored to generate the desired nucleophilic radicals [228, 229]. α -Trialkylsilylamines additionally provide the advantage of being more easily oxidised ($E_{\text{ox}} \leq +0.4$ V vs Fc^{+/0}) than analogous regular amines, thereby facilitating electron transfer to the PC [228]. They are also synthetically readily obtained by silylalkylation of the corresponding primary or secondary amine [230]. Consequently, a number of reports describing the usage of α -trialkylsilylamines as precursors to α -aminoalkyl radicals, generated by either organic or noble metal PCs, have emerged [224, 229-239].

Here, we set out to investigate the generation and utilisation of α -aminoalkyl radicals by visible light photoredox catalysis using [Fe(III)(phtmeimb)₂]PF₆ (**11**) as PC. The choice of PC was rationalised by the 2 ns-lifetime of the ²LMCT state of said complex, its capacity to act as a suitable photooxidant (+0.97 V vs Fc) as well as proven ability to engage in diffusion-controlled bimolecular quenching processes with amines as electron donors [12, 40, 138]. Said α -aminoalkyl radicals were trapped by electron-deficient alkenes, such as Michael acceptors, giving rise to a high degree of functionalisation within one reaction step.

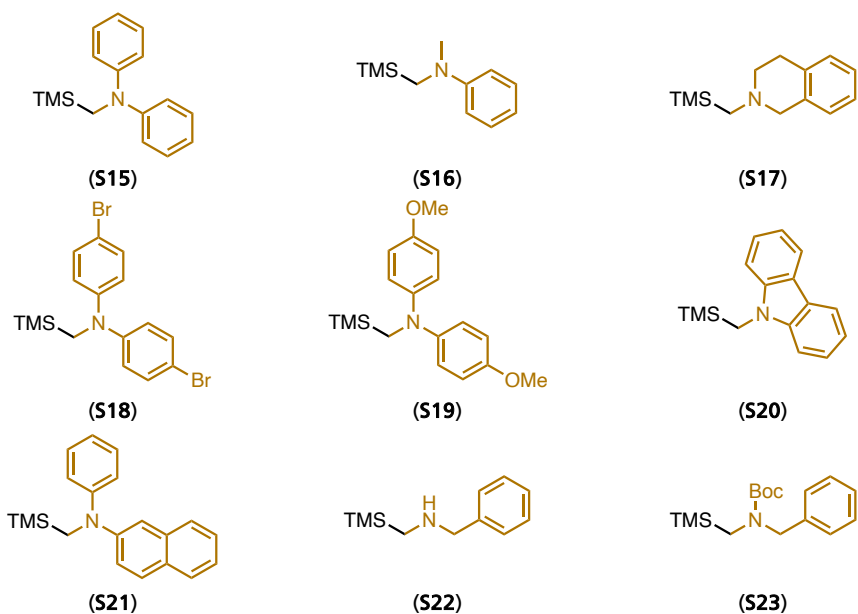
The activity of our PC (**11**) was probed using the highly electrophilic Michael acceptor diethyl ethylidenemalonate (**S14**) and *N*-phenyl-*N*-((trimethylsilyl)methyl)aniline (**S15**) as model substrates, utilising green light irradiation (530 nm). Optimisation of the reaction conditions gave rise to a reliable protocol by which the desired product (**P17**) was afforded in quantitative yield (92 % NMR yield after aqueous work-up) in 15 h with a PC-loading of 1 mol% and equimolar amounts of the two starting materials (**S14**) and (**S15**) using DMF as reaction solvent. When enones such as (**S14**) are used for the trapping of the α -aminoalkyl radical obtained from an α -trialkylsilylamine, formation of the corresponding silyl enol ether can ensue [224]. However, due to the aqueous work-up conducted in the course of product isolation, said silyl enol ethers are hydrolysed, affording the desired products. Control experiments using FeBr₂ and [Fe(II)(bpy)₃](PF₆)₂ (**8**) gave no product, while use of [Fe(III)(btz)₃](PF₆)₃ (**9**) afforded only 12 % of (**P17**). Interestingly, under the reaction conditions employed here whilst using blue light irradiation (450 nm), application of [Ru(II)(bpy)₃]²⁺ (**1**) as PC gave rise to only 64 % (NMR yield after aqueous work-up) of (**3a**), which was ascribed to its propensity to undergo rapid photodegradation.



Scheme 6.4: Visible light-driven aminomethylation of diethyl ethylidenemalonate (**S14**) with *N*-phenyl-*N*-((trimethylsilyl)methyl)aniline (**S15**) catalysed by (**11**). Adapted from Paper III.

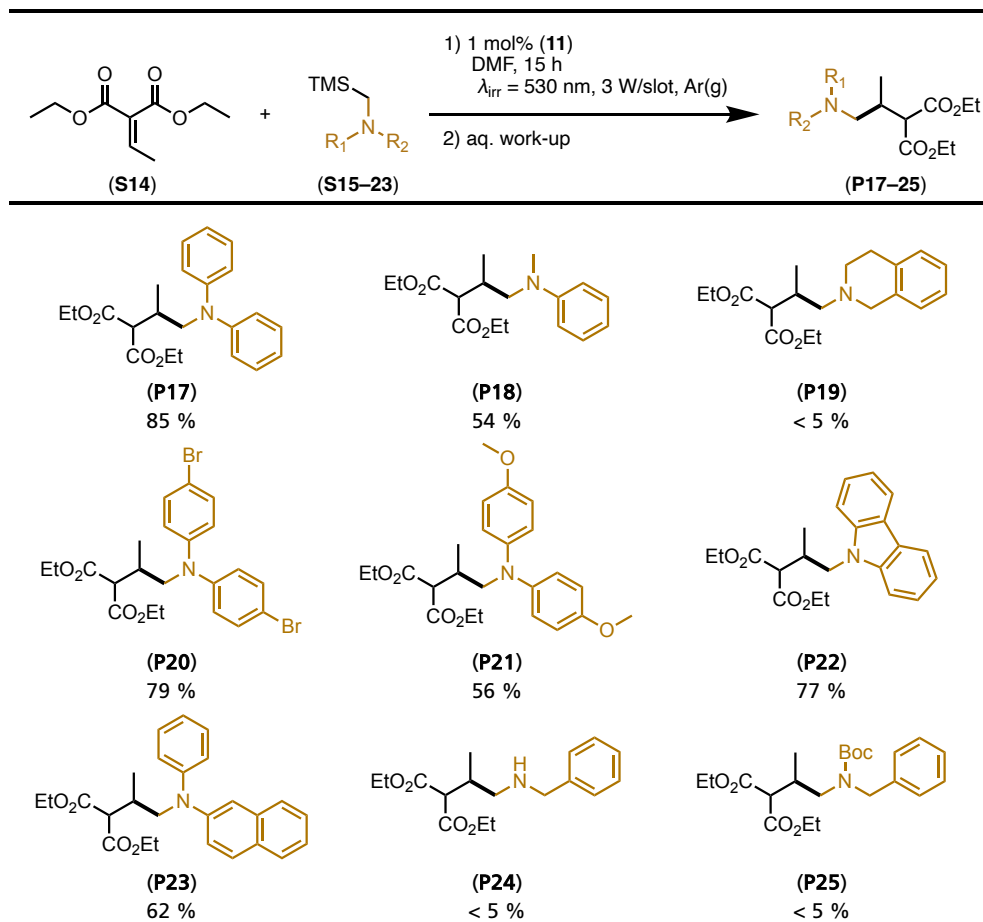
Table 6.2 provides an overview of the α -trimethylsilyl(TMS)amines used as precursors for the generation of α -aminoalkyl radicals in this study, all of which were obtained by facile silylalkylation of commercially available primary or secondary amines. These substrates feature different aromatic and/or aliphatic *N*-substituents as well as a secondary amine, to explore potential limitations of our protocol.

Table 6.2: Overview of the α -trimethylsilylamines investigated in this study.



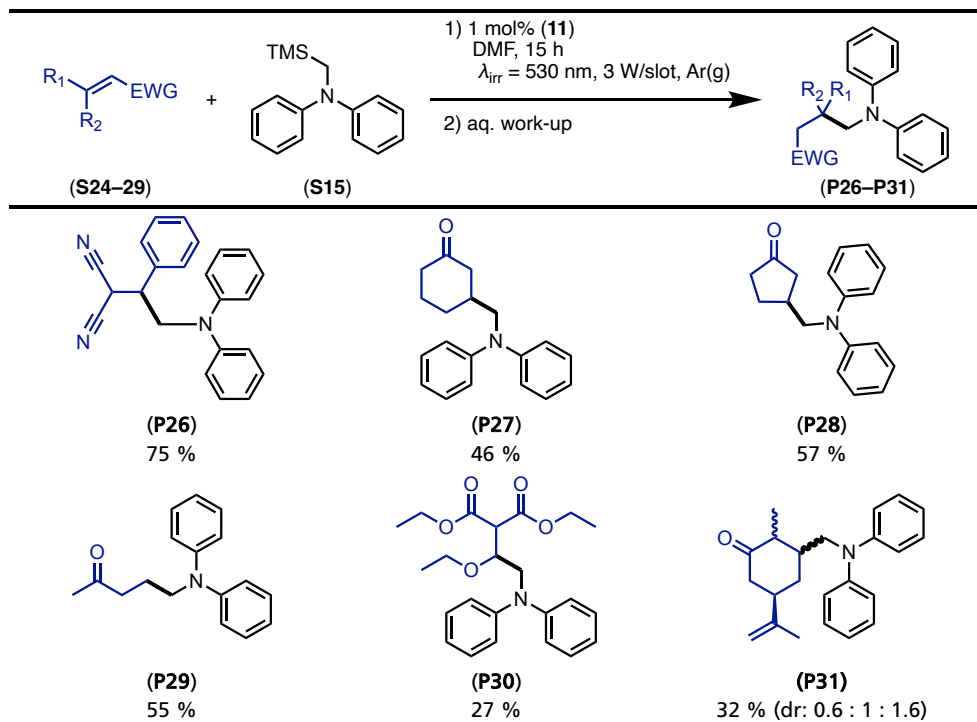
The applicability of our protocol to said α -trimethylsilylamines (Table 6.3) as well as to a range of electron-poor alkenes (Table 6.4) was subsequently explored. Thus, we were able to demonstrate that aromatic amines (**S15**, **S18–21**) afforded the desired products of their reaction with (**S14**) in fair to good yields. However, aliphatic amine (**S17**), gave the corresponding product (**P19**) only in trace amounts, as observed by LC–MS, despite attempts at further optimising the reaction conditions for this specific reaction. Such lack of reactivity has been encountered in some other studies as well and can likely be ascribed to undesired side reactions such as protodesilylation. The latter leads to premature deactivation of the highly reactive α -aminoalkyl radical [237], assuming that the SET from (**S17**) to (**11**) occurs with sufficient efficiency. This is further in line with the results obtained using (**S16**), which harbours one aliphatic and one aromatic *N*-substituent, where the desired product (**P18**) was afforded in 54 % yield, which is lower than the yield for (**P17**). We also tested the compatibility of our reaction system with a secondary amine (**S22**), as well as its Boc-protected analogue (**S23**), neither of which resulted in product formation. This lack of reactivity was attributed to the comparatively more challenging oxidation of secondary amines and carbamates [240].

Table 6.3: Scope and isolated yields for the visible light-mediated aminomethylation of (**S14**) by different α -trimethylsilylamines using the optimised conditions. Adapted from Paper III.

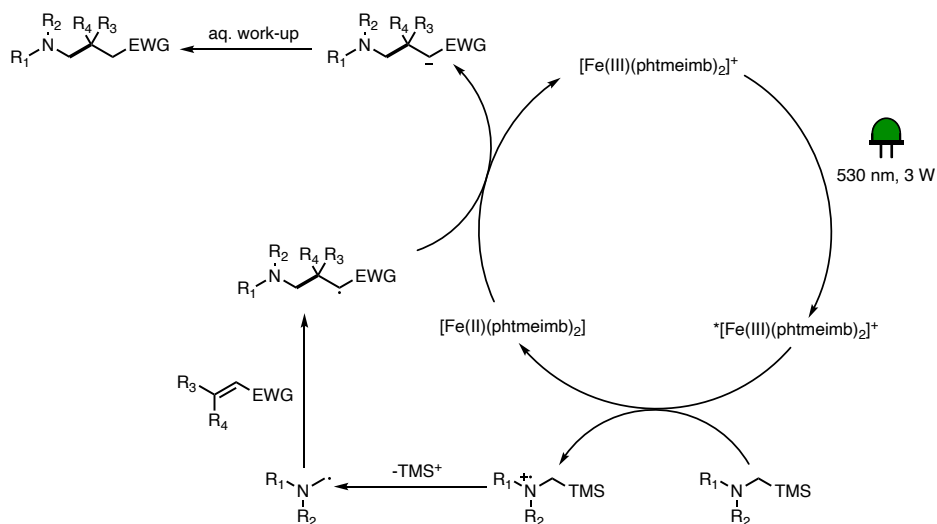


Additionally, different electron-deficient alkenes were also screened in reactions with the most reactive α -trimethylsilylamine (**S15**) (Table 6.4). As expected, the more electrophilic substrate benzylidene malononitrile (**S24**) afforded the product (**P26**) in good yield of 75 %, while the reaction products (**P27–29**) were obtained in slightly lower yields (45–57 %). Introduction of additional electron-donating substituents such as for (**S28**), which is otherwise structurally similar to the model substrate (**S14**), expectedly resulted in a rather low yield of 27 %. Use of *R*-(-)-carvone (**S29**) as substrate furthermore gave a mixture of three diastereomers (**P31**) with a combined yield of 32 %, which demonstrated good regioselectivity for electrophilic double bonds as addition to the terminal nucleophilic double bond did not occur. The lower yield of this reaction compared to (**P27**) can be rationalised by the increase in steric bulk going from (**S25**) to (**S29**).

Table 6.4: Scope and isolated yields for the visible light-mediated aminomethylations of different electron-deficient alkenes by **(1a)** under the optimised conditions. Adapted from Paper III.



We proposed that the reaction for the addition of α -aminoalkyl radicals to electron-deficient alkenes catalysed by Fe(III)-NHC complex **(11)** followed the mechanism presented in Scheme 6.5. There, we invoke the single electron oxidation of the α -trimethylsilylamine by the ES of our PC, which should be thermodynamically feasible based on the redox potentials of the involved species and the fact that the 2 LMCT state of **(11)** has been shown to be sufficiently long-lived to allow for diffusion-controlled bimolecular quenching processes. Said quenching event would consequently afford the Fe(II)-GS and the amine radical cation, the latter of which forms the desired α -aminoalkyl radical upon desilylation. Trapping of the α -aminoalkyl radical by the electron-poor alkene and subsequent reduction of the resulting newly formed radical-adduct would give rise to the desired product and furthermore restore the original Fe(III)-GS, allowing for the reaction to proceed in a catalytic fashion.



Scheme 6.5: Proposed reaction mechanism for the photocatalytic aminomethylation of electron-deficient alkenes using reductive quenching of the excited state of (11). Reprinted from Paper III.

We consequently set out to investigate the first proposed step of the catalytic reaction—the SET from the α -trimethylsilylamine to the ES of (11). Steady-state emission quenching studies for ES reaction of (11) with three different α -trimethylsilylamines (S15–17) in DMF were therefore performed (Figure 6.3, left column). In all three cases, appreciable emission quenching was observed, while ES reactions between our PC and the Michael acceptor used in the model reaction (S14) could be excluded. For (S15) and (S16), the Stern–Volmer plot exhibited an upward curvature. This is indicative of a combination of dynamic and static quenching as discussed in Chapter 3.3.1. Therefore, the dynamic quenching rate constants k_q were determined independently utilising time-correlated single photon counting (TCSPC), a time-resolved emission spectroscopy technique. The thereby obtained values were in line with the data afforded by steady-state spectroscopy. The static quenching constants K_S were thus also extracted, using the method described in Chapter 3.3.1 and the experimentally determined respective dynamic quenching constants K_D . The relevant ES quenching data is shown in Table 6.5. Overall, the k_q values obtained for (S15–17) were comparable to quenching rate constants that have previously been determined for the reaction of (11) with trialkylamines, while being approximately one order of magnitude slower than what has been observed for aromatic amines [40]. The nature of the quenching event was investigated by ns-TA spectroscopy (Figure 6.3, right column), where features corresponding to the Fe(II)-GS as well as bleach of the Fe(III)-GS of (11) were observed, indicative of RQ. The longevity of the TA feature ascribed to the Fe(II)-GS (several milliseconds), furthermore shows that α -trimethylsilylamines are rather suitable electron donors for (11), due to the lack of charge recombination between the electron transfer products.

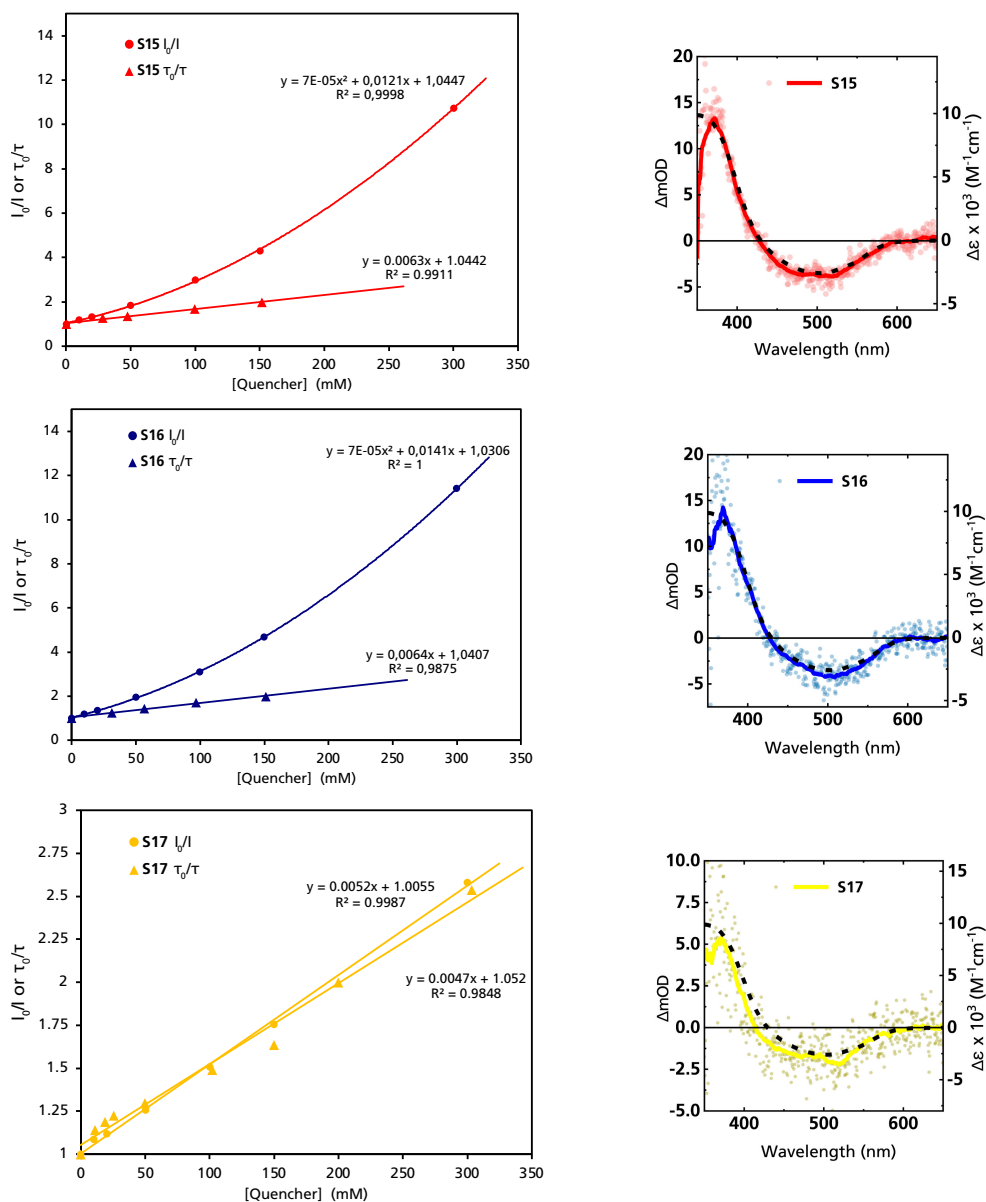
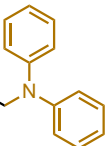
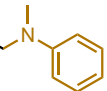
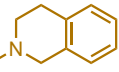
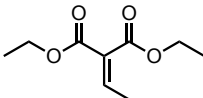


Figure 6.3: left column: Stern–Volmer plots derived from the steady-state and time-resolved emission quenching of $[\text{Fe}(\text{III})(\text{phtmeimb})_2]^+$ (**11**) (0.16 mM) in DMF with substrates (**S15–17**) with the corresponding emission spectra and TCSPC traces shown in the Supporting Information. right column: ns-TAS spectra of $[\text{Fe}(\text{III})(\text{phtmeimb})_2]^+$ (**11**) (0.15 mM) and substrates (**S15–17**) (104, 101, 88 mM, respectively) in DMF upon 465 nm (30 μs delay, 21.4 ± 0.1 mJ/pulse) excitation (data smoothed by Adjacent Averaging method) and differential absorption spectrum of the metal-centred reduction based on spectroelectrochemistry in MeCN (---). Adapted from Paper III.

To gain further insights into the efficiency of the generation of charge-separated electron transfer products, the CEYs for substrates (S15–S17) were determined, giving results ranging from 9 % for (S17) to 15 % for (S15) and 22 % for (S16) (Table 6.5) in DMF, which is higher than what has previously been observed for the RQ of (11) by tertiary amines in the same solvent [40]. When looking at the CEYs of (S17) but particularly (S16), the reasonably efficient cage escape of the electron transfer products appears somewhat counterintuitive considering that for (S17) no product formation was observed in the photocatalytic reaction, while use of (S16) resulted in a significantly lower yield than in the case of (S15) (Table 6.3), despite the latter’s lower CEYs. These discrepancies are therefore like to arise from differences in efficiency of the subsequent steps of the catalytic cycle or possible unproductive side reactions, such as the previously mentioned protodesilylation [237].

Table 6.5: Excited state quenching data for [Fe(III)(phtmeimb)₂]PF₆ (11) in DMF. (K_S = static quenching constant, K_D = Stern–Volmer quenching constant for dynamic quenching, k_q = bimolecular quenching constant, η_q = quenching yield, η_{ce} = cage escape yield, $\eta_q\eta_{ce}$ = quantum yield). CEYs calculated under the assumption that the extinction coefficients of Fe(III) and Fe(II) in DMF are similar to those in acetonitrile (see details of calculations in SI).

Quencher	[Fe(phtmeimb) ₂]PF ₆ (11) τ_0 (² LMCT) = 1.6 ns (in DMF)					
	K_S (M ⁻¹)	K_D (M ⁻¹)	k_q (10 ⁹ M ⁻¹ s ⁻¹)	η_q ([Q]/M)	η_{ce}	$\eta_q\eta_{ce}$ ([Q]/M)
 Substrate (S15)	9.9	6.3	3.7	0.67 (0.1)	0.15	0.10 (0.1)
 Substrate (S16)	11.3	6.4	4.0	0.68 (0.1)	0.22	0.15 (0.1)
 Substrate (S17)	n.a.	5.2	2.8	0.34 (0.1)	0.09	0.03 (0.1)
 Substrate (S14)	n.a.	n.a.	n.a.	0 (≤ 0.3)	n.a.	0 (≤ 0.3)

Consequently, we set out to further elucidate the steps following the initial SET using TA spectroscopy. There, we were able to observe the degradation of an absorption feature at 600 nm, which decays with a lifetime of 244 ns—indicative of an intramolecular process. Said feature was assigned to the intermittent radical cation degrading into the α -aminoalkyl radical by loss of the TMS-functionality. Subsequent

addition of the Michael acceptor (S14) resulted in the recovery of the Fe(III)-GS of (11) being observed, which is in accordance with the last step of the photocatalytic cycle proposed in Scheme 6.5, where the radical-adduct between the Michael acceptor and the α -aminoalkyl radical is reduced by the Fe(II)-GS.

Overall, in this study, [Fe(III)(phtmeimb)₂]PF₆ (11) has been established as a reasonably efficient PC for the visible light-mediated aminomethylation of electron-deficient alkenes by in situ generation of highly nucleophilic α -aminoalkyl radicals. This method has allowed for the one step-synthesis of functionalised *N*-containing products, thus adding to the to date still very small repertoire of synthetically valuable reactions driven by outer-sphere SET from a CT state of a photoactive iron complex. Certain limitations with regard to the substrate scope for α -trimethylsilylamines featuring aliphatic *N*-substituents, imposed by potential side reactions, were observed. However, overall yields, especially when using aromatic α -trimethylsilylamines, were fair to good and direct comparison to the archetypal [Ru(II)(bpy)₃]Cl₂ (1) under comparable reaction conditions showed the superior performance of our Fe(III)-NHC catalyst. The underlying mechanism was furthermore extensively investigated, revealing that RQ of the ²LMCT state of (11) by the α -trimethylsilylamines takes place with reasonably efficient bimolecular quenching rates and appreciable CEYs and that the Fe(III)-GS is recovered by SET to the radical-adduct, thus providing experimental support for the essential steps of the entire catalytic cycle.

6.3 Conclusions

Photoredox catalysis in organic synthesis using TM-based PCs has conventionally relied on diffusion-controlled bimolecular quenching of CT states. Recent improvements regarding the design of photoactive complexes based on iron, such as the introduction of NHC-ligands, have aided in mitigating the inherently poor photophysical and -chemical properties encountered in complexes that structurally resemble noble metal-PCs. Thus, their investigation as PCs for driving different organic transformations, both concerning their synthetic applicability but also, and maybe more importantly so, their behaviour from a mechanistic standpoint, presented the next step for this comparatively new field to undergo further—and hopefully more rapid—development.

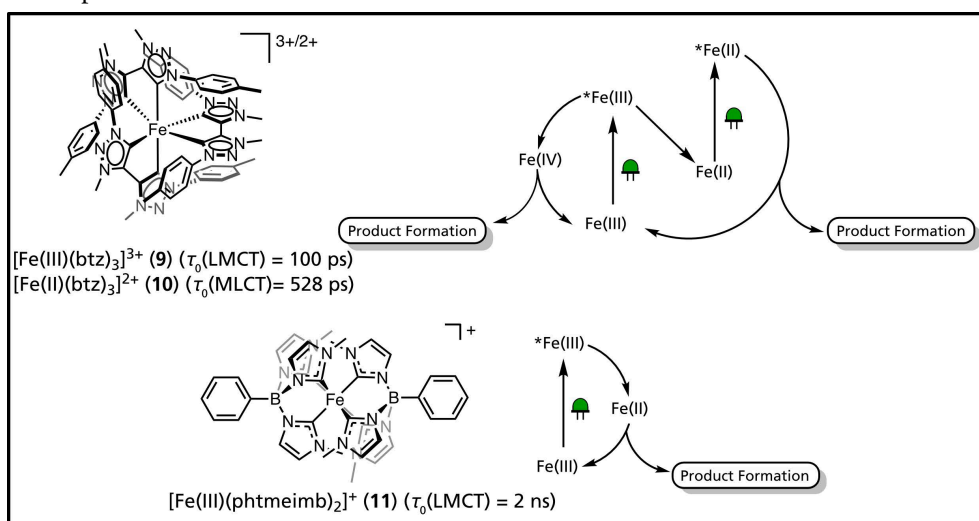


Figure 6.4: Illustration of the different reaction modes of Fe(III)-NHC complexes **(9)** and **(11)** utilising for the reactions presented in Paper II and III.

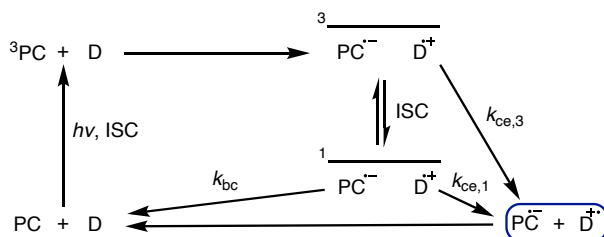
In Paper II, $[\text{Fe}(\text{III})(\text{btz})_3]^{3+}$ (**9**) was found to be a suitable PC to drive ATRA reactions involving reactive alkyl halides, both in an RQ as well as an OQ pathway. For the former, we invoked the involvement of not just one but two excitations within the same catalytic turnover. This was possible due to the fact that both the Fe(III)-NHC complex (**9**) and its Fe(II)-congener (**10**) are photoactive and exhibit lifetimes of their ESs, an $^2\text{LMCT}$ and $^3\text{MLCT}$ respectively, that range in the hundreds of picoseconds, as well as relatively strong absorption at the irradiation wavelength (530 nm). Through this a conPET mechanism, more energy is accumulated in one catalytic turnover than in the corresponding single photon mechanism, and such a reactivity can be considered as mimicry of the Z-scheme seen in natural photosynthesis. Additionally, the reaction via OQ allowed for product formation via single photon excitation of (**9**), whilst omitting the use of sacrificial reagents. But more importantly, with this study we were

able to show that even sub-ns lifetimes of the CT ESs of a PC can be sufficient to drive a photocatalytic reaction with good efficacies provided that the bimolecular quenching step is reasonably efficient and that CEYs of the electron-transfer products are high. While a longer ES lifetime is still indubitably advantageous, we can conclude from this investigation that photoactive compounds exhibiting what would generally be considered too short ES lifetimes should not be immediately disregarded for photocatalytic application, before further knowledge of their photochemical properties has been obtained.

Additionally, in the study described in Paper III, the 2 ns-ES lifetime of $[\text{Fe}(\text{III})(\text{phtmeimb})_2]^+$ (**11**) was exploited to effect aminomethylation reactions of electron-deficient alkenes. There, RQ of the $^2\text{LMCT}$ resulted in single electron oxidation of α -trimethylsilylamines, giving rise to the amine radical cation, which then undergoes desilylation affording the desired very nucleophilic, neutral radical. The α -aminoalkyl radicals could thus be trapped by suitable electrophiles, here electron-deficient double bonds, resulting in the rapid functionalisation of the amines in a one step-reaction. With this investigation, the currently still rather limited range of synthetically useful reactions catalysed by bimolecular quenching of a CT state of an iron complex was expanded, giving rise to a number of functionalised *N*-containing products in fair to good yields. The variety of substrates as well as catalytic efficiencies were comparable to systems relying on organic or noble metal-PCs, including limitations encountered in some of these systems, such as the use of aliphatic amines not resulting in efficient product formation. The lack of reactivity likely originates from undesired side reactions. This was further supported by the observation of bimolecular quenching with both aromatic and aliphatic α -trimethylsilylamines as well as reasonably high CEYs, indicating that—particularly at higher concentrations—these compounds can act as very good quenchers for (**11**). As such they could also be interesting for further exploration in other reactions, where they might also be used as sacrificial electron donors. Additionally, we were able to spectroscopically track the later steps of the reaction, mapping the entire photocatalytic cycle to obtain a more complete picture of the different reaction steps.

7 Excited state dynamics of an Fe(II) *Hexa*-NHC Complex (Paper IV)

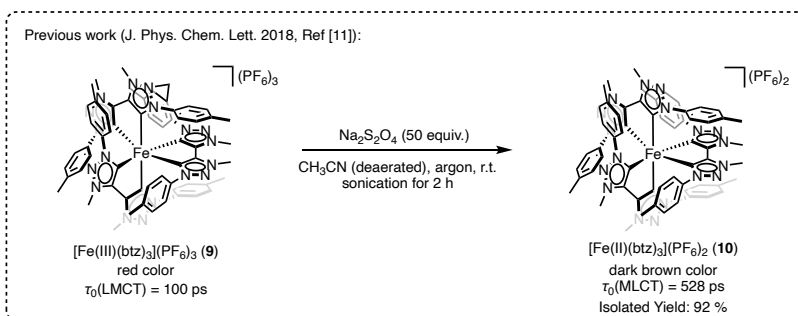
While Fe(III)-NHC complexes have been successfully applied in an artificial photosynthesis reaction as well as organic photoredox catalysis [40, 43-45, 139, 140], there is still on-going work towards finding Fe(II)-NHC complexes with long-lived CT states. This is due to the fact that they are expected to be even stronger photo-reductants than their Fe(III)-counterparts, broadening the range of possible application. Higher CEYs might also be obtained by SET from the $^3\text{MLCT}$ states that are found in Fe(II)-complexes, than what has so far been observed for Fe(III)-systems featuring $^2\text{LMCT}$ states, as a result of the spin-forbidden recombination of triplet radical pairs [241]. The latter refers to the fact that upon reduction of a triplet state by an electron donor, a spin-correlated pair exhibiting the multiplicity of the ES of the PC is initially afforded [242]. For said radical pair, geminate back-combination within the solvent cage is spin-forbidden. However, for TM-based PCs, which feature heavy atoms, ISC leads to interconversion between the triplet and singlet radical pair, presenting a competing pathway through which aforementioned back-combination can still take place [242, 243], as illustrated in Scheme 7.1.



Scheme 7.1: Schematic illustration of the reaction pathways of the triplet ES of TM-based PCs in presence of an electron donor. Adapted from [241] with permission. © 2020 The Authors. Chemistry – A European Journal published by Wiley-VCH GmbH.

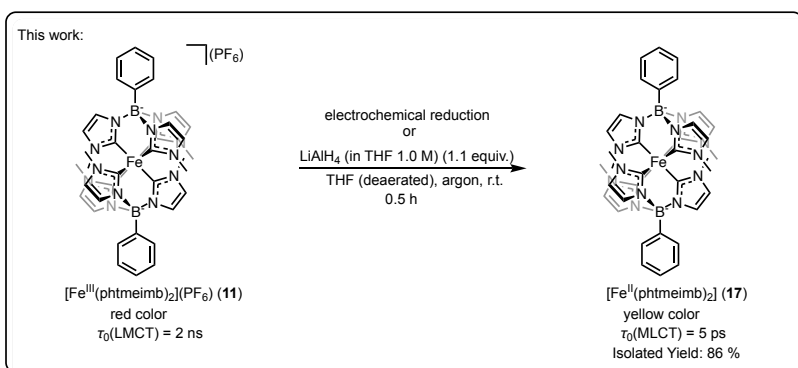
In a previous report, it has been shown that reduction of $[\text{Fe(III)(btz)}_3]^{3+}$ (**9**), a homoleptic *hexa*-NHC complex harbouring the bidentate ligand btz, affords its Fe(II)-congener (**10**). Said complex exhibits a non-emissive $^3\text{MLCT}$ state with an ES lifetime of 528 ps in acetonitrile [10, 11], which can be used for a photoredox reaction driven by both the $^2\text{LMCT}$ state of (**9**) as well as the $^3\text{MLCT}$ state of (**10**) via consecutive

bimolecular quenching events as demonstrated in Paper II. This type of reactivity, somewhat resembling the Z-Scheme known from natural photosynthesis, is particularly interesting as it allows for the accumulation of more energy within the same catalytic cycle, thus giving access to energetically more demanding reactions than what would be possible in a single photon mechanism [244].



Scheme 7.2: Previous work demonstrating the chemical reduction of (**9**) to (**10**) [11]. Adapted from Paper IV.

Consequently, uncovering similar reactivity in other Fe-NHC complexes could allow for rapid further development of the field of iron photocatalysis. Here, $[\text{Fe}(\text{III})(\text{phtmeimb})_2]^+$ (**11**)—also a homoleptic *hexa*-NHC complex, featuring the tripodal tridentate ligand phtmeimb, with a $^2\text{LMCT}$ lifetime of 2 ns—was considered a promising candidate. It had previously been demonstrated, that electrochemical reduction of (**11**) to $[\text{Fe}(\text{II})(\text{phtmeimb})_2]$ (**17**) is possible at a potential of -1.16 V vs $\text{Fc}^{+/0}$. Complex (**17**) has been found to also be photoactive exhibiting an absorption band at 348 nm ($\epsilon = 10\,850 \text{ M}^{-1}\text{cm}^{-1}$), tentatively ascribed to an MLCT transition [12]. This assignment has been further corroborated by the computational study of the GS electronic structure of (**17**) presented in this study.



Scheme 7.3: Overview of the transformation of (**11**) to (**17**) by electrochemical or chemical reduction. Adapted from Paper IV.

Here, we showed that chemical reduction of $[\text{Fe}(\text{III})(\text{phtmeimb})_2]\text{PF}_6$ (**11**) was possible using LiAlH_4 as reductant in THF, upon which a colour change from red to yellow was observed (Scheme 7.3). The corresponding UV–VIS absorption spectrum supported the formation of (**17**) exhibiting the same changes as seen for the product obtained by electrochemical reduction (Figure 7.1).

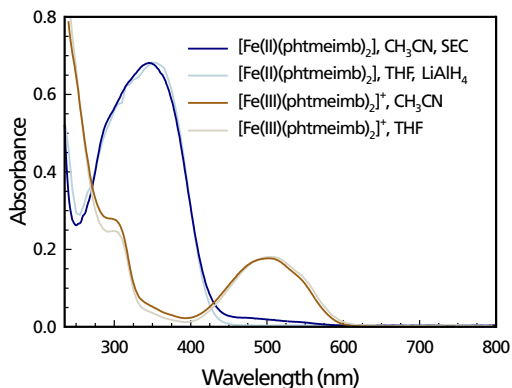


Figure 7.1: UV–VIS absorption spectra of the Fe(III)-NHC (**11**) in acetonitrile (brown) and THF (beige) and of the Fe(II)-NHC complex (**17**) obtained by spectroelectrochemistry in acetonitrile (dark blue) and by chemical reduction by LiAlH_4 in THF. The spectra obtained in THF were scaled at the maxima of the LMCT and MLCT bands, respectively. Adapted from Paper IV.

Isolation of the Fe(II)-NHC complex (**17**) was possible (86 %) but further handling and characterisations proved challenging, as even inside a glovebox, a successive colour change back to the original red was observed, indicating rather rapid re-oxidation. Due to this, NMR spectroscopic characterisation of (**17**) was performed by in situ chemical reduction under inert atmosphere using deaerated $\text{THF-}d_8$ in presence of a slight excess of LiAlH_4 in a sealed NMR tube. The excess of LiAlH_4 served to ensure that no degradation back to the Fe(III)-state occurred for the duration of the measurements. Both the ^1H NMR spectrum as well as the ^{13}C NMR spectrum exhibited well-resolved peaks, as expected for a diamagnetic compound such as (**17**). Interestingly, a substantial downfield shift of 216.9 ppm for the carbene-carbon signal was observed, likely originating from the strongly electron-donating effect the NHC-functionality imposes upon the metal centre. This is very much in line with chemical shifts of the carbene-carbon in the *hexa*-carbene Fe(II)-complex (**10**), where the pertinent signal appears at 206.7 ppm [11].

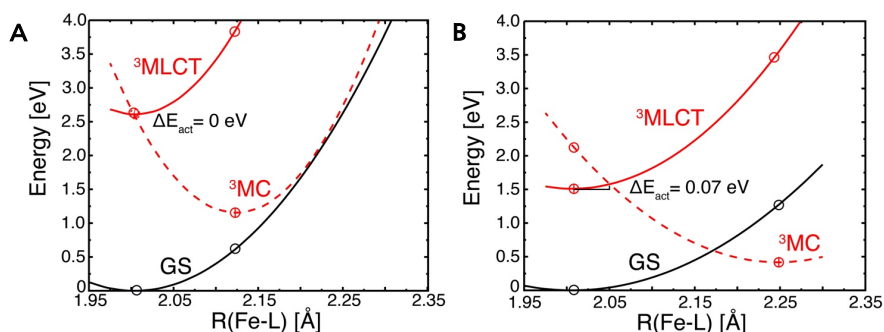


Figure 7.2: Extrapolated diabatic harmonic singlet and triplet potential energy surfaces for A) [Fe(II)(phtmeimb)₂] (17) and B) [Fe(II)(btz)₃]²⁺ (10) along an effective one-dimensional average Fe–C reaction coordinate calculated at B3LYP+D2/6-311G*, SDD (Stuttgart/Dresden pseudopotentials and basis set) level of theory in acetonitrile. ³MLCT (red solid line), ³MC (red dashed line), GS (black solid line). Reprinted from Paper IV.

Investigation of the excited state dynamics of (17) revealed a markedly shorter ³MLCT lifetime of only 5 ps compared to the 2 ns-lifetime of the Fe(III)-ES. Due to the fact that a significant increase in ES lifetime was observed when going from Fe(III)-NHC complex (9) to its Fe(II)-analogue (10), the question of why the opposite was found for (11) arose. Consequently, the differences in lifetime between (10) and (17) were rationalised by activation barriers and Hamiltonian coupling constants for the transition to MC states obtained by computational methods. These indicated that in the case of (17) the comparatively shorter lifetime of the ³MLCT state can partly be ascribed to the higher energy of this state resulting in an essentially barrierless transition to the ³MC state (Figure 7.2, Table 7.1).

Table 7.1: Calculated thermodynamic parameters for (17) and (10) at B3LYP+D2/6-311G*(C, H, O, N), SDD(Fe) level of theory in acetonitrile using the polarizable continuum model (PCM). (ΔE_{act} = activation energy, ΔE = driving force, λ = reorganisation energy, H_{AB} = electronic coupling constant).

	ΔE_{act} (eV)	ΔE (eV)	λ (eV)	H_{AB} (Bohr ⁻¹)
[Fe(II)(phtmeimb) ₂] (17)	0.00	-1.45	1.35	0.083
[Fe(II)(btz) ₃] ²⁺ (10)	0.07	-1.09	1.89	0.026

In Paper I, where we presented HERs sensitised by the Fe(III)-NHC complex (11), we established that the complex exhibits substantially higher photostability in acetonitrile than the archetypal [Ru(II)(bpy)₃]²⁺ (1), which had been ascribed to the strong nature of the Fe–C(carbene) bond as well as the fact that the phtmeimb-ligands of (11) are tridentate, giving rise to a more rigid framework and thus improved structural integrity. In light of that, we set out to investigate the photostability of its Fe(II)-congener (17) in the presence of LiAlH₄ under irradiation at 375 nm. There, we observed changes in the MLCT absorption band at about 350 nm, already after 15–30 min. After 60 min,

significant degradation of the complex was noted and at 90 min, the MLCT band had essentially vanished. This lack of photostability for the Fe(II)-complex might be a consequence of weakening of the Fe–C(carbene) bonds in the MC states through which the CT state is decaying.

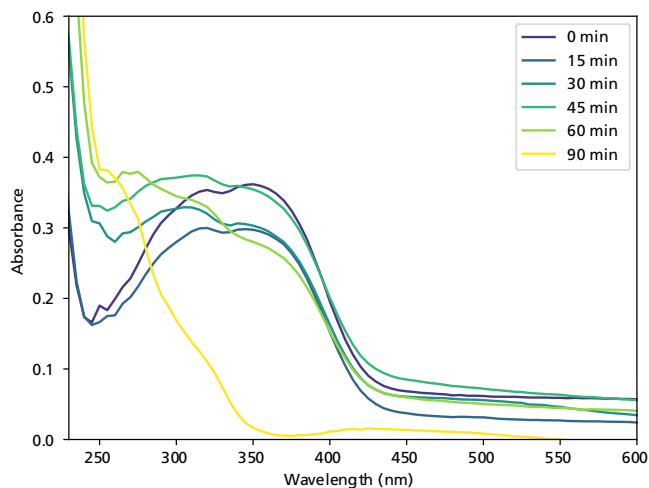


Figure 7.3: Photostability study for (17) (0.05 mM in THF + 1.5 equiv. LiAlH₄) under irradiation at 375 nm. Reprinted from Paper IV.

The photostability of $[\text{Fe}(\text{II})(\text{btz})_3]^{2+}$ (10) was subsequently also investigated as a reference using irradiation at 525 nm in anhydrous acetonitrile (Figure 7.4A) as well as in a binary acetonitrile:water mixture (9:1) (Figure 7.4B). In both cases, substantial changes of the corresponding absorption spectra were observed already within 60 min, with the shoulder peaks at 450 nm and 510 nm decreasing in intensity. These changes were more pronounced in the presence of water and especially so upon irradiation overnight, where the characteristic absorption bands of (10) had completely disappeared. Both under anhydrous conditions and in presence of water, precipitation of decomposition products was observed within few hours.

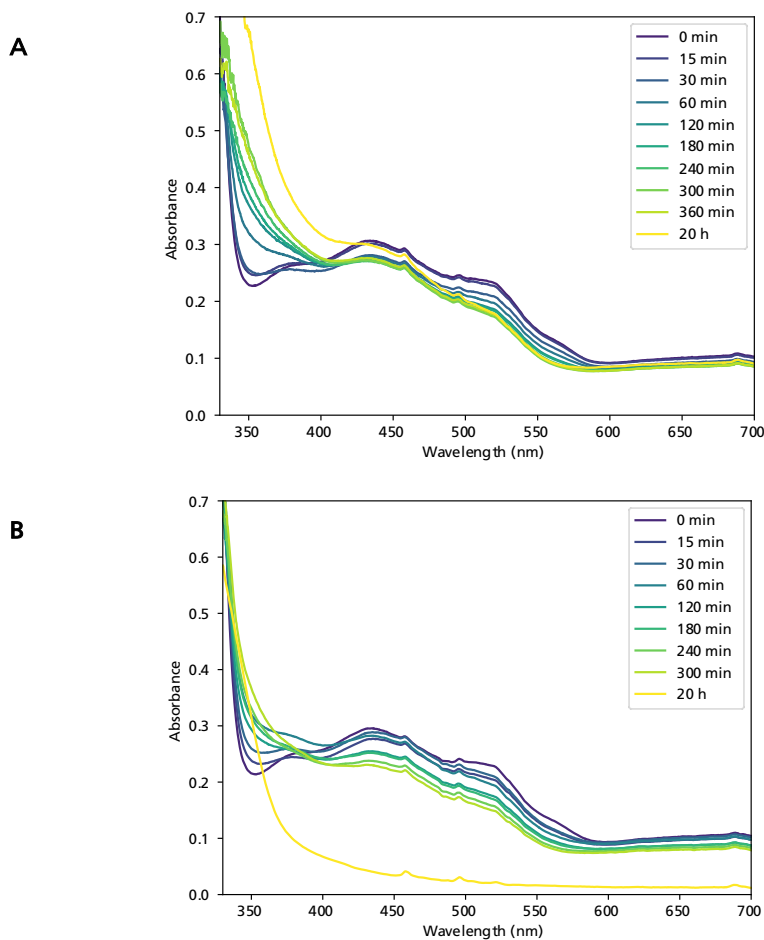


Figure 7.4: A) Photostability study for $[\text{Fe}(\text{II})(\text{btz})_3](\text{PF}_6)_2$ (**10**) (0.4 mM in acetonitrile) under irradiation at 525 nm. B) Photostability study for $[\text{Fe}(\text{II})(\text{btz})_3](\text{PF}_6)_2$ (**10**) (0.4 mM in acetonitrile: H_2O , 9:1 v/v) under irradiation at 525 nm. Reprinted from Paper IV.

Based on these results, it appears that Fe(II)-*hexa*-NHC complexes are prone to photodegradation to a similar extent as more classical systems, such as $[\text{Ru}(\text{II})(\text{bpy})_3]^{2+}$ (**1**). However, although photostability is highly desirable for applications in photocatalysis, the apparent lability of (**10**) does not seem to have strongly detrimental effects on its applicability for photoredox catalysis of (**9**), where—under RQ conditions—(**10**) partakes as an intermediate species such as in Paper II [44, 139].

To conclude, in this study, the ES lifetime of the $^3\text{MLCT}$ state of $[\text{Fe}(\text{II})(\text{phtmeimb})_2]$ (**17**) was determined to be 5 ps, which is significantly shorter than the 2 ns-lifetime of the $^2\text{LMCT}$ of its Fe(III)-congener. This relation was also compared to the $[\text{Fe}(\text{III}/\text{II})(\text{btz})_3]^{3+/2+}$ (**9/10**) couple, where the Fe(III)-complex exhibits a 100 ps-

lifetime of its $^2\text{LMCT}$, while the $^3\text{MLCT}$ state of the Fe(II)-congener has a lifetime of 528 ps and is thus more long-lived [10, 11]. The surprisingly short lifetime of the $^3\text{MLCT}$ state of (17) most likely precludes the possibility for efficient diffusion-controlled photochemical reactions. The differences between the $^3\text{MLCT}$ states of (17) and (10) were attributed to the fact that the former's CT state of higher energy undergoes an essentially barrierless transition to the ^3MC state. This is in so far interesting as it would be expected that the tridentate phtmeimb-ligands featured in this complex destabilise the ^3MC state to a higher degree than the btz-ligands. In contrast to that, such a decay via MC-centred states is less favourable for the Fe(III)-NHC complex (11) due to the spin-forbidden nature of the $^2\text{LMCT} \rightarrow ^4\text{MC}$ transition. Additionally, the diamagnetic complex (17) was characterised by NMR spectroscopy, revealing well-resolved peaks and a notable downfield shift of the carbene-C signal, attributed to its strong electron-donation to the coordination centre. The photostability of this complex was also investigated and compared to (10), revealing that both Fe(II)-NHC complexes were prone to degradation within much shorter time than the Fe(III)-complex (11). This shows that simple reduction of existing Fe(III)-NHC complexes with reasonably long $^2\text{LMCT}$ lifetimes does not necessarily give rise to Fe(II)-NHC species that also showcase long $^3\text{MLCT}$ lifetimes. Consequently, the pursuit for long-lived MLCT states of Fe(II)-complexes remains a challenging endeavour, with very few successful examples to date [11, 245-248].

8 Heterogenisation of Fe(III)-NHC Complexes for Photoredox Catalysis

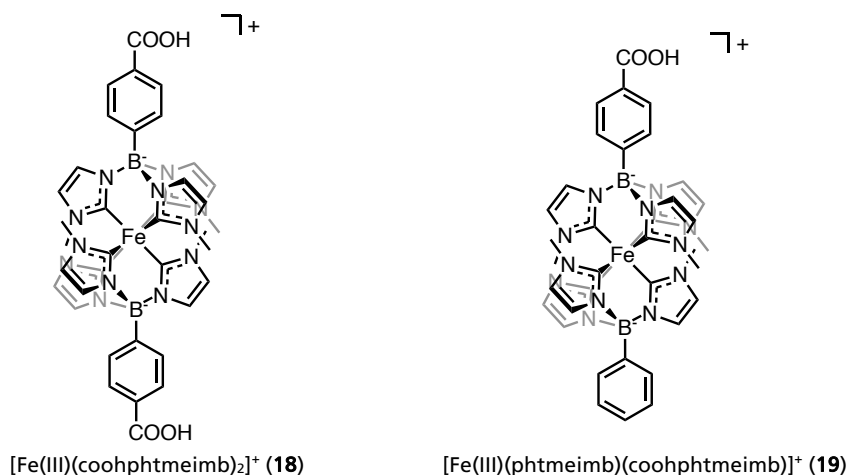
8.1 Background and Motivation

A range of reports, including the studies presented in Paper I–III, have clearly established that Fe-complexes featuring strongly σ -donating NHC, can partake in outer-sphere SET from CT states to drive diffusion-controlled photocatalytic processes. The reactivities observed from Fe-PCs were somewhat comparable to established noble metal-PCs. With iron being highly Earth-abundant, especially compared to ruthenium or iridium, Fe-complexes could be viewed as more sustainable alternatives to the latter. However, what needs to be taken into consideration beyond the abundance of the metal centre, is also the more elaborate ligand design and labour-intensive preparation required for the NHC-ligands discussed herein, which can include multi-step synthesis. Furthermore, yields for the synthesis of the Fe-NHC complexes can also be low, due to the sensitivity of the complexation step to moisture as well as possible formation of undesired side products. Therefore, one approach to making photoactive Fe-NHC complexes even more sustainable is their heterogenisation on inert metal oxide particles via a suitable anchoring group present on the ligand framework. This strategy would consequently allow for the facile separation of the photocatalytic component from the reaction mixture via simple techniques such as filtration or centrifugation, enabling straight-forward reusability.

$[\text{Fe(III)}(\text{phtmeimb})_2]^+$ (11) has been established as a promising candidate for use in photocatalytic reactions owing to the lifetime of 2 ns of its $^2\text{LMCT}$ state, strong absorption of green light, as well as its photostability. As a result of the formerly discussed photostability of (11), it has been shown that the PC could be recovered in 88 % yield following a successful dehalogenation reaction and a subsequent reaction using the recovered material again led to full conversion of the starting material [40]. Furthermore, it has been observed that introduction of different substituents, be that electron-donating ($-\text{MeO}$) or -withdrawing ($-\text{Br}$, $-\text{COOH}$), on the 4-position of the phenyl-moiety featured in the phtmeimb-ligand, induces barely any changes in the ES lifetime, absorption features and redox chemistry compared to the parent complex (11) [249]. Based on these insights, the Fe(III)-NHC complex

$[\text{Fe}(\text{coohphtmeimb})_2]\text{PF}_6$ (**18**) (coohphtmeimb = (4-carboxyphenyl)tris(3-methylimidazolin-2-ylidene)borate) could be an interesting candidate for immobilisation on solid support.

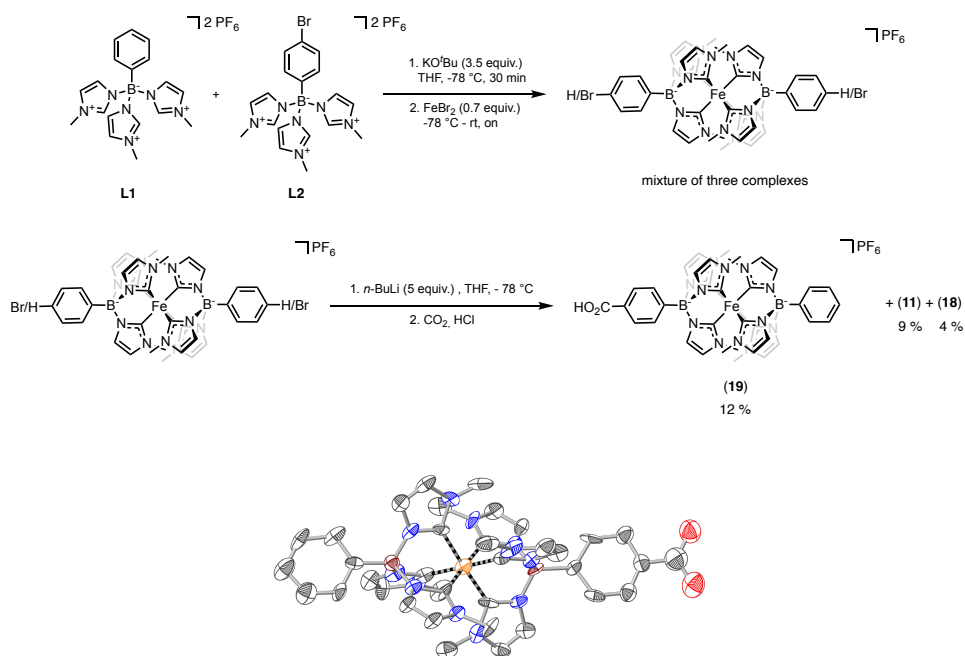
In this chapter, early results for the heterogenisation of two Fe(III)-NHC complexes on nanoparticles (NPs) are presented, where their solvent stability as well as application in a photocatalytic model reaction were investigated. The two complexes in question are the known PS (**18**), as well as a newly synthesised and characterised heteroleptic Fe(III)-NHC complex, $[\text{Fe}(\text{III})(\text{phtmeimb})(\text{coohphtmeimb})]\text{PF}_6$ (**19**), featuring both the unsubstituted phtmeimb-ligand as well as the carboxy-substituted coohphtmeimb-ligand. For the solid support, Al_2O_3 -NPs were chosen, as Al_2O_3 has a wide band gap (8.45–9.9 eV) and a high energy conduction band. Consequently, electron injection from the attached Fe-PC should not take place, resulting in the metal oxide acting as an essentially inert support [250].



8.2 Synthesis of Fe(III)-NHC complex (19)

Based on the syntheses of (**11**) and (**18**) [12, 249], a synthetic route for the heteroleptic complex (**19**) was devised (Scheme 8.1). Previous reports attempting the direct preparation of the Fe(III)-NHC complex (**18**) from the NHC-precursor featuring the carboxylic acid-moiety had been unsuccessful, which is why the corresponding bromo-substituted complex had been synthesised and isolated before subsequent conversion to the desired product (**18**) by carboxylation. Therefore, equimolar amounts of the NHC-precursors $[\text{phtmeimbH}_3](\text{PF}_6)_2$ ($\text{phtmeimbH}_3 = [\text{phenyltris}(3\text{-methyl-}1H\text{-imidazol-}3\text{-ium-}1\text{-yl)borate}]^{2+}$) (**L1**) and $[\text{brphtmeimbH}_3](\text{PF}_6)_2$ ($\text{brphtmeimbH}_3 = (4\text{-bromophenyl)tris}(3\text{-methyl-}1H\text{-imidazol-}3\text{-ium-}1\text{-yl)borate}]^{2+}$) (**L2**) were used for the

complexation, where the carbene was generated in situ at $-78\text{ }^{\circ}\text{C}$ by addition of a strong base (potassium *tert*-butoxide, KO^tBu), after which FeBr₂ was added. This led to the formation of a statistical mixture of the heteroleptic complex and the two corresponding homoleptic species. Due to the fact that the polarity difference between the three different complexes was not sufficiently large for separation via chromatography, the purified mixture was subjected to the next step. There, a lithium-halogen exchange was performed, after which CO₂ was used as an electrophile to trap the anion, giving rise to a mixture of the desired heteroleptic product (19) along with the homoleptic species (11) and (18). As a result of introducing the carboxylic-acid moieties affording the heteroleptic complex (19) and complex (18), which harbour one and two carboxy-groups respectively, it was then possible to separate the products by column chromatography.



Scheme 8.1: Synthetic route towards the heteroleptic Fe(III)-NHC complex (19) and its molecular structure based on X-ray crystallography data. Yields are given over two steps.

The identity and purity of this new heteroleptic complex (19) was established by ¹H NMR and ¹³C NMR spectroscopy, high-resolution mass spectrometry (HRMS) as well as elemental analysis and was in accordance with the proposed molecular structure. Not entirely unsurprisingly, comparison of the steady-state absorption spectra of the heteroleptic complex (19) to the homoleptic analogues (11) and (18) revealed essentially identical absorption features (Figure 8.1). Additionally, the same was also observed for the corresponding steady-state emission spectra (Figure 10.3, Supporting Information).

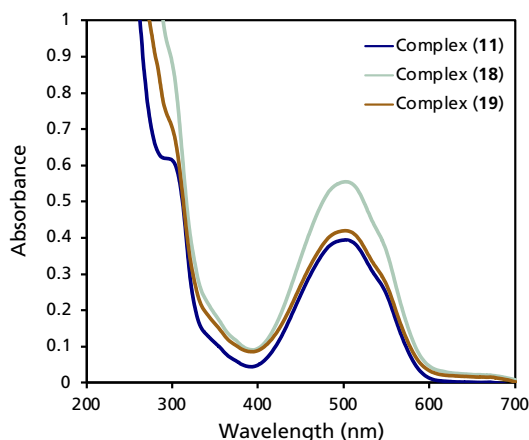


Figure 8.1: Steady-state absorption spectra of the homoleptic Fe(III)-NHC complexes (11) and (18) as well as their heteroleptic analogue (19) in MeOH.

8.3 Preparation of Al₂O₃-(18) and Al₂O₃-(19) and Solvent Stability Studies

With the two Fe(III)-NHC complexes—equipped with suitable anchoring groups—in hand, the heterogenisations on Al₂O₃-NPs were performed. This was done following a modified literature procedure [250, 251], where the NPs were stirred in a solution of the PC overnight in the dark (Supporting Information for experimental details). The loading of dye-molecules attached to the Al₂O₃-NPs was determined using the so-called depletion method. There, the decrease in concentration of PC in the solution after sensitisation is measured utilising UV–VIS absorption spectroscopy.

For Al₂O₃-(19), concentrations of 0.17 mM and 0.28 mM of the heteroleptic dye were used for the initial sensitisation, while concentrations of 0.25 mM and 0.5 mM of the homoleptic dye were employed for the preparation of Al₂O₃-(18), which resulted in the loadings of PC on Al₂O₃ shown in Table 8.1. This range of concentrations was chosen to afford initial insight into the effect the loading of PC on the Al₂O₃-NPs would have on the reactivity. Notably, when comparing the sensitisation using a 0.25 mM solution of (18) and a 0.28 M solution of (19) (Table 8.1), higher coverage was obtained for the former (Al₂O₃-(18)-A), which can likely be attributed to the presence of two carboxylic acid-moieties increasing the chances for anchoring to the metal oxide-surface.

Table 8.1: Surface loadings obtained for the sensitisation of Al₂O₃-NPs using (18) and (19). ^aconcentration of the PC-solution used for the sensitisation. ^bmmol of PC per mg Al₂O₃ as determined by the depletion method.

		[PC] (mM) ^a	PC loading on the NP-surface (mmol mg ⁻¹) ^b
Al ₂ O ₃ -(18)	A	0.25	2.32·10 ⁻⁵
	B	0.50	4.87·10 ⁻⁵
Al ₂ O ₃ -(19)	A	0.17	1.29·10 ⁻⁵
	B	0.28	2.08·10 ⁻⁵

The thereby solid-supported catalysts Al₂O₃-(18) and Al₂O₃-(19) (Figure 8.2) were then investigated for their stability in a range of different solvents with respect to possible catalyst desorption under irradiation at 530 nm for 2 h (Figure 8.3). Following irradiation, the catalysts were separated from the supernatant solution by centrifugation and the latter was subsequently analysed by UV–VIS absorption spectroscopy. In general, similar trends for both Al₂O₃-(18) and Al₂O₃-(19) were observed, where visible leaching of the PC into the solution—as indicated by the appearance of an absorption band at around 500 nm attributed to the ²LMCT transition of both (18) and (19)—occurred to varying degrees when using water, methanol, DMSO and to a smaller extent DMF. Meanwhile, acetonitrile, THF, toluene, DCM and chloroform appeared to be well-tolerated. Due to the commonplace usage of the latter solvents, this could potentially allow for the application of the heterogenised PCs in different photocatalytic reactions.

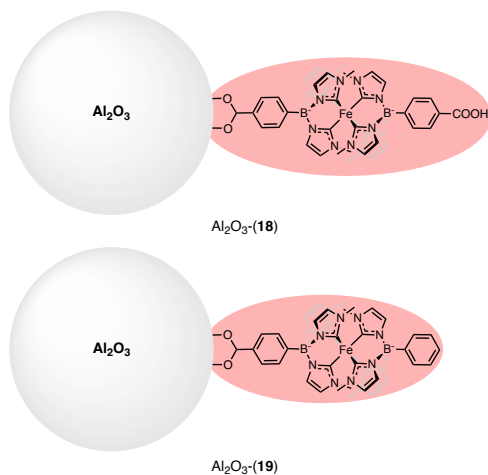


Figure 8.2: Schematic Illustration of the heterogenised Fe(III)-NHC complexes (18) and (19) affording Al₂O₃-(18) and Al₂O₃-(19) respectively.

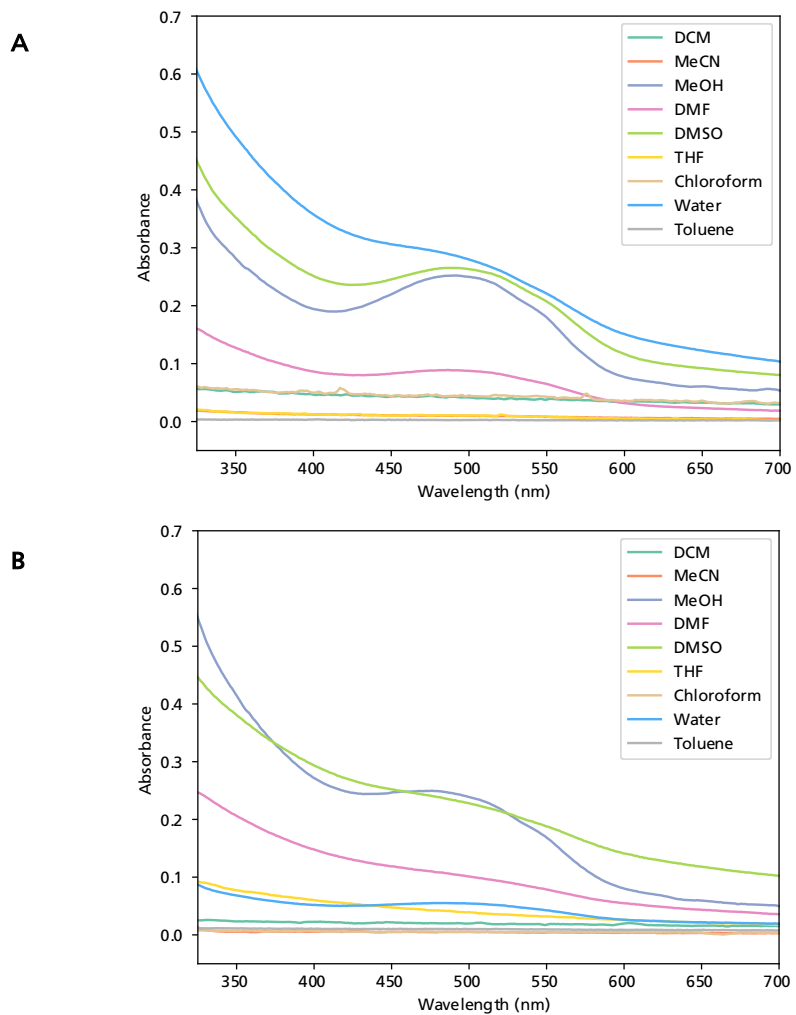
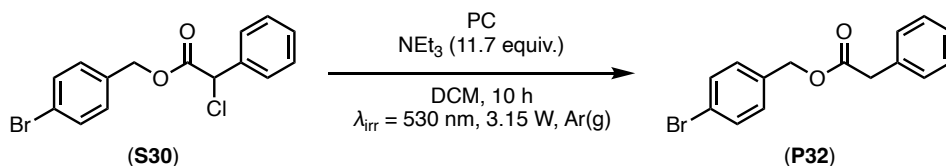


Figure 8.3: Stability of A) $\text{Al}_2\text{O}_3\text{-}(18)\text{-B}$ and B) $\text{Al}_2\text{O}_3\text{-}(19)\text{-B}$ in different solvents under irradiation at 530 nm for 2 h (3 W/slot).

8.4 Investigation of the Photocatalytic Activity & Reusability

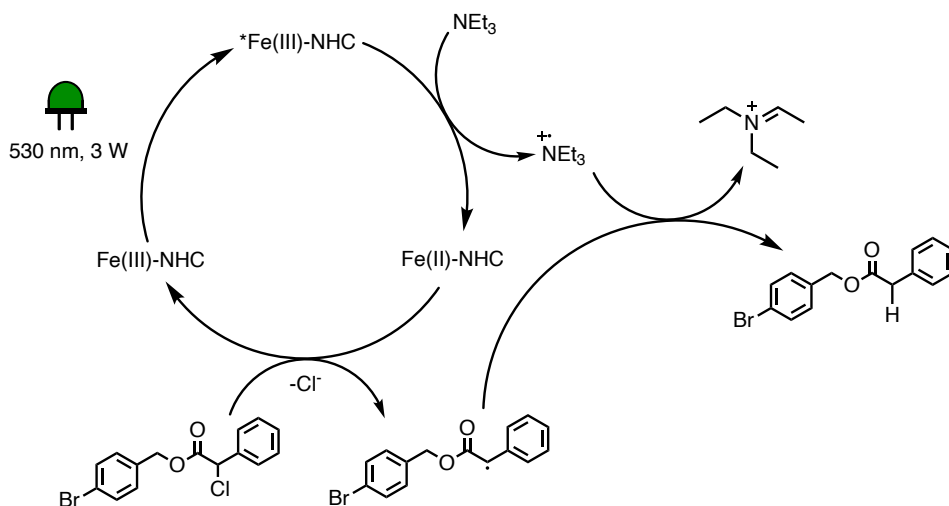
Having determined that the heterogenised Fe(III)-NHC complexes exhibit considerable stability towards desorption in different solvents under irradiation, the next step was to investigate their photocatalytic activity and reusability. For this, a simple dehalogenation, which had previously been performed by Troian-Gautier and co-workers using the parent complex $[\text{Fe(III)(phtmeimb)}_2]^+$ (11) [40], was chosen as the model reaction.



Scheme 8.2: Dehalogenation of (S30) to afford (P32) using Al₂O₃-(18) and Al₂O₃-(19) as catalysts.

There, both Al₂O₃-(18) and Al₂O₃-(19) were added (30 mg of the sensitised NPs resulting in PC-loadings of 0.26 mol% and 0.46 mol% for Al₂O₃-(19)-A and Al₂O₃-(19)-B respectively and 0.42 mol% and 0.92 mol% for Al₂O₃-(18)-A and Al₂O₃-(18)-B respectively). The dehalogenation of 4-bromobenzyl 2-chloro-2-phenylacetate (S30) to 4-bromobenzyl 2-phenylacetate (P32) was performed using NEt₃ both as sacrificial reductant as well as a hydrogen source required for the formation of the desired product in DCM as reaction solvent.

The reaction catalysed by the sensitised NPs presumably follows a very similar mechanism to the one reported for the unsubstituted parent-complex $[\text{Fe(III)(phtmeimb)}_2]\text{PF}_6$ (11) [40], which is shown in Scheme 8.3. There, it was proposed that the Fe(III)-ES is reductively quenched by NEt₃, giving rise to the amine radical cation and the Fe(II)-GS. The Fe(II)-GS subsequently transfers an electron to (S30), leading to cleavage of the C(sp³)-Cl bond, forming a neutral radical intermediate. The amine radical cation, as previously discussed in Chapter 5.2, can subsequently undergo radical abstraction of an α-hydrogen, ultimately affording the desired dehalogenated product (P32) and an iminium cation.



Scheme 8.3: Proposed mechanism for the dehalogenation of (**S30**) to afford (**P32**) using an Fe(III)-NHC complex as PC and NEt₃ as sacrificial reductant and proton source. Adapted with permission from [40]. © 2021 American Chemical Society.

The reactions were vigorously stirred while irradiating at 530 nm for 10 h under inert argon atmosphere. Thereafter, the solid-supported PCs were separated from the reaction mixture by centrifugation, rinsed thoroughly with the reaction solvent and dried. The conversion of (**S30**) to (**P32**) was quantified by ¹H NMR spectroscopy. Control reactions using no catalyst or unsensitised Al₂O₃ led to no product formation. Meanwhile, in the first reaction run, near quantitative conversion (93 %) of the starting material was observed for Al₂O₃-**(18)-B**, while 76 % was observed for Al₂O₃-**(18)-A** consistent with a lower PC-concentration present in the reaction. The same trend was observed for Al₂O₃-**(19)-A** and **-B**. The overall catalyst concentrations for these reactions were lower, resulting in lower conversions (46 % and 66 %).

For both Al₂O₃-**(18)** and Al₂O₃-**(19)**, the catalytic activity steadily dropped over the course of four reaction runs, but the most significant decreases were observed during the fourth run (Figure 8.4). This also coincided with the noticeable decolouration of the NPs after the third reaction run. However, regardless of that, product formation was still maintained overall.

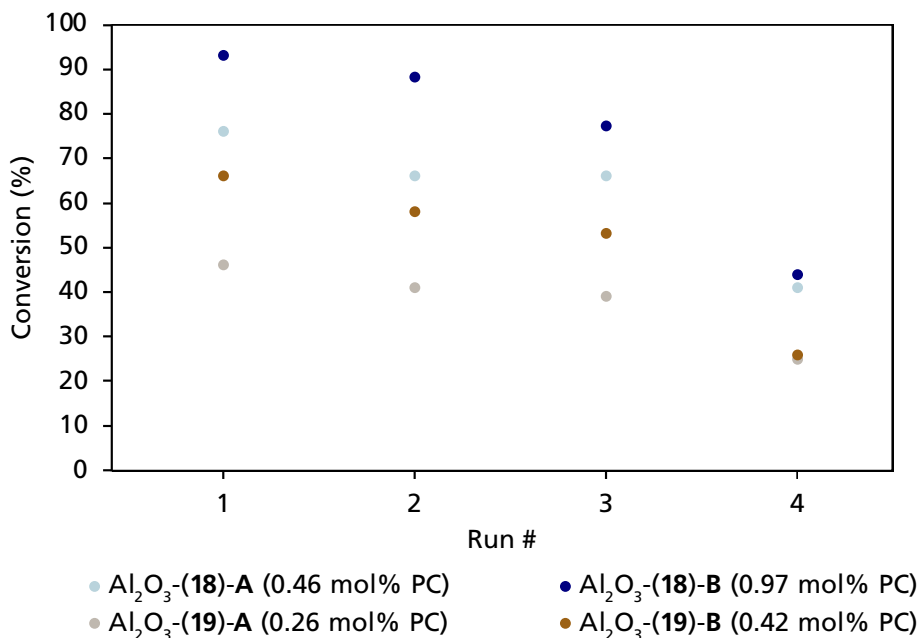
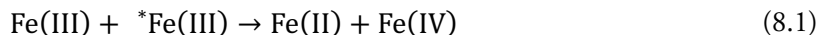


Figure 8.4: Reusability of Al₂O₃-(18) and Al₂O₃-(19) at different catalyst-loadings in a dehalogenation reaction. (mol% of PC in relation to the starting material **530**, conversion determined by ¹H NMR spectroscopy)

When considering the photocatalytic activity in relation to the surface coverage, the possibility of symmetry-breaking charge-separation (SBCS) also needs to be taken into account (Eq. (8.1)). Such reactivity has previously been reported for [Fe(III)(phtmeimb)₂]⁺ (**11**) both in solution at high concentrations (70 mM) [252], as well as upon deposition on solid films [253].



There, an excited Fe(III)-molecule and a GS Fe(III)-molecule, can engage in SET, affording the Fe(II)- and Fe(IV)-GS. The impact such reactivity can have for heterogenised photocatalysis is as of now not sufficiently explored and further investigations will be needed. While this way of accessing the Fe(II)-GS can provide the reducing equivalents needed for parts of the reaction to be driven while omitting the use of sacrificial reductants, the SET from the ES is a necessary step in some reactions and thus, SBCS could pose an issue for certain photocatalytic transformations, such as the herein shown dehalogenation. However, in the systems we have investigated here, it appears that higher surface coverage in the given concentration range is still beneficial to photocatalytic activity.

8.5 Conclusion and Future Plans

Although the investigations presented in this chapter are still at a rather early stage, the stability of the Al_2O_3 -NP-supported Fe(III)-NHC complexes Al_2O_3 -(**18**) and Al_2O_3 -(**19**) in different solvents and demonstration of their photocatalytic activity in a dehalogenation reaction show that this approach towards making these PCs even more sustainable might be promising.

Optimisation of the PC-loading on the NPs will be required in the future, although simultaneously, the potential charge-disproportionation between Fe(III)-ESs and Fe(III)-GSs should be taken into account. The use of co-adsorbents—molecules that feature anchoring groups and thus also attach to the metal oxide surface and that can serve as spacers between the dye-molecules without participating in the photocatalytic reaction—could also be investigated with respect to their impact on photocatalytic activity and possible prevention of SBCS.

Furthermore, improving the strength of binding to the metal-oxide surface could be beneficial, with the goal of decreasing the degree of PC-desorption and subsequent decline in catalytic activity. To this end, different anchoring groups could be tested which might allow for stronger binding to the metal oxide-surface. Additionally, other inert support materials could furthermore be investigated, such as SiO_2 , indium tin oxide (ITO) or ZrO_2 .

Once the heterogenised Fe(III)-NHC complexes have been optimised with regard to their composition, the scope of photoredox reactions can be expanded beyond dehalogenation reactions and the reusability under different reaction conditions can be studied.

9 Concluding Remarks & Outlook

Photoactive complexes based on iron with sufficiently long ES lifetimes to allow for diffusion-controlled SET from their CT states have been considered a holy grail for many years. The inherently unfavourable photophysical properties of many such compounds have thus presented a rather large obstacle towards achieving the desired reactivity—an issue that was mitigated by the introduction of strongly σ -donating ligands, which aid in counteracting the rapid deactivation of the ES. The resulting Fe-NHC complexes featured substantially longer ES lifetimes of their CT states, ranging from hundreds of ps to the low ns. Regardless of the fact that longer ES lifetimes than that have oftentimes been stated as crucial for bimolecular reactions, the goal of this thesis work was to investigate the potential applicability of Fe-NHC complexes for photocatalysis, shining a light on their merits and possible limitations and give insight into mechanistic aspects that could aid the improvement of such systems, be that through adjustments to the catalyst design or modification of reaction conditions. Consequently, Fe-NHC complexes have been employed as PSs for artificial photosynthesis and photoredox catalysis of organic reactions in this work, and the underlying mechanisms have been investigated thoroughly.

Chapter 5 addressed the investigation of $[\text{Fe}(\text{III})(\text{phtmeimb})_2]^+$ (**11**) as PS in HERs (Paper I), where the 2 ns-lifetime of this complex' $^2\text{LMCT}$ state was utilised, to generate hydrogen gas from an organic acid, $[\text{HNEt}_3][\text{BF}_4]$, using either Pt-colloids or a molecular PRC based on Earth-abundant cobalt (**12**) (Paper I). There, TONs of up to 1300 were obtained under green light irradiation, vastly outcompeting previous attempts at producing hydrogen with Fe-NHC complexes as the light-harvesting component of the reaction system. While initial reaction rates for our complex (**11**) were significantly lower compared to the archetypal $[\text{Ru}(\text{II})(\text{bpy})_3]^{2+}$ (**1**), superior long-term photostability allowed for sustained hydrogen evolution over a longer time, effectively resulting in the production of larger amounts of hydrogen. The difference in initial TOFs was rationalised by the fact that, while the quenching rates for the bimolecular quenching of (**11**) with the trialkylamine-based sacrificial reductants in the reaction solvent acetonitrile were sufficiently high to indicated that this step occurred via a diffusion-controlled process, the CEYs of the electron transfer products were rather low (2–3 %). These results were furthermore in line with the overall quantum yields for the hydrogen production of 1.1–1.3 % using (**11**). Attempts at improving the reactivity through increasing the CEYs by changing the reaction solvent acetonitrile to, amongst

others, DCM—a solvent known to enable significantly higher CEYs for the RQ of (11) by trialkylamines than acetonitrile—resulted in no or significantly less hydrogen being produced. Therefore, we could show that while certain changes to the reaction conditions can prove beneficial to isolated steps of the reaction mechanism, for more complex reactions, these effects can be multi-faceted and thus more challenging to exploit, as the reactivity might be impeded in another step. Hydrogen evolution from water was not feasible under the reaction conditions used in this study, as was shown upon replacement of $[\text{HNEt}_3][\text{BF}_4]$ with water as a proton source, where the protons for the product formation were presumably obtained through the decomposition pathways undergone by the trialkylamines used as sacrificial reductants. While the poor solubility of (11) might partially contribute to the lack of hydrogen production from water, the reasons for the inactivity are still unclear. In order to improve upon the herein described system, further investigations and modifications will thus be needed. One such change could be the use of other sacrificial reductants.

Additionally, CO_2 -reduction to CO, sensitised by (11), was attempted with different reduction catalysts. However, no catalytic CO-formation has been observed, warranting further testing in the future. Change of the sacrificial electron donor could also prove beneficial in this case, as higher quenching efficiencies might be needed to drive this thermodynamically challenging process. Furthermore, to enhance the catalytic performance of Fe-NHC complexes as PS for reduction reactions in artificial photosynthesis, the design of compounds with not just sufficiently long ES lifetimes but also higher reducing power being accessed in the Fe(II)-GS is essential, so that certain reaction steps do not rely on the generation of reducing decomposition products such as α -aminoalkyl radicals or $\text{CO}_2^{\cdot-}$.

In light of these problems, particularly in the case of artificial photosynthesis reactions, the use of molecular dyads or anchoring of the Fe-NHC complexes to semiconductor materials could be advantageous, allowing for the circumvention of several issues associated with diffusion-controlled SET processes.

In Chapter 6, some of the first substantiated examples of organic photoredox reactions driven by outer-sphere quenching of the CT states of Fe-NHC complexes are presented. The results of Paper II showcase that $[\text{Fe}(\text{III})(\text{btz})_3]^{3+/2+}$ (9)/(10)—a complex with two photoactive oxidation states exhibiting sub-ns lifetimes of the $^2\text{LMCT}$ state of the Fe(III)- and $^3\text{MLCT}$ state of the Fe(II)-congener—could be used to drive a benchmark photoredox reaction, the ATRA reaction, under green light irradiation. Bimolecular RQ of the ES of the Fe(III)-PC (9) gave access to the Fe(II)-GS (10), which itself also undergoes excitation at the irradiation wavelength, affording the even more strongly reducing Fe(II)-ES. Thereby, two photons per catalytic turnover are utilised, giving access to the higher energy required to catalyse the target reaction under these reaction conditions in a mechanistic facsimile of the Z-scheme known from photosynthesis. Furthermore, the OQ of the ES of (9) was used for efficient product formation whilst

allowing for the omission of sacrificial reagents—albeit higher catalyst loadings were needed to maintain comparable reactivities between the two routes. This study in particular showcases that even ES lifetimes in the hundreds of picoseconds are sufficient for photoredox catalysis via collisional quenching of CT states in iron-based PCs—given that the bimolecular quenching occurs at appreciable rates and that the cage escape of electron-transfer products is sufficiently high.

The study in Paper III featuring $[\text{Fe}(\text{III})(\text{phtmeimb})_2]^+$ (11) highlights that these PCs can furthermore catalyse synthetically valuable reactions beyond classical benchmark reactions that have been demonstrated as a proof-of-principle to study the photochemical properties of these systems. There, aminomethylations of electron-deficient alkenes are made possible by SET from α -trimethylsilylamines to the $^2\text{LMCT}$ state of (11), giving rise to the Fe(II)-GS and amine radical cations that undergo bond fission of the Si–C(α)-bond to afford the corresponding α -aminoalkyl radicals. Said highly nucleophilic α -aminoalkyl radicals could be trapped by electron-poor alkenes, allowing for the synthesis of highly functionalised *N*-containing compounds within just one step. Through mechanistic investigations, it was revealed that the quenching of the $^2\text{LMCT}$ state of (11) transpired via a combination of dynamic and static quenching. While collisional quenching rates were similar to previously reported values found for regular tertiary amines, the CEYs in DMF of the resulting electron-transfer products were higher for α -trimethylsilylamines. This, along with the fact that α -aminoalkyl radical formation occurs more selectively from these species, makes α -trimethylsilylamines attractive quenchers for (11), not only for the generation of synthetic building blocks but also for example to produce reducing species in a more efficient and targeted fashion for e.g., artificial photosynthesis applications. In this study, we were furthermore able to spectroscopically follow the recovery of the Fe(III)-GS, corresponding to catalytic turnover, giving insight into a part of the catalytic cycle that is usually less thoroughly explored. Consequently, the results described in that chapter serve to showcase both the opportunities but also some of the limitations associated with Fe-NHC complexes in the context of photoredox catalysis for organic transformations.

Both for artificial photosynthesis reactions as well as organic photoredox catalysis, the comparatively low reducing power of the herein encountered Fe(II)-GSs impose restrictions on the applicability of these complexes. However, as shown in Paper II, sequential excitation of two photoactive oxidation states, if feasible, can aid in boosting the reactivity. In Chapter 7 (Paper IV), $[\text{Fe}(\text{II})(\text{phtmeimb})_2]$ (17) was investigated with regard to its photophysical and -chemical properties, due to the 2 ns-lifetime of its Fe(III)-congener (11). There, it was however found that this Fe(II)-complex possesses a $^3\text{MLCT}$ lifetime of only 5 ps, attributed to an essentially barrierless decay to the ^3MC state, which precludes its utilisation for photocatalytic applications relying on diffusion-controlled bimolecular quenching processes. Characterisation of (17) by NMR

spectroscopy revealed a strong downfield shift of the carbene-C (216.9 ppm), attesting to the σ -donating properties of the NHC-motif. Since the corresponding Fe(III)-complex (11) had exhibited remarkable photostability as demonstrated in Paper I, the photodegradation of [Fe(II)(phtmeimb)₂] (17) and [Fe(II)(btz)₃]²⁺ (10) was also investigated by irradiation at 375 nm and 525 nm respectively. In both cases, degradation within few hours was observed, likely as a result of the Fe–C(carbene) bond being weakened in the MC state. With Fe(II)-complexes exhibiting long-lived ³MLCT states remaining elusive, the photostability of Fe(III)-NHC complexes such as (11) offers additional motivation for ²LMCT state-driven photocatalysis, beyond the so far reported applications, not to be disregarded.

One major incentive for the studies described in this thesis was to establish Fe-NHC complexes as a more sustainable alternative to noble metal-based PSs for photocatalytic applications. However, the fact that quantum yields of the reactions performed with these complexes are comparatively low and their syntheses involve several steps, some of which can be low-yielding, invites the question of whether their sustainability can actually be considered a key advantage at this point in time. Consequently, in some instances, it could be argued that the catalytic efficiencies, better quantum yields and overall reactivities that can be accessed via noble metal-PSs, as well as their commercial availability or facile synthetic preparation, might validate their usage over Fe-NHC complexes. However, the sheer abundance of iron, combined with the demonstrated superior photostability of the Fe(III)-*hexa*-NHC complex with the longest ES lifetime to date, still makes a compelling case for the sustainability of these systems. Therefore, in Chapter 8, the photostability of (11) and its favourable photophysical properties, which remain unchanged upon introduction of carboxylic acid-moieties on the phenyl-groups present in this molecule, were utilised in an attempt to improve the recyclability of Fe(III)-NHC PCs by heterogenisation via anchoring to an inert solid support. There, Al₂O₃ NPs were sensitised with the homoleptic complex [Fe(coohphtmeimb)₂]PF₆ (18) as well as the newly synthesised heteroleptic complex [Fe(phtmeimb)(coohphtmeimb)]PF₆ (19) and the solvent stability of the resulting heterogenised PCs was investigated. Furthermore, the photocatalytic activity and recyclability of the heterogenised Fe(III)-NHC complexes were probed in a simple dehalogenation reaction, revealing that over four runs conversion of the starting material can be observed, although it gradually decreases. This study is currently still at an early stage, but could serve to facilitate the reusability of Fe(III)-NHC complexes in photocatalytic applications—although further optimisations are needed.

The investigations presented in this thesis have, amongst other things, revealed that Fe(III)-*hexa*-NHC complexes exhibit substantially improved photostability compared to the prevalent archetypal noble metal PSs. The examples of photocatalytic applications using Fe-NHC complexes discussed herein furthermore aid in counteracting the general notion that rather long ES lifetimes are crucial for reactions

to be driven via diffusion-controlled outer-sphere electron transfer reactions, whilst not negating that extending them further would most certainly be advantageous and thus remains desirable. However, the Fe-NHC complexes currently at our disposal exhibit limited redox potentials and low CEYs. While the latter could potentially be improved by modification of the reaction conditions, adjustment to the former necessitate changes in structural design. These issues currently pose barriers for the more widespread application of Fe-NHC complexes in photocatalysis. Nevertheless, studies such as the ones presented in this thesis work, can give invaluable information about mechanistic intricacies that govern the observed reactivity, paving the way for future optimisations. The interplay between synthetic organic and organometallic chemistry, computational chemistry and spectroscopic techniques is crucial to expediting the development of the field of photocatalysis and by utilising insights from all of these areas iron could potentially face a bright future.

10 Supporting Information

10.1 CO₂-Reduction sensitised by an Fe(III)-NHC complex

10.1.1 General Information

All solvents and sacrificial reductants were obtained from commercial suppliers and used without further purification. [Fe(phtmeimb)₂]PF₆ (**11**) [12], [Co(TIM)Br₂]Br (**13**) [189], [Co(L^{N3})Cl](OTf)₂ (**14**) [190], *fac*-[Re(bpy)(CO)₃(MeCN)] (**15**) [191] and *fac*-[Re(bpy)(CO)₃Cl] (**16**) [254] were synthesised according to literature procedure. CO₂ was purchased from Linde Gas and used directly from the gas cylinder.

10.1.2 Experimental Details

Photoreactions were conducted in a TAK120 AC photoreactor purchased from HK Testsysteme GmbH. Irradiation was performed using the green LED array ($\lambda_{\text{irr}} = 530 \text{ nm}$, 3.15 W/slot unless otherwise indicated) and a reaction temperature of 28–32 °C. Reaction solutions were contained in 4.9 mL clear glass vials with screw caps featuring a PTFE/silicone septum and flushed with CO₂ (g) for 5 min.

The amount of CO in the headspace was determined using a custom-built Raman based spectrometer. To this end, amount of CO dissolved in the solvent was considered to be very minor compared to the amount in the headspace.

10.1.3 Results

Table S1: Testing of the photocatalytic reduction of CO₂ to CO using [Co(TIM)Br₂]Br (**13**) as catalyst and [Fe(III)(phtmeimb)₂]PF₆ (**11**) as PS ($\lambda_{\text{irr}} = 530$ nm, 3.15 W/slot, all results given as an average of duplicate measurements, n.d. = not detected, ^aTON = mol H₂ / mol PRC).

Cat	[Cat] (mM)	PS	[PS] (mM)	Sacrificial Reductant	[Q] (M)	Solvent	Time (h)	CO (μmol)	TON ^a
(13)	10	(11)	1	TEA	0.5	MeCN: MeOH (4:3)	18	2.41	<1
(13)	10	(11)	1	TEOA	0.5	MeCN: MeOH (4:3)	18	4.45	<1
(13)	10	(11)	1	TEA	1	MeCN: MeOH (4:3)	18	2.52	<1
(13)	10	(11)	1	TEOA	1	MeCN: MeOH (4:3)	18	4.59	<1
(13)	1	(11)	1	TEOA	0.5	DMF	21	n.d.	–
(13)	2	(11)	1	TEOA	0.5	DMF	21	n.d.	–
(13)	5	(11)	1	TEOA	0.5	DMF	21	n.d.	–
(13)	10	(11)	1	TEOA	0.5	DMF	21	n.d.	–

Table S2: Testing of the photocatalytic reduction of CO₂ to CO using [Co(L^{N3})Cl](OTf)₂ (**14**) as catalyst and [Fe(III)(phtmeimb)₂]PF₆ (**11**) as PS ($\lambda_{\text{irr}} = 530$ nm, 3.15 W/slot, n.d. = not detected, ^aTON = mol H₂ / mol PRC).

Cat	[Cat] (mM)	PS	[PS] (mM)	Sacrificial Reductant	[Q] (M)	Solvent	Time (h)	CO (μmol)	TON ^a
(14)	1	(11)	1	TEA	0.5	DMF	20	n.d.	–
(14)	1	(11)	1	TEOA	0.5	DMF	20	n.d.	–
(14)	1	–	–	TEA	0.5	DMF	20	n.d.	–

Table S3: Testing of the photocatalytic reduction of CO₂ to CO using *fac*-[Re(bpy)(CO)₃(MeCN)] (**15**) as catalyst and [Fe(III)(phtmeimb)₂]PF₆ (**11**) as PS (λ_{irr} = 530 nm, n.d. = not detected, ^aTON = mol H₂ / mol PRC, ^b3.15 W/slot, ^c1.51 W/slot).

Cat	[Cat] (mM)	PS	[PS] (mM)	Sacrificial Reductant	[Q] (M)	Solvent	Time (h)	CO (μ mol)	TON ^a
(15) ^b	0.5	(11)	0.5	TEOA	0.5	DMF	20	19.1	19
(15) ^b	0.5	–	–	TEOA	0.5	DMF	20	30.3	30
(15) ^c	0.5	(11)	0.5	TEOA	0.5	DMF	20	12.9	13
(15) ^c	0.5	–	–	TEOA	0.5	DMF	20	6.5	7

Table S4: Testing of the photocatalytic reduction of CO₂ to CO using *fac*-[Re(bpy)(CO)₃Cl] (**16**) as catalyst and [Fe(III)(phtmeimb)₂]PF₆ (**11**) as PS (λ_{irr} = 530 nm, 1.51 W/slot, n.d. = not detected, ^aTON = mol H₂ / mol PRC).

Cat	[Cat] (mM)	PS	[PS] (mM)	Sacrificial Reductant	[Q] (M)	Solvent	Time (h)	CO (μ mol)	TON ^a
(16)	0.5	(11)	0.5	TEOA	0.5	DMF	20	34.1	34
(16)	0.5	–	–	TEOA	0.5	DMF	20	52.0	52

10.2 Heterogenisation of Fe(III)-NHC Complexes for Photoredox Catalysis

10.2.1 Materials & Methods

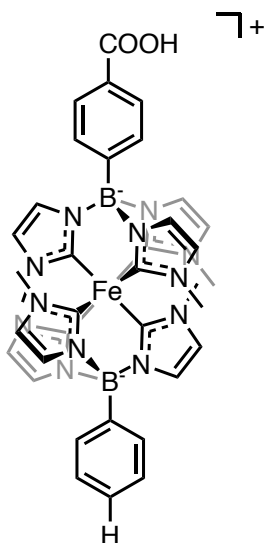
10.2.1.1 Synthesis and Characterisation

The ligands L1 and L2 as well as complex (18) were prepared following literature procedures [12, 249]. All solvents used in work-up procedures, for silica gel or alumina column chromatography, and for sensitisation of Al₂O₃-nanoparticles were obtained from commercial suppliers and used without further purification. THF was dried over Na/benzophenone and subsequently distilled under nitrogen prior to use. Flash column chromatography was performed using Merck silica gel (pore size 60 Å, 230–400 mesh particle size, particle size 0.043–0.063 mm) or Merck aluminium oxide 90 active neutral (0.063–0.200 mm, 70–230 mesh ASTM). NMR spectra were recorded at ambient temperature on a BrukerAvance II 400 MHz NMR spectrometer (400/101 MHz ¹H/¹³C). Chemical shifts (δ) for ¹H and ¹³C NMR spectra are reported in parts per million (ppm), relative to the residual solvent peak of the respective NMR solvent (DMSO-*d*₆ ($\delta_{\text{H}} = 2.50$ and $\delta_{\text{C}} = 39.5$ ppm)). Coupling constants (*J*) are given in Hertz (Hz), with the multiplicities being denoted as follows: singlet (s), doublet (d), triplet (t), quartet (q), quintet (qi), multiplet (m), broad (br). NMR spectra for ¹³C were recorded with decoupling from ¹H. Electrospray ionization–high resolution mass spectrometry (ESI–HRMS) and atmospheric pressure chemical ionization (APCI) for mass spectrometry were recorded on a Waters Micromass Q-ToF micro mass spectrometer. Elemental analyses were performed by Mikroanalytisches Laboratorium KOLBE (Oberhausen, Germany).

10.2.1.2 Photocatalytic Reactions

Photoreactions were conducted in a TAK120 AC photoreactor purchased from HK Testsysteme GmbH. Irradiation was performed using the green LED array ($\lambda_{\text{irr}} = 530$ nm, 3.15 W/slot unless otherwise indicated) and a reaction temperature of 28–32 °C. Reaction solutions were contained in 4.9 mL clear glass vials with screw caps featuring a PTFE/silicone septum.

10.2.2 Synthesis of the Fe(III)-NHC complex (19)



[Fe(III)(phtmeimb)(coohphtmeimb)]⁺ (19)

[Phenyltris(3-methyl-1*H*-imidazol-3-ium-1-yl)borate] di(hexafluorophosphate) (L1) (1.45 g, 2.32 mmol, 0.5 equiv.) and [(4-bromophenyl)tris(3-methyl-1*H*-imidazol-3-ium-1-yl)borate] di(hexafluorophosphate) (L2) (1.63 g, 2.32 mmol, 0.5 equiv.) were dried in vacuo overnight at 80 °C. Potassium *tert*-butoxide (1 M in THF, 16.3 mL, 16.24 mmol, 3.5 equiv.) was added dropwise to a suspension of (L1) and (L2) in dry THF (80 mL) at -78 °C affording a light-yellow solution. After stirring for 30 min at that temperature, the cooling was removed and a solution of FeBr₂ (699 mg, 3.25 mmol, 0.7 equiv.) in THF (30 mL) was added at once after the yellow ligand solution had turned to a dark orange colour. The reaction mixture turned dark brown and was allowed to reach room temperature before stirring overnight in the dark under Ar (g). The mixture was exposed to air, leading to a colour change to burgundy red, and the solvent was removed under reduced pressure. The residue was taken up in DCM and filtered through a pad of celite and dried over MgSO₄ before concentrating and drying in vacuo. The red residue was then dissolved in a minute amount of DCM before reprecipitation by addition of diethyl ether, which was repeated twice. The precipitate was purified by silica gel column chromatography (3.5 × 17 cm, toluene : acetonitrile, 3:1, v/v) affording a dark red solid, which was a mixture of the desired heteroleptic precursor-complex [Fe(III)(phtmeimb)(brphtmeimb)]PF₆ and the homoleptic analogues [Fe(III)(brphtmeimb)₂]PF₆ and [Fe(III)(phtmeimb)₂]PF₆ (11). (Yield of the mixture: 803 mg)

This mixture (803 mg) was suspended in anhydrous THF after drying in vacuo at 45 °C overnight and cooled to -78 °C. *n*-BuLi (2.5 M in hexanes, 1.8 mL, 1.8 mmol, 5 equiv.) was added dropwise leading to a colour change to dark yellow. The reaction mixture was stirred at that temperature for 1.5 h. CO₂ (g, from a gas cylinder) was bubbled through the solution, upon which it changed colour from yellow back to red. The cooling was removed and stirring was continued at room temperature for another hour before removing the CO₂-inlet. The solvent was then removed under reduced pressure and the burgundy red residue was suspended in water, acidified with HPF₆ (55 % aq., to pH 2) and stirred vigorously for 1 h. The resulting fluffy red precipitate was filtered, washed with water and dried in vacuo overnight.

The mixture of products was separated by column chromatography (activated neutral alumina, acetonitrile → acetonitrile : water 4:1, v/v → acetonitrile : water 2:1 + 1 % HCl v/v) affording the desired product (**19**) (247 mg, 12 % over 2 steps) as well as the homoleptic complexes (**11**) (184 mg, 9 % over 2 steps) and (**18**) (87 mg, 4 %, over 2 steps).

¹H NMR (400 MHz, DMSO-*d*₆): δ 14.82 (s, 2H), 14.68 (s, 2H), 11.00–10.87 (m, 2H), 10.49–10.29 (m, 2H), 9.82–9.65 (m, 1H), 5.07 (s, 18H), 1.11 (s, 3H), 1.02 (s, 3H), -11.85 (s, 3H), -12.12 (s, 3H). ¹³C NMR (101 MHz, DMSO-*d*₆): δ 169.5, 139.3 (d, J = 18.2 Hz), 133.2, 132.3, 131.6, 130.9, 49.4 (d, J = 39.5 Hz), 16.0, 14.9, -29.7. ESI-HRMS calculated m/z = 762.2933, found m/z = 763.2951 for C₃₇H₄₀B₂N₁₂O₂Fe⁺; calculated m/z = 144.9642, found m/z = 144.9635 for PF₆⁻. Elemental analysis for C₃₇H₄₀B₂N₁₂O₂FePF₆ (% calcd, % found): C (48.98, 48.91), H (4.44, 4.41), N (18.53, 18.51).

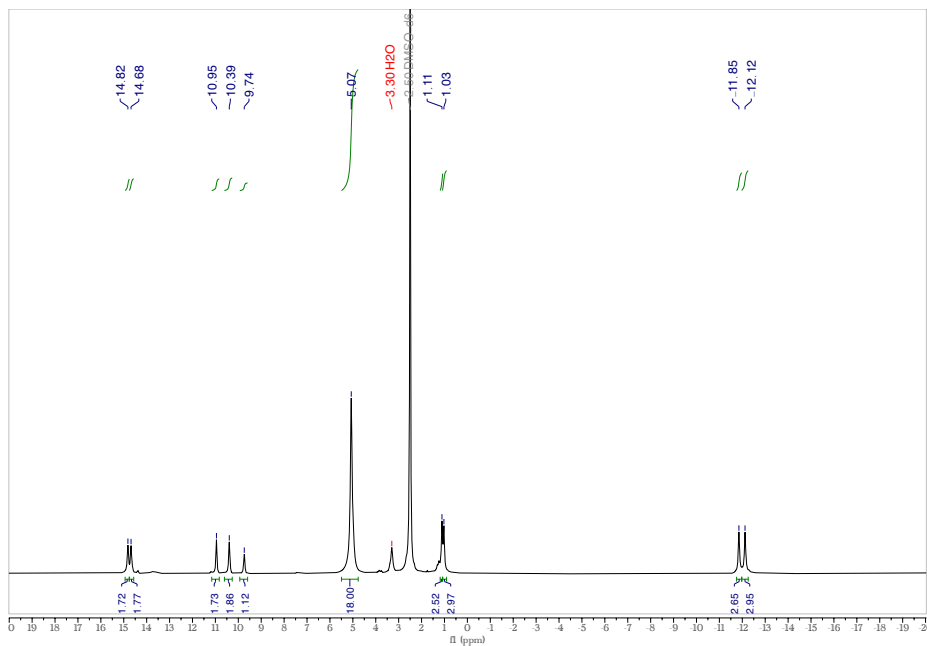


Figure 10.1: ^1H NMR (400 Hz) spectrum of (19) in $\text{DMSO}-d_6$.

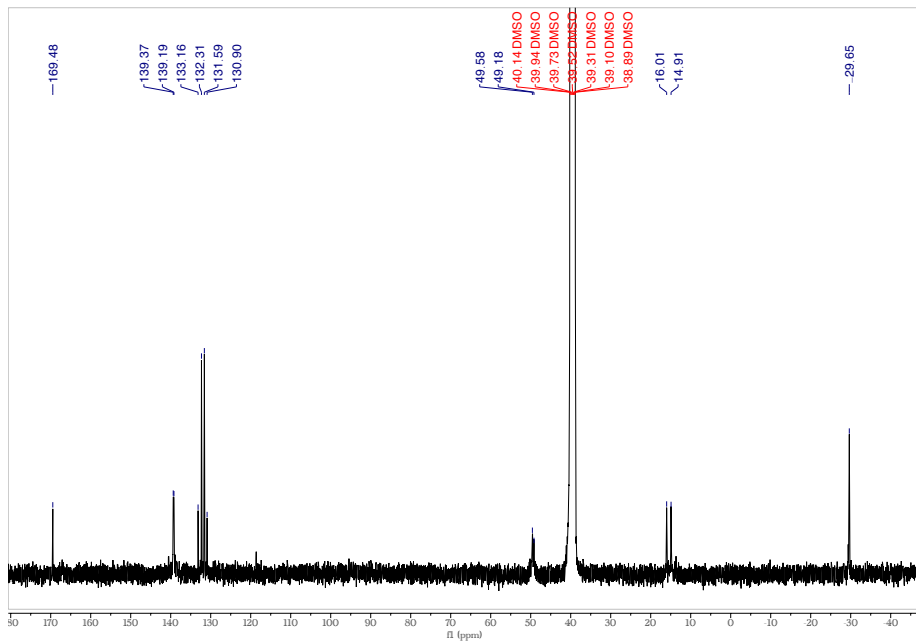


Figure 10.2: ^{13}C NMR (101 Hz) spectrum of (19) in $\text{DMSO}-d_6$.

10.2.3 Steady-State Emission Spectroscopy

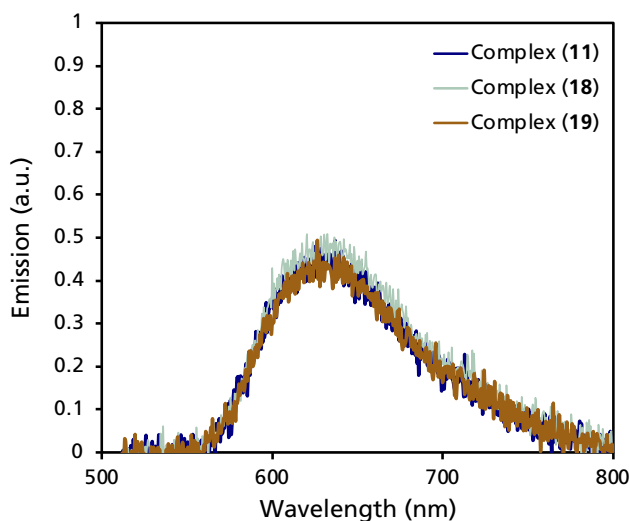


Figure 10.3: Steady-state emission spectra of the Fe(III)-NHC complexes (11), (18) and (19) in MeOH.

10.2.4 Preparation of the sensitised Al₂O₃-Nanoparticles

The preparation of the sensitised Al₂O₃-NPs was performed using a modified literature procedure [251]. To 100 mg Al₂O₃ (nanopowder, <50 nm particle size (TEM)), 10 mL of a solution of the PC in methanol with the indicated concentration was added and the resulting suspension was stirred in the dark overnight. Thereafter, the sensitised Al₂O₃-NPs were separated from the supernatant solution by centrifugation and washed thrice with methanol before drying in vacuo. The PC-loading on the NP-surface was determined using the depletion method, where the consumption of the dye from the sensitisation solution is quantified by UV–VIS absorption spectroscopy.

10.2.5 Photocatalytic Dehalogenations

A 4.9 mL clear glass vial was charged with 4-bromobenzyl 2-chloro-2-phenylacetate (S30) (0.15 mmol, 50.65 mg), NEt₃ (1.76 mmol, 254 μL) in DCM (2.5 mL) the respective PC (30 mg) before flushing with Ar (g) for 3 min. The samples were then irradiated at 530 nm (3.15 W/slot) under vigorous stirring for 10 h. Upon completion, the PC was separated from the reaction solution by centrifugation, washed with DCM and dried for further usage. The conversion of starting material to product was determined using ¹H NMR spectroscopy.

Acknowledgements

During the four years of my PhD studies, I had the pleasure of enjoying the constant support of a large number of amazing people without whom the work presented within this thesis would not have been possible.

First of all, I would like to sincerely thank my supervisor **Kenneth** for giving me the opportunity to pursue my PhD studies in his research group and to work on engaging and challenging projects. I have also appreciated that you have not just allowed but encouraged me to work on my own ideas and have always heard me out, even if we did not agree at all times. Thank you for all your support!

Furthermore, I would like to express my gratitude to my co-supervisor **Ola**. I have learnt a lot during my time in your research group as a MSc student, which I truly enjoyed, and I have valued your support both back then and during my PhD. Thank you also to **Ulf N.**, for your work as my department representative and the helpful discussions we had during my ISP meetings and staff appraisal talks.

CAS has been a very open and welcoming workplace and I want to thank all former and current members for making it so. In particular, thank you to **Maria** and **Sara** for your unfailing support in all administrative matters, to **Kornelije** for help with instruments and other issues in the lab, to **KC Purchase**, especially **Katarina F.**, for all the assistance with buying chemicals and equipment as well as **Sofia**, **Annette** and **Fiona** for all help with HRMS and our LC-MS and **Zoltán** for your never-ceasing efforts and help with NMR-related issues. I also had the pleasure of teaching during my PhD studies, which has been a very gratifying experience, and here I want to thank **Sophie Manner** for all your support.

There is one particular group of people at CAS that I have cherished immensely during my PhD—the **KW group**, both past and current members. Particularly the PhD students have been nothing but supportive, inspiring and motivating throughout my time here and I am more than happy to say that I do not see you just as my colleagues but as my friends. In no particular order, thank you: **Anna**, I am very grateful to have had you as my friend, Pepsi-buddy and never-ending source of memes and reels. You have always had an open ear when I wanted to vent and have given perspective when needed. **Jesper**, my “PhD twin”. We applied to the same position and started on the exact same day, worked together on several shared projects, were office and course

mates. I have truly appreciated sharing this entire journey with you! Thank you also for your feedback on my thesis! **Samuel**, your wit, sense of humour and kindness are just some of the attributes I have valued throughout our joint time here—but most importantly you have been an amazing Lucia-buddy! **Valtýr**, you have been nothing but fun, warm and welcoming ever since I joined the group and our time as lab mates has been something I cherish a lot—despite my nagging about the cleanliness. You have also been a great neighbour and friend! **Lisa**, thank you for helping me get started in the group with administrative- and research-related matters and for the collaboration on the ATRA project and the Perspective article, through all of which I learnt a lot. **Vicky**, thank you for your input on chemistry questions and for sharing some Chinese recipes and dishes with me! **Eric**, it has been a lot of fun spending time with you, both in the lab and outside of it. I appreciate that you don't take yourself too seriously and can always take a joke. **Clara**, you have been a great addition to the group and it has been great getting to know you. I am very excited to see you continue the work on the photocatalysis projects! Furthermore, I'd like to thank the Postdocs that have been in our group and from whom I have learned a lot, be that research-related or on a personal level: **Simon K.**, **Hao**, **Om**, **Alpesh**, **Yogesh**, **Suresh**, **Dnyaneshwar**, **Arvind** and **Abhishek**. I also want to express my sincere appreciation for my students **Benjamin** and **Simon H.** for your hard work on Paper III. It has been a real pleasure to supervise both of you and to have you as fellow group members!

Thank you also to fellow CAS-PhD students that I got to meet and spend time with over the years, be that in courses, through teaching or social activities: **Nitish**, **Fredrik**, **Roberto**, **Joachim**, **Mikélis**, **Simon E.**, **Mattias**, **Leo**, **Oksana**, **Josep**, and many more.

Throughout my PhD studies I also had the privilege of collaborating with a number of researchers outside of our group, through all of whom I have learned a lot. I want to extend my gratitude towards all of them, both named and unnamed, but in particular to **Catherine** and **Reiner** at Uppsala University for all your work contributing to all papers presented in this thesis and the fruitful discussions we have had over the years. Thank you also to everyone at ChemPhys, whom I have in one way or another worked together with, but first and foremost the members of the former Junior FeCAB group, **Linneá**, **Pavel**, **Nils**, **Yen** and **Iria**. Also thank you to our collaborators in the US, **Elena** and **Mawuli**, for the computational work in Paper IV and interesting discussions.

I furthermore want to thank **Tea**, **Hanna** and **Ante**. You were my first Swedish friends and I am very grateful to have met you during our MSc studies. Thank you for many evenings spent together and countless fun moments, which have helped me take a mental break from my research when it was most needed!

Another source of calm and stress relief during my time here in Lund has been all the time spent playing recreational volleyball at Lunds VK and I am grateful to all my friends and teammates there for this great outlet.

But most importantly, none of this would have been even remotely possible without the unwavering support of my family. **Mama** und **Papa**, ihr habt mich mein ganzes Leben lang unterstützt und dazu ermuntert, meine Träume und Ziele zu verfolgen. Ohne euch wäre ich niemals so weit gekommen und ich werde nie ausdrücken können, wie dankbar ich bin, euch zu haben. **Danijel**, dich als großen Bruder zu haben, bedeutet, immer jemanden zu haben, auf den ich mich vollkommen verlassen und zu dem ich aufblicken kann. Danke für alles! Želela bih takođe od srca da se zahvalim svojim **babama** i **dedama**, kako živima tako i nažalost preminulima, što su bili tako važan deo mog života i što su me podržavali svako na svoj način.

Last but most certainly not least, I want to thank my fiancé **Lukas**. Over the past almost 10 years together, you have unfailingly supported, encouraged and inspired me. I am immensely glad that you chose to move to Sweden for your own PhD studies, which led me to follow and share in this adventure with you. I cannot wait to see what our next step together will be and to face new adventures with you by my side.

Aleksandra Ilić
Lund, April 2024

References

1. Megía, P.J., Vizcaíno, A.J., Calles, J.A., and Carrero, A., *Hydrogen Production Technologies: From Fossil Fuels toward Renewable Sources. A Mini Review*. Energy & Fuels, 2021. **35**(20): p. 16403-16415.
2. BP. *Statistical Review of World Energy*. 2021; Available from: <https://www.bp.com/content/dam/bp/business-sites/en/global/corporate/pdfs/energy-economics/statistical-review/bp-stats-review-2021-full-report.pdf>.
3. OECD, *World Energy Outlook 2023*. 2023.
4. Amin, M., Shah, H.H., Fareed, A.G., Khan, W.U., Chung, E., Zia, A., Rahman Farooqi, Z.U., and Lee, C., *Hydrogen production through renewable and non-renewable energy processes and their impact on climate change*. Int. J. Hydrogen Energy, 2022. **47**(77): p. 33112-33134.
5. IPCC, *Climate Change 2021: The Physical Science Basis. Contribution of Working Group I to the Sixth Assessment Report of the Intergovernmental Panel on Climate Change*, V. Masson-Delmotte, P. Zhai, A. Pirani, S.L. Connors, C. Péan, S. Berger, N. Caud, Y. Chen, L. Goldfarb, M.I. Gomis, M. Huang, K. Leitzell, E. Lonnoy, J.B.R. Matthews, T.K. Maycock, T. Waterfield, O. Yelekçi, R. Yu, and B. Zhou, Editors. 2021: Cambridge University Press. In Press.
6. Morton, O., *Solar energy: a new day dawning? Silicon Valley sunrise*. Nature, 2006. **443**(7107): p. 19-22.
7. *Tables for Reference Solar Spectral Irradiances: Direct Normal and Hemispherical on 37° Tilted Surface*. ASTM International.
8. Gueymard, C.A., *The sun's total and spectral irradiance for solar energy applications and solar radiation models*. Solar Energy, 2004. **76**(4): p. 423-453.
9. Narayanam, J.M. and Stephenson, C.R., *Visible light photoredox catalysis: applications in organic synthesis*. Chem. Soc. Rev., 2011. **40**(1): p. 102-13.

10. Chábera, P., Liu, Y., Prakash, O., Thyraug, E., Nahhas, A.E., Honarfar, A., Essen, S., Fredin, L.A., Harlang, T.C., Kjær, K.S., Handrup, K., Ericson, F., Tatsuno, H., Morgan, K., Schnadt, J., Häggström, L., Ericsson, T., Sobkowiak, A., Lidin, S., Huang, P., Styring, S., Uhlig, J., Bendix, J., Lomoth, R., Sundström, V., Persson, P., and Wärnmark, K., *A low-spin Fe(III) complex with 100-ps ligand-to-metal charge transfer photoluminescence*. *Nature*, 2017. 543(7647): p. 695-699.
11. Chábera, P., Kjær, K.S., Prakash, O., Honarfar, A., Liu, Y., Fredin, L.A., Harlang, T.C.B., Lidin, S., Uhlig, J., Sundström, V., Lomoth, R., Persson, P., and Wärnmark, K., *Fe^{II} Hexa N -Heterocyclic Carbene Complex with a 528 ps Metal-to-Ligand Charge-Transfer Excited-State Lifetime*. *J. Phys. Chem. Lett.* 2018. 9(3): p. 459-463.
12. Kjær, K.S., Kaul, N., Prakash, O., Chábera, P., Rosemann, N.W., Honarfar, A., Gordivska, O., Fredin, L.A., Bergquist, K.E., Haggstrom, L., Ericsson, T., Lindh, L., Yartsev, A., Styring, S., Huang, P., Uhlig, J., Bendix, J., Strand, D., Sundström, V., Persson, P., Lomoth, R., and Wärnmark, K., *Luminescence and reactivity of a charge-transfer excited iron complex with nanosecond lifetime*. *Science*, 2019. 363(6424): p. 249-253.
13. Gong, J., Li, C., and Wasielewski, M.R., *Advances in solar energy conversion*. *Chem. Soc. Rev.*, 2019. 48(7): p. 1862-1864.
14. Fujishima, A. and Honda, K., *Electrochemical photolysis of water at a semiconductor electrode*. *Nature*, 1972. 238(5358): p. 37-8.
15. Sun, X., Jiang, S., Huang, H., Li, H., Jia, B., and Ma, T., *Solar Energy Catalysis*. *Angew. Chem. Int. Ed. Engl.*, 2022. 61(29): p. e202204880.
16. Swierk, J.R., *The Cost of Quantum Yield*. *Org. Process Res. Dev.*, 2023. 27(7): p. 1411-1419.
17. Sender, M. and Ziegenbalg, D., *Light Sources for Photochemical Processes – Estimation of Technological Potentials*. *Chem. Ing. Tech.*, 2017. 89(9): p. 1159-1173.
18. Buglioni, L., Raymenants, F., Slattery, A., Zondag, S.D.A., and Noel, T., *Technological Innovations in Photochemistry for Organic Synthesis: Flow Chemistry, High-Throughput Experimentation, Scale-up, and Photoelectrochemistry*. *Chem. Rev.*, 2022. 122(2): p. 2752-2906.
19. Marzo, L., Pagire, S.K., Reiser, O., and Konig, B., *Visible-Light Photocatalysis: Does It Make a Difference in Organic Synthesis?* *Angew. Chem. Int. Ed. Engl.*, 2018. 57(32): p. 10034-10072.
20. Michelin, C. and Hoffmann, N., *Photosensitization and Photocatalysis—Perspectives in Organic Synthesis*. *ACS Catal.*, 2018. 8(12): p. 12046-12055.
21. Kaufhold, S. and Wärnmark, K., *Design and Synthesis of Photoactive Iron N-Heterocyclic Carbene Complexes*. *Catalysts*, 2020. 10(1): p. 132.

22. Shaw, M.H., Twilton, J., and MacMillan, D.W.C., *Photoredox Catalysis in Organic Chemistry*. J. Org. Chem., 2016. **81**(16): p. 6898-6926.
23. Hossain, A., Engl, S., Lutsker, E., and Reiser, O., *Visible-Light-Mediated Regioselective Chlorosulfonylation of Alkenes and Alkynes: Introducing the Cu(II) Complex [Cu(dap)Cl₂] to Photochemical ATRA Reactions*. ACS Catal., 2019. **9**(2): p. 1103-1109.
24. Engl, S. and Reiser, O., *Making Copper Photocatalysis Even More Robust and Economic: Photoredox Catalysis with [Cu^{II}(dmp)₂Cl]Cl*. Eur. J. Org. Chem., 2020. **2020**(10): p. 1523-1533.
25. Tinker, L.L., McDaniel, N.D., Curtin, P.N., Smith, C.K., Ireland, M.J., and Bernhard, S., *Visible light induced catalytic water reduction without an electron relay*. Chem. - Eur. J., 2007. **13**(31): p. 8726-32.
26. Lazarides, T., McCormick, T., Du, P., Luo, G., Lindley, B., and Eisenberg, R., *Making hydrogen from water using a homogeneous system without noble metals*. J. Am. Chem. Soc., 2009. **131**(26): p. 9192-4.
27. Zhang, P., Wang, M., Na, Y., Li, X., Jiang, Y., and Sun, L., *Homogeneous photocatalytic production of hydrogen from water by a bioinspired [Fe₂S₂] catalyst with high turnover numbers*. Dalton Trans., 2010. **39**(5): p. 1204-6.
28. Prier, C.K., Rankic, D.A., and MacMillan, D.W.C., *Visible light photoredox catalysis with transition metal complexes: Applications in organic synthesis*. Chem. Rev. 2013. **113**(7): p. 5322-5363.
29. Luo, S.P., Mejia, E., Friedrich, A., Pazidis, A., Junge, H., Surkus, A.E., Jackstell, R., Denurra, S., Gladiali, S., Lochbrunner, S., and Beller, M., *Photocatalytic water reduction with copper-based photosensitizers: a noble-metal-free system*. Angew. Chem. Int. Ed. Engl., 2013. **52**(1): p. 419-23.
30. Srivastava, V. and Singh, P.P., *Eosin Y catalysed photoredox synthesis: a review*. RSC Advances, 2017. **7**(50): p. 31377-31392.
31. Dau, H., Fujita, E., and Sun, L., *Artificial Photosynthesis: Beyond Mimicking Nature*. ChemSusChem, 2017. **10**(22): p. 4228-4235.
32. Yuan, Y.J., Yu, Z.T., Chen, D.Q., and Zou, Z.G., *Metal-complex chromophores for solar hydrogen generation*. Chem. Soc. Rev., 2017. **46**(3): p. 603-631.
33. Shon, J.-H. and Teets, T.S., *Photocatalysis with Transition Metal Based Photosensitizers*. Comments Inorg. Chem., 2019. **40**(2): p. 53-85.
34. Liu, Q., Huo, C., Fu, Y., and Du, Z., *Recent progress in organophotoredox reaction*. Org. Biomol. Chem., 2022. **20**(34): p. 6721-6740.
35. Twilton, J., Le, C., Zhang, P., Shaw, M.H., Evans, R.W., and MacMillan, D.W.C., *The merger of transition metal and photocatalysis*. Nat. Rev. Chem., 2017. **1**(7).

36. Shon, J.-H. and Teets, T.S., *Molecular Photosensitizers in Energy Research and Catalysis: Design Principles and Recent Developments*. ACS Energy Lett., 2019. 4(2): p. 558-566.
37. Earley, J.D., Zieleniewska, A., Ripberger, H.H., Shin, N.Y., Lazorski, M.S., Mast, Z.J., Sayre, H.J., McCusker, J.K., Scholes, G.D., Knowles, R.R., Reid, O.G., and Rumbles, G., *Ion-pair reorganization regulates reactivity in photoredox catalysts*. Nat. Chem., 2022. 14(7): p. 746-753.
38. Olmsted, J. and Meyer, T.J., *Factors affecting cage escape yields following electron-transfer quenching*. J. Phys. Chem., 1987. 91(6): p. 1649-1655.
39. Hoffman, M.Z., *Cage escape yields from the quenching of excited tris(bipyridyl)ruthenium²⁺ by methylviologen in aqueous solution*. J. Phys. Chem., 1988. 92(12): p. 3458-3464.
40. Aydogan, A., Bangle, R.E., Cadranel, A., Turlington, M.D., Conroy, D.T., Cauet, E., Singleton, M.L., Meyer, G.J., Sampaio, R.N., Elias, B., and Troian-Gautier, L., *Accessing Photoredox Transformations with an Iron(III) Photosensitizer and Green Light*. J. Am. Chem. Soc., 2021. 143(38): p. 15661-15673.
41. Wang, C., Li, H., Bürgin, T.H., and Wenger, O.S., *Cage escape governs photoredox reaction rates and quantum yields*. Nat. Chem., 2024.
42. DiLuzio, S., Connell, T.U., Mdluli, V., Kowalewski, J.F., and Bernhard, S., *Understanding Ir(III) Photocatalyst Structure–Activity Relationships: A Highly Parallelized Study of Light-Driven Metal Reduction Processes*. J. Am. Chem. Soc., 2022. 144(3): p. 1431-1444.
43. Schwarz, J., Ilic, A., Johnson, C., Lomoth, R., and Warnmark, K., *High turnover photocatalytic hydrogen formation with an Fe(III) N-heterocyclic carbene photosensitizer*. Chem. Commun., 2022. 58(35): p. 5351-5354.
44. Ilic, A., Schwarz, J., Johnson, C., de Groot, L.H.M., Kaufhold, S., Lomoth, R., and Wärmarm, K., *Photoredox catalysis via consecutive ²LMCT- and ³MLCT-excitation of an Fe(III/II)-N-heterocyclic carbene complex*. Chem. Sci., 2022. 13(32): p. 9165-9175.
45. Ripak, A., De Kreijger, S., Sampaio, R.N., Vincent, C.A., Cauet, E., Jabin, I., Tambar, U.K., Elias, B., and Troian-Gautier, L., *Photosensitized Activation of Diazonium Derivatives for C-B Bond Formation*. Chem Catal., 2023. 3(2).
46. Sittel, S., Sell, A.C., Hofmann, K., Wiedemann, C., Nau, J.P., Kerzig, C., Manolikakes, G., and Heinze, K., *Visible-Light Induced Fixation of SO₂ into Organic Molecules with Polypyridine Chromium(III) Complexes*. ChemCatChem, 2023. 15(6): p. e202201562.
47. Sutin, N. and Creutz, C., *Light induced electron transfer reactions of metal complexes*. Pure Appl. Chem., 1980. 52(12): p. 2717-2738.

48. Harriman, A., Porter, G., and Wilowska, A., *Photoreduction of benzo-1,4-quinone sensitised by metalloporphyrins*. J. Chem. Soc., Faraday Transa. 2, 1983. 79(6): p. 807-16.
49. Mandal, K. and Hoffman, M.Z., *Solution medium control of the photoredox yield in the Ru(bpy)₃²⁺/methyl viologen/EDTA system*. J. Phys. Chem., 1984. 88(2): p. 185-187.
50. Lucia, L.A. and Schanze, K.S., *Cage escape yields for photoinduced bimolecular electron transfer reactions of Re(I) complexes*. Inorg. Chim. Acta, 1994. 225(1-2): p. 41-49.
51. Wolff, H.-J., Burssher, D., and Steiner, U.E., *Spin-orbit coupling controlled spin chemistry of Ru(bpy)₃²⁺ photooxidation: Detection of strong viscosity dependence of in-cage backward electron transfer rate*. Pure Appl. Chem., 1995. 67(1): p. 167-174.
52. Manoj, N., Ajit Kumar, R., and Gopidas, K.R., *Photophysical and electron transfer studies of a few 2,6-dimethyl-4-(alkylphenyl)pyrylium and thiopyrylium derivatives*. J. Photochem. Photobiol., A, 1997. 109(2): p. 109-118.
53. S. Jayanthi, S. and Ramamurthy, P., *Photoinduced electron transfer reactions of 2,4,6-triphenylpyrylium: solvent effect and charge-shift type of systems*. Phys. Chem. Chem. Phys., 1999. 1(20): p. 4751-4757.
54. Miedlar, K. and Das, P.K., *Tris(2,2'-bipyridine)ruthenium(II)-sensitized photooxidation of phenols. Environmental effects on electron transfer yields and kinetics*. J. Am. Chem. Soc., 1982. 104(26): p. 7462-7469.
55. Ohno, T. and Lichtin, N.N., *Electron transfer in the quenching of triplet methylene blue by complexes of iron(II)*. J. Am. Chem. Soc., 1980. 102(14): p. 4636-4643.
56. Delaire, J.A., Sanquer-Barrie, M., and Webber, S.E., *Role of electrostatic interaction in light-induced charge separation in polyelectrolyte-bound vinylidiphenylanthracene*. J. Phys. Chem., 1988. 92(5): p. 1252-1257.
57. Kikuchi, K., Hoshi, M., Niwa, T., Takahashi, Y., and Miyashi, T., *Heavy-atom effects on the excited singlet-state electron-transfer reaction*. J. Phys. Chem., 1991. 95(1): p. 38-42.
58. Gibbons, D.J., Farawar, A., Mazzella, P., Leroy-Lhez, S., and Williams, R.M., *Making triplets from photo-generated charges: observations, mechanisms and theory*. Photochem. Photobiol. Sci., 2020. 19(2): p. 136-158.
59. Ji, Y., DiRocco, D.A., Kind, J., Thiele, C.M., Gschwind, R.M., and Reibarkh, M., *LED-Illuminated NMR Spectroscopy: A Practical Tool for Mechanistic Studies of Photochemical Reactions*. ChemPhotoChem, 2019. 3(10): p. 984-992.

60. Braslavsky, S.E., *Glossary of terms used in photochemistry, 3rd edition (IUPAC Recommendations 2006)*. Pure Appl. Chem., 2007. 79(3): p. 293-465.
61. De Kreijger, S., Gillard, M., Elias, B., and Troian-Gautier, L., *Spectroscopic Techniques to Unravel Mechanistic Details in Light-Induced Transformations and Photoredox Catalysis*. ChemCatChem, 2024. 16(1): p. e202301100.
62. Arias-Rotondo, D.M. and McCusker, J.K., *The photophysics of photoredox catalysis: a roadmap for catalyst design*. Chem. Soc. Rev., 2016. 45(21): p. 5803-5820.
63. Rehm, D. and Weller, A., *Kinetics of Fluorescence Quenching by Electron and H-Atom Transfer*. Isr. J. Chem., 1970. 8(2): p. 259-271.
64. Strieth-Kalthoff, F. and Glorius, F., *Triplet Energy Transfer Photocatalysis: Unlocking the Next Level*. Chem, 2020. 6(8): p. 1888-1903.
65. Balzani, V., Bergamini, G., Campagna, S., and Puntoriero, F., *Photochemistry and Photophysics of Coordination Compounds: Overview and General Concepts*, in *Photochemistry and Photophysics of Coordination Compounds I*, 2007: Springer Berlin Heidelberg: Berlin, Heidelberg.
66. Cravencoco, A., Ye, C., Gräfenstein, J., and Börjesson, K., *Interplay between Förster and Dexter Energy Transfer Rates in Isomeric Donor–Bridge–Acceptor Systems*. J. Phys. Chem. A, 2020. 124(36): p. 7219-7227.
67. Strieth-Kalthoff, F., James, M.J., Teders, M., Pitzer, L., and Glorius, F., *Energy transfer catalysis mediated by visible light: principles, applications, directions*. Chem. Soc. Rev., 2018. 47(19): p. 7190-7202.
68. Sahoo, H., *Förster resonance energy transfer – A spectroscopic nanoruler: Principle and applications*. J. Photochem. Photobiol. C: Photochem. Rev., 2011. 12(1): p. 20-30.
69. Förster, T., *Energiewanderung und Fluoreszenz*. Naturwissenschaften, 1946. 33(6): p. 166-175.
70. Mikhnenko, O.V., Blom, P.W.M., and Nguyen, T.-Q., *Exciton diffusion in organic semiconductors*. Energy Environ. Sci., 2015. 8(7): p. 1867-1888.
71. Marchini, M., Bergamini, G., Cozzi, P.G., Ceroni, P., and Balzani, V., *Photoredox Catalysis: The Need to Elucidate the Photochemical Mechanism*. Angew. Chem. Int. Ed., 2017. 56(42): p. 12820-12821.
72. de Groot, L.H.M., Ilic, A., Schwarz, J., and Wärnmark, K., *Iron Photoredox Catalysis—Past, Present, and Future*. J. Am. Chem. Soc., 2023. 145(17): p. 9369-9388.
73. Pitre, S.P., McTiernan, C.D., and Scaiano, J.C., *Understanding the Kinetics and Spectroscopy of Photoredox Catalysis and Transition-Metal-Free Alternatives*. Acc. Chem. Res., 2016. 49(6): p. 1320-30.

74. Swords, W.B. and Yoon, T.P., *Transient absorption spectroscopy in visible-light photocatalysis*, in *Photochemistry: Volume 50*, 2022: The Royal Society of Chemistry.
75. Balzani, V., Ceroni, P., and Juris, A., *Photochemistry and Photophysics: Concepts, Research, Applications*. 2014: Wiley.
76. Lakowicz, J.R., *Principles of Fluorescence Spectroscopy*. 2006: Springer NY.
77. Genovese, D., Cingolani, M., Rampazzo, E., Prodi, L., and Zaccheroni, N., *Static quenching upon adduct formation: a treatment without shortcuts and approximations*. *Chem. Soc. Rev.*, 2021. **50**(15): p. 8414-8427.
78. Farr, E.P., Quintana, J.C., Reynoso, V., Ruberry, J.D., Shin, W.R., and Swartz, K.R., *Introduction to Time-Resolved Spectroscopy: Nanosecond Transient Absorption and Time-Resolved Fluorescence of Eosin B*. *J. Chem. Educ.*, 2018. **95**(5): p. 864-871.
79. Porter, G.-N. and Norrish, R.G.W., *Flash photolysis and spectroscopy. A new method for the study of free radical reactions*. *Proc. R. Soc. Lond. A. Mathematical and Physical Sciences*, 1950. **200**(1061): p. 284-300.
80. Porter, G., *Flash Photolysis and Some of Its Applications*. *Science*, 1968. **160**(3834): p. 1299-1307.
81. Elgrishi, N., Rountree, K.J., McCarthy, B.D., Rountree, E.S., Eisenhart, T.T., and Dempsey, J.L., *A Practical Beginner's Guide to Cyclic Voltammetry*. *J. Chem. Educ.*, 2017. **95**(2): p. 197-206.
82. Compton, R.G. and Banks, C.E., *Understanding Voltammetry (Third Edition)*. 2018: World Scientific Publishing Company.
83. Pavlishchuk, V.V. and Addison, A.W., *Conversion constants for redox potentials measured versus different reference electrodes in acetonitrile solutions at 25°C*. *Inorg. Chim. Acta*, 2000. **298**(1): p. 97-102.
84. Gagne, R.R., Koval, C.A., and Lisensky, G.C., *Ferrocene as an internal standard for electrochemical measurements*. *Inorg. Chem.*, 1980. **19**(9): p. 2854-2855.
85. Cadranel, A., Pieslinger, G.E., Tongying, P., Kuno, M.K., Baraldo, L.M., and Hodak, J.H., *Spectroscopic signatures of ligand field states in {Ru^{II}(imine)} complexes*. *Dalton Trans.*, 2016. **45**(13): p. 5464-5475.
86. Sampaio, R.N., Troian-Gautier, L., and Meyer, G.J., *A Charge-Separated State that Lives for Almost a Second at a Conductive Metal Oxide Interface*. *Angew. Chem. Int. Ed.*, 2018. **57**(47): p. 15390-15394.
87. Glaser, F., Kerzig, C., and Wenger, O.S., *Sensitization-initiated electron transfer via upconversion: mechanism and photocatalytic applications*. *Chem. Sci.*, 2021. **12**(29): p. 9922-9933.

88. Bürgin, T.H., Glaser, F., and Wenger, O.S., *Shedding Light on the Oxidizing Properties of Spin-Flip Excited States in a Cr^{III} Polypyridine Complex and Their Use in Photoredox Catalysis*. J. Am. Chem. Soc., 2022. 144(31): p. 14181-14194.
89. Swords, W.B., Chapman, S.J., Hofstetter, H., Dunn, A.L., and Yoon, T.P., *Variable Temperature LED–NMR: Rapid Insights into a Photocatalytic Mechanism from Reaction Progress Kinetic Analysis*. J. Org. Chem., 2022. 87(17): p. 11776-11782.
90. Weil J.A and Bolton J.R., *Electron Paramagnetic Resonance: Elementary Theory and Practical Applications*. 2006: Wiley.
91. Goswami, M., Chirila, A., Rebreyend, C., and de Bruin, B., *EPR Spectroscopy as a Tool in Homogeneous Catalysis Research*. Top. Catal., 2015. 58(12): p. 719-750.
92. Williams, P.J.H., Boustead, G.A., Heard, D.E., Seakins, P.W., Rickard, A.R., and Chechik, V., *New Approach to the Detection of Short-Lived Radical Intermediates*. J. Am. Chem. Soc., 2022. 144(35): p. 15969-15976.
93. Kuhn, H.J., Braslavsky, S.E., and Schmidt, R., *Chemical actinometry (IUPAC Technical Report)*. Pure Appl. Chem., 2004. 76(12): p. 2105-2146.
94. Rabani, J., Mamane, H., Pousty, D., and Bolton, J.R., *Practical Chemical Actinometry—A Review*. Photochem. Photobiol., 2021. 97(5): p. 873-902.
95. Cismesia, M.A. and Yoon, T.P., *Characterizing Chain Processes in Visible Light Photoredox Catalysis*. Chem. Sci., 2015. 6(10): p. 5426-5434.
96. Ripak, A., De Kreijger, S., Elias, B., and Troian-Gautier, L., *A protocol for determining cage-escape yields using nanosecond transient absorption spectroscopy*. STAR Protoc., 2023. 4(2): p. 102312.
97. Dedeian, K., Djurovich, P.I., Garces, F.O., Carlson, G., and Watts, R.J., *A new synthetic route to the preparation of a series of strong photoreducing agents: fac-tris-ortho-metalated complexes of iridium(III) with substituted 2-phenylpyridines*. Inorg. Chem., 2002. 30(8): p. 1685-1687.
98. Lytle, F.E. and Hercules, D.M., *Luminescence of tris(2,2'-bipyridine)ruthenium(II) dichloride*. J. Am. Chem. Soc., 2002. 91(2): p. 253-257.
99. Day, J.I., Teegardin, K., Weaver, J., and Chan, J., *Advances in Photocatalysis: A Microreview of Visible Light Mediated Ruthenium and Iridium Catalyzed Organic Transformations*. Org. Process Res. Dev., 2016. 20(7): p. 1156-1163.
100. Schmid, L., Kerzig, C., Prescimone, A., and Wenger, O.S., *Photostable Ruthenium(II) Isocyanoborato Luminophores and Their Use in Energy Transfer and Photoredox Catalysis*. JACS Au, 2021. 1(6): p. 819-832.

101. Gray, H.B. and Maverick, A.W., *Solar chemistry of metal complexes*. Science, 1981. 214(4526): p. 1201-5.
102. Bozic-Weber, B., Constable, E.C., and Housecroft, C.E., *Light harvesting with Earth abundant d-block metals: Development of sensitizers in dye-sensitized solar cells (DSCs)*. Coord. Chem. Rev., 2013. 257(21-22): p. 3089-3106.
103. Larsen, C.B. and Wenger, O.S., *Photoredox Catalysis with Metal Complexes Made from Earth-Abundant Elements*. Chem. - Eur. J., 2018. 24(9): p. 2039-2058.
104. Wenger, O.S., *Photoactive Complexes with Earth-Abundant Metals*, J. Am. Chem. Soc., 2018. 140(42): p. 13522-13533.
105. Glaser, F. and Wenger, O.S., *Recent progress in the development of transition-metal based photoredox catalysts*. Coord. Chem. Rev., 2020. 405.
106. Förster, C. and Heinze, K., *Photophysics and photochemistry with Earth-abundant metals – fundamentals and concepts*, Chem. Soc. Rev., 2020. 49: p. 1057-1070.
107. Mitani, M., Kato, I., and Koyama, K., *Photoaddition of alkyl halides to olefins catalyzed by copper(I) complexes*. J. Am. Chem. Soc., 2002. 105(22): p. 6719-6721.
108. Pirtsch, M., Paria, S., Matsuno, T., Isobe, H., and Reiser, O., *[Cu(dap)₂Cl] as an efficient visible-light-driven photoredox catalyst in carbon-carbon bond-forming reactions*. Chem. - Eur. J., 2012. 18(24): p. 7336-40.
109. Bagal, D.B., Kachkovskiy, G., Knorn, M., Rawner, T., Bhanage, B.M., and Reiser, O., *Trifluoromethylchlorosulfonylation of alkenes: evidence for an inner-sphere mechanism by a copper phenanthroline photoredox catalyst*. Angew. Chem. Int. Ed. Engl., 2015. 54(24): p. 6999-7002.
110. Pintauer, T., *Towards the development of highly active copper catalysts for atom transfer radical addition (ATRA) and polymerization (ATRP)‡*. Chemical Papers, 2016. 70(1): p. 22-42.
111. Rawner, T., Lutsker, E., Kaiser, C.A., and Reiser, O., *The Different Faces of Photoredox Catalysts: Visible-Light-Mediated Atom Transfer Radical Addition (ATRA) Reactions of Perfluoroalkyl Iodides with Styrenes and Phenylacetylenes*. ACS Catal. 2018. 8(5): p. 3950-3956.
112. Hossain, A., Engl, S., Lutsker, E., and Reiser, O., *Visible-Light-Mediated Regioselective Chlorosulfonylation of Alkenes and Alkynes: Introducing the Cu(II) Complex [Cu(dap)Cl₂] to Photochemical ATRA Reactions*. ACS Catal., 2018. 9(2): p. 1103-1109.
113. Herr, P., Kerzig, C., Larsen, C.B., Haussinger, D., and Wenger, O.S., *Manganese(I) complexes with metal-to-ligand charge transfer luminescence and photoreactivity*. Nat. Chem., 2021. 13(10): p. 956-962.

114. Stevenson, S.M., Shores, M.P., and Ferreira, E.M., *Photooxidizing chromium catalysts for promoting radical cation cycloadditions*. *Angew. Chem. Int. Ed. Engl.*, 2015. **54**(22): p. 6506-10.
115. Büldt, L.A. and Wenger, O.S., *Chromium complexes for luminescence, solar cells, photoredox catalysis, upconversion, and phototriggered NO release*. *Chem. Sci.*, 2017. **8**(11): p. 7359-7367.
116. Sinha, N., Wegeberg, C., Haussinger, D., Prescimone, A., and Wenger, O.S., *Photoredox-active Cr(0) luminophores featuring photophysical properties competitive with Ru(II) and Os(II) complexes*. *Nat. Chem.*, 2023. **15**(12): p. 1730-1736.
117. Wang, C., Wegeberg, C., and Wenger, O.S., *First-Row d(6) Metal Complex Enables Photon Upconversion and Initiates Blue Light-Dependent Polymerization with Red Light*. *Angew. Chem. Int. Ed. Engl.*, 2023. **62**(43): p. e202311470.
118. Chan, A.Y., Ghosh, A., Yarranton, J.T., Twilton, J., Jin, J., Arias-Rotondo, D.M., Sakai, H.A., McCusker, J.K., and MacMillan, D.W.C., *Exploiting the Marcus inverted region for first-row transition metal-based photoredox catalysis*. *Science*, 2023. **382**(6667): p. 191-197.
119. Herr, P., Glaser, F., Buldt, L.A., Larsen, C.B., and Wenger, O.S., *Long-Lived, Strongly Emissive, and Highly Reducing Excited States in Mo(0) Complexes with Chelating Isocyanides*. *J. Am. Chem. Soc.*, 2019. **141**(36): p. 14394-14402.
120. Crabtree, R.H., *The Organometallic Chemistry of the Transition Metals*. 2019: Wiley.
121. Dierks, P., Vukadinovic, Y., and Bauer, M., *Photoactive iron complexes: more sustainable, but still a challenge*. *Inorg. Chem. Front.*, 2022. **9**(2): p. 206-220.
122. McCusker, J.K., *Electronic structure in the transition metal block and its implications for light harvesting*. *Science*, 2019. **363**(6426): p. 484-488.
123. Pyykko, P., *Relativistic effects in structural chemistry*. *Chem. Rev.*, 1988. **88**(3): p. 563-594.
124. Kaupp, M., *The role of radial nodes of atomic orbitals for chemical bonding and the periodic table*. *J. Comput. Chem.*, 2007. **28**(1): p. 320-325.
125. Liu, Y., Persson, P., Sundström, V., and Wärnmark, K., *Fe N-Heterocyclic Carbene Complexes as Promising Photosensitizers*. *Acc. Chem. Res.*, 2016. **49**(8): p. 1477-85.
126. Juban, E.A., Smeigh, A.L., Monat, J.E., and McCusker, J.K., *Ultrafast dynamics of ligand-field excited states*. *Coord. Chem. Rev.*, 2006. **250**(13-14): p. 1783-1791.

127. Cannizzo, A., Milne, C.J., Consani, C., Gawelda, W., Bressler, C., van Mourik, F., and Chergui, M., *Light-induced spin crossover in Fe(II)-based complexes: The full photocycle unraveled by ultrafast optical and X-ray spectroscopies*. *Coord. Chem. Rev.*, 2010. **254**(21-22): p. 2677-2686.
128. Hauser, A., *Light-Induced Spin Crossover and the High-Spin→Low-Spin Relaxation*, in *Spin Crossover in Transition Metal Compounds II*, 2004: Springer Berlin Heidelberg: Berlin, Heidelberg.
129. Papai, M., Vanko, G., de Graaf, C., and Rozgonyi, T., *Theoretical Investigation of the Electronic Structure of Fe(II) Complexes at Spin-State Transitions*. *J. Chem. Theory Comput.*, 2013. **9**(1): p. 509-519.
130. Sousa, C., de Graaf, C., Rudavskiy, A., Broer, R., Tatchen, J., Etinski, M., and Marian, C.M., *Ultrafast deactivation mechanism of the excited singlet in the light-induced spin crossover of [Fe(2,2'-bipyridine)₃]²⁺*. *Chem. - Eur. J.*, 2013. **19**(51): p. 17541-51.
131. Jamula, L.L., Brown, A.M., Guo, D., and McCusker, J.K., *Synthesis and characterization of a high-symmetry ferrous polypyridyl complex: approaching the ⁵T₂^βT₁ crossing point for Fe(II).* *Inorg. Chem.*, 2014. **53**(1): p. 15-7.
132. Mengel, A.K.C., Förster, C., Breivogel, A., Mack, K., Ochsmann, J.R., Laquai, F., Ksenofontov, V., and Heinze, K., *A heteroleptic push-pull substituted iron(II) bis(tridentate) complex with low-energy charge-transfer states*. *Chem. – Eur. J.*, 2015. **21** p. 704-714.
133. Wachtler, M., Kubel, J., Barthelmes, K., Winter, A., Schmiedel, A., Pascher, T., Lambert, C., Schubert, U.S., and Dietzek, B., *Energy transfer and formation of long-lived ³MLCT states in multimetallic complexes with extended highly conjugated bis-terpyridyl ligands*. *Phys. Chem. Chem. Phys.*, 2016. **18**(4): p. 2350-60.
134. Wenger, O.S., *Is Iron the New Ruthenium?* *Chem. - Eur. J.*, 2019. **25**(24): p. 6043-6052.
135. Liu, Y., Harlang, T., Canton, S.E., Chabera, P., Suarez-Alcantara, K., Fleckhaus, A., Vithanage, D.A., Goransson, E., Corani, A., Lomoth, R., Sundstrom, V., and Warnmark, K., *Towards longer-lived metal-to-ligand charge transfer states of iron(II) complexes: an N-heterocyclic carbene approach*. *Chem. Commun.*, 2013. **49**(57): p. 6412-4.
136. Liu, Y., Kjær, K.S., Fredin, L.A., Chábera, P., Harlang, T., Canton, S.E., Lidin, S., Zhang, J., Lomoth, R., Bergquist, K.-E.E., Persson, P., Wärnmark, K., Sundström, V., Kjær, K.S., Fredin, L.A., Chábera, P., Harlang, T., Canton, S.E., Lidin, S., Zhang, J., Lomoth, R., Bergquist, K.-E.E., Persson, P., Wärnmark, K., and Sundström, V., *A Heteroleptic Ferrous Complex with Mesoionic Bis(1,2,3-triazol-5-ylidene) Ligands: Taming the MLCT Excited State of Iron(II)*. *Chem. - Eur. J.*, 2015. **21** p. 3628-3639.

137. Lindh, L., Chábera, P., Rosemann, N.W., Uhlig, J., Wärnmark, K., Yartsev, A., Sundström, V., and Persson, P., *Photophysics and Photochemistry of Iron Carbene Complexes for Solar Energy Conversion and Photocatalysis*. *Catalysts*, 2020. **10**(3): p. 315.
138. Rosemann, N.W., Chábera, P., Prakash, O., Kaufhold, S., Wärnmark, K., Yartsev, A., and Persson, P., *Tracing the Full Bimolecular Photocycle of Iron(III)-Carbene Light Harvesters in Electron-Donating Solvents*. *J. Am. Chem. Soc.*, 2020. **142**(19): p. 8565-8569.
139. Jang, Y.J., An, H., Choi, S., Hong, J., Lee, S.H., Ahn, K.H., You, Y., and Kang, E.J., *Green-Light-Driven Fe(III)(btz)₃ Photocatalysis in the Radical Cationic [4+2] Cycloaddition Reaction*. *Org. Lett.*, 2022. **24**(24): p. 4479-4484.
140. Aydogan, A., Bangle, R.E., De Kreijger, S., Dickenson, J.C., Singleton, M.L., Cauët, E., Cadranet, A., Meyer, G.J., Elias, B., Sampaio, R.N., and Troian-Gautier, L., *Mechanistic investigation of a visible light mediated dehalogenation/cyclisation reaction using iron(III), iridium(III) and ruthenium(II) photosensitizers*. *Catal. Sci. Technol.*, 2021. **11**(24): p. 8037-8051.
141. Cui, Z., Ding, J., Gao, Y., and Li, F., *Organic Light-Emitting Diodes Based on an Iron(III) Complex with Doublet Emission*. *CCS Chemistry*, 2022. **4**(9): p. 2953-2958.
142. Barber, J. and Tran, P.D., *From natural to artificial photosynthesis*. *J. R. Soc. Interface*, 2013. **10**(81): p. 20120984.
143. Hammarström, L. and Wasielewski, M.R., *Biomimetic approaches to artificial photosynthesis*. *Energy Environ. Sci.*, 2011. **4**(7): p. 2339-2339.
144. Hammarström, L. and Styring, S., *Proton-coupled electron transfer of tyrosines in Photosystem II and model systems for artificial photosynthesis: the role of a redox-active link between catalyst and photosensitizer*. *Energy Environ. Sci.*, 2011. **4**(7): p. 2379-2388.
145. Whang, D.R. and Apaydin, D.H., *Artificial Photosynthesis: Learning from Nature*. *ChemPhotoChem*, 2018. **2**(3): p. 148-160.
146. Hammarström, L., *Accumulative Charge Separation for Solar Fuels Production: Coupling Light-Induced Single Electron Transfer to Multielectron Catalysis*. *Acc. Chem. Res.*, 2015. **48**(3): p. 840-850.
147. IEA. *The Future of Hydrogen*. Available from: <https://www.iea.org/reports/the-future-of-hydrogen>.
148. Tollefson, J., *Hydrogen vehicles: Fuel of the future?* *Nature*, 2010. **464**(7293): p. 1262-4.

149. de Kleijne, K., de Coninck, H., van Zelm, R., Huijbregts, M.A.J., and Hanssen, S.V., *The many greenhouse gas footprints of green hydrogen*. Sustainable Energy Fuels, 2022. 6(19): p. 4383-4387.
150. Ismail, A.A. and Bahnemann, D.W., *Photochemical splitting of water for hydrogen production by photocatalysis: A review*. Sol. Energy Mater. Sol. Cells, 2014. 128: p. 85-101.
151. Junge, H., Rockstroh, N., Fischer, S., Brückner, A., Ludwig, R., Lochbrunner, S., Kühn, O., and Beller, M., *Light to Hydrogen: Photocatalytic Hydrogen Generation from Water with Molecularly-Defined Iron Complexes*. Inorganics, 2017. 5(1).
152. Watanabe, M., *Dye-sensitized photocatalyst for effective water splitting catalyzt*. Sci. Technol. Adv. Mater., 2017. 18(1): p. 705-723.
153. Wang, Y., Suzuki, H., Xie, J., Tomita, O., Martin, D.J., Higashi, M., Kong, D., Abe, R., and Tang, J., *Mimicking Natural Photosynthesis: Solar to Renewable H(2) Fuel Synthesis by Z-Scheme Water Splitting Systems*. Chem Rev, 2018. 118(10): p. 5201-5241.
154. Ng, B.J., Putri, L.K., Kong, X.Y., Teh, Y.W., Pasbakhsh, P., and Chai, S.P., *Z-Scheme Photocatalytic Systems for Solar Water Splitting*. Adv. Sci., 2020. 7(7): p. 1903171.
155. Karkas, M.D., Verho, O., Johnston, E.V., and Akermark, B., *Artificial photosynthesis: molecular systems for catalytic water oxidation*. Chem. Rev., 2014. 114(24): p. 11863-2001.
156. Morris, A.J., Meyer, G.J., and Fujita, E., *Molecular approaches to the photocatalytic reduction of carbon dioxide for solar fuels*. Acc. Chem. Res., 2009. 42(12): p. 1983-94.
157. Neatu, S., Macia-Agullo, J.A., and Garcia, H., *Solar light photocatalytic CO₂ reduction: general considerations and selected bench-mark photocatalysts*. Int. J. Mol. Sci., 2014. 15(4): p. 5246-62.
158. Yamazaki, Y., Takeda, H., and Ishitani, O., *Photocatalytic reduction of CO₂ using metal complexes*. J. Photochem. and Photobiol. C: Photochem. Rev., 2015. 25: p. 106-137.
159. Chen, L., Guo, Z., Wei, X.G., Gallenkamp, C., Bonin, J., Anxolabehere-Mallart, E., Lau, K.C., Lau, T.C., and Robert, M., *Molecular Catalysis of the Electrochemical and Photochemical Reduction of CO₂ with Earth-Abundant Metal Complexes. Selective Production of CO vs HCOOH by Switching of the Metal Center*. J. Am. Chem. Soc., 2015. 137(34): p. 10918-21.
160. Takeda, H., Cometto, C., Ishitani, O., and Robert, M., *Electrons, Photons, Protons and Earth-Abundant Metal Complexes for Molecular Catalysis of CO₂ Reduction*. ACS Catal., 2016. 7(1): p. 70-88.

161. Seo, H., Katcher, M.H., and Jamison, T.F., *Photoredox activation of carbon dioxide for amino acid synthesis in continuous flow*. Nat. Chem., 2017. **9**(5): p. 453-456.
162. Pellegrin, Y. and Odobel, F., *Sacrificial electron donor reagents for solar fuel production*. C. R. Chimie, 2017. **20**(3): p. 283-295.
163. Lowe, G.A., *Enabling artificial photosynthesis systems with molecular recycling: A review of photo- and electrochemical methods for regenerating organic sacrificial electron donors*. Beilstein J. Org. Chem., 2023. **19**: p. 1198-1215.
164. Du, P., Schneider, J., Luo, G., Brennessel, W.W., and Eisenberg, R., *Visible Light-Driven Hydrogen Production from Aqueous Protons Catalyzed by Molecular Cobaloxime Catalysts*. Inorg. Chem., 2009. **48**(11): p. 4952-4962.
165. Park, H., Ou, H.-H., Kang, U., Choi, J., and Hoffmann, M.R., *Photocatalytic conversion of carbon dioxide to methane on TiO₂/CdS in aqueous isopropanol solution*. Catal. Today, 2016. **266**: p. 153-159.
166. Li, L., Duan, L., Wen, F., Li, C., Wang, M., Hagfeldt, A., and Sun, L., *Visible light driven hydrogen production from a photo-active cathode based on a molecular catalyst and organic dye-sensitized p-type nanostructured NiO*. Chem. Commun., 2012. **48**(7): p. 988-990.
167. Sander, A.C., Maji, S., Francàs, L., Böhnisch, T., Dechert, S., Llobet, A., and Meyer, F., *Highly Efficient Binuclear Ruthenium Catalyst for Water Oxidation*. ChemSusChem, 2015. **8**(10): p. 1697-1702.
168. Huber, Fabian L., Amthor, S., Schwarz, B., Mizaikoff, B., Streb, C., and Rau, S., *Multi-phase real-time monitoring of oxygen evolution enables in operando water oxidation catalysis studies*. Sustainable Energy & Fuels, 2018. **2**(9): p. 1974-1978.
169. Wood, R.W., *The Raman Effect with Hydrochloric Acid Gas: the 'Missing Line.'* Nature, 1929. **123**(3095): p. 279-279.
170. Schiel, D. and Richter, W., *Use of Raman spectrometry in gas analysis*. Fresenius' Zeitschrift für analytische Chemie, 1987. **327**(3): p. 335-337.
171. Knebl, A., Yan, D., Popp, J., and Frosch, T., *Fiber enhanced Raman gas spectroscopy*. TrAC, Trends Anal. Chem., 2018. **103**: p. 230-238.
172. Niklas, C., Wackerbarth, H., and Ctistis, G., *A Short Review of Cavity-Enhanced Raman Spectroscopy for Gas Analysis*. Sensors, 2021. **21**(5): p. 1698.
173. Schwarz, J., Ilic, A., Kaufhold, S., Ahokas, J., Myllyperkiö, P., Pettersson, M., and Wärnmark, K., *Simultaneous non-invasive gas analysis in artificial photosynthesis reactions using rotational Raman spectroscopy*. Sustainable Energy & Fuels, 2022. **6**(19): p. 4388-4392.

174. Zimmer, P., Müller, P., Burkhardt, L., Schepper, R., Neuba, A., Steube, J., Dietrich, F., Flörke, U., Mangold, S., Gerhards, M., and Bauer, M., *N-Heterocyclic Carbene Complexes of Iron as Photosensitizers for Light-Induced Water Reduction*. Eur. J. Inorg. Chem., 2017. **2017**(11): p. 1504-1509.
175. Huber-Gedert, M., Nowakowski, M., Kertmen, A., Burkhardt, L., Lindner, N., Schoch, R., Herbst-Irmer, R., Neuba, A., Schmitz, L., Choi, T.K., Kubicki, J., Gawelda, W., and Bauer, M., *Fundamental Characterization, Photophysics and Photocatalysis of a Base Metal Iron(II)-Cobalt(III) Dyad*. Chem. - Eur. J., 2021. **27**(38): p. 9905-9918.
176. Rodenberg, A., Oraziotti, M., Probst, B., Bachmann, C., Alberto, R., Baldrige, K.K., and Hamm, P., *Mechanism of Photocatalytic Hydrogen Generation by a Polypyridyl-Based Cobalt Catalyst in Aqueous Solution*. Inorg. Chem., 2015. **54**(2): p. 646-657.
177. Bhattacharyya, K. and Das, P.K., *Nanosecond transient processes in the triethylamine quenching of benzophenone triplets in aqueous alkaline media. Substituent effect, ketyl radical deprotonation, and secondary photoreduction kinetics*. J. Phys. Chem., 2002. **90**(17): p. 3987-3993.
178. Wayner, D.D.M., McPhee, D.J., and Griller, D., *Oxidation and reduction potentials of transient free radicals*. J. Am. Chem. Soc., 2002. **110**(1): p. 132-137.
179. Lai, R.Y. and Bard, A.J., *Electrogenerated Chemiluminescence. 70. The Application of ECL to Determine Electrode Potentials of Tri-n-propylamine, Its Radical Cation, and Intermediate Free Radical in MeCN/Benzene Solutions*. J. Phys. Chem. A, 2003. **107**(18): p. 3335-3340.
180. Izutsu, K., *Acid-base Dissociation Constants in Dipolar Aprotic Solvents*. 1990: Blackwell Scientific Publications.
181. Beatty, J.W. and Stephenson, C.R., *Amine Functionalization via Oxidative Photoredox Catalysis: Methodology Development and Complex Molecule Synthesis*. Acc. Chem. Res., 2015. **48**(5): p. 1474-84.
182. Hu, J., Wang, J., Nguyen, T.H., and Zheng, N., *The chemistry of amine radical cations produced by visible light photoredox catalysis*. Beilstein J. Org. Chem., 2013. **9**: p. 1977-2001.
183. Draper, F., Doeven, E.H., Adcock, J.L., Francis, P.S., and Connell, T.U., *Extending Photocatalyst Activity through Choice of Electron Donor*. J. Org. Chem., 2023. **88**(10): p. 6445-6453.
184. Nelsen, S.F. and Ippoliti, J.T., *The deprotonation of trialkylamine cation radicals by amines*. J. Am. Chem. Soc., 1986. **108**(16): p. 4879-4881.

185. Zhang, X., Yeh, S.-R., Hong, S., Freccero, M., Albin, A., Falvey, D.E., and Mariano, P.S., *Dynamics of α -CH Deprotonation and α -Desilylation Reactions of Tertiary Amine Cation Radicals*. J. Am. Chem. Soc., 1994. 116(10): p. 4211-4220.
186. Dempsey, J.L., Brunschwig, B.S., Winkler, J.R., and Gray, H.B., *Hydrogen evolution catalyzed by cobaloximes*. Acc. Chem. Res., 2009. 42(12): p. 1995-2004.
187. Sun, Z., Ma, T., Tao, H., Fan, Q., and Han, B., *Fundamentals and Challenges of Electrochemical CO₂ Reduction Using Two-Dimensional Materials*. Chem, 2017. 3(4): p. 560-587.
188. Bonin, J., Maurin, A., and Robert, M., *Molecular catalysis of the electrochemical and photochemical reduction of CO₂ with Fe and Co metal based complexes*. Recent advances. Coord. Chem. Rev., 2017. 334: p. 184-198.
189. Matsuoka, S., Yamamoto, K., Ogata, T., Kusaba, M., Nakashima, N., Fujita, E., and Yanagida, S., *Efficient and selective electron mediation of cobalt complexes with cyclam and related macrocycles in the p-terphenyl-catalyzed photoreduction of carbon dioxide*. J. Am. Chem. Soc., 2002. 115(2): p. 601-609.
190. Obermeier, M., Beckmann, F., Schaer, R.S., Wenger, O.S., and Schwalbe, M., *Sensitized Photocatalytic CO₂ Reduction With Earth Abundant 3d Metal Complexes Possessing Dipicolyl-Triazacyclononane Derivatives*. Front. Chem., 2021. 9: p. 751716.
191. Morimoto, T., Nakajima, T., Sawa, S., Nakanishi, R., Imori, D., and Ishitani, O., *CO₂ Capture by a Rhenium(I) Complex with the Aid of Triethanolamine*. J. Am. Chem. Soc., 2013. 135(45): p. 16825-16828.
192. Morimoto, T., Nishiura, C., Tanaka, M., Rohacova, J., Nakagawa, Y., Funada, Y., Koike, K., Yamamoto, Y., Shishido, S., Kojima, T., Saeki, T., Ozeki, T., and Ishitani, O., *Ring-Shaped Re(I) Multinuclear Complexes with Unique Photofunctional Properties*. J. Am. Chem. Soc., 2013. 135(36): p. 13266-13269.
193. Sullivan, B.P., Bolinger, C.M., Conrad, D., Vining, W.J., and Meyer, T.J., *One- and two-electron pathways in the electrocatalytic reduction of CO₂ by fac-Re(bpy)(CO)₃Cl (bpy = 2,2'-bipyridine)*. J. Chem. Soc., Chem. Commun., 1985(20): p. 1414-1416.
194. Hawecker, J., Lehn, J.-M., and Ziessel, R., *Photochemical and Electrochemical Reduction of Carbon Dioxide to Carbon Monoxide Mediated by (2,2'-Bipyridine)tricarbonylchlororhenium(I) and Related Complexes as Homogeneous Catalysts*. Helv. Chim. Acta, 1986. 69(8): p. 1990-2012.
195. Caspar, J.V. and Meyer, T.J., *Application of the energy gap law to nonradiative, excited-state decay*. J. Phys. Chem., 1983. 87(6): p. 952-957.

196. Qu, Y. and Duan, X., *Progress, challenge and perspective of heterogeneous photocatalysis*. Chem. Soc. Rev., 2013. 42(7): p. 2568-2580.
197. Wu, L.-Z., Chen, B., Li, Z.-J., and Tung, C.-H., *Enhancement of the Efficiency of Photocatalytic Reduction of Protons to Hydrogen via Molecular Assembly*. Acc. Chem. Res., 2014. 47(7): p. 2177-2185.
198. Crisenza, G.E.M. and Melchiorre, P., *Chemistry glows green with photoredox catalysis*. Nat. Commun., 2020. 11(1): p. 803.
199. Douglas, J.J., Sevrin, M.J., and Stephenson, C.R.J., *Visible Light Photocatalysis: Applications and New Disconnections in the Synthesis of Pharmaceutical Agents*. Org. Process Res. Dev., 2016. 20(7): p. 1134-1147.
200. Nicholls, T.P., Leonori, D., and Bissember, A.C., *Applications of visible light photoredox catalysis to the synthesis of natural products and related compounds*. Nat. Prod. Rep., 2016. 33(11): p. 1248-1254.
201. McAtee, R.C., McClain, E.J., and Stephenson, C.R.J., *Illuminating Photoredox Catalysis*. Trends Chem, 2019. 1(1): p. 111-125.
202. Nicewicz, D.A. and Nguyen, T.M., *Recent Applications of Organic Dyes as Photoredox Catalysts in Organic Synthesis*. ACS Catal., 2013. 4(1): p. 355-360.
203. Glaser, F., Aydogan, A., Elias, B., and Troian-Gautier, L., *The great strides of iron photosensitizers for contemporary organic photoredox catalysis: On our way to the holy grail?* Coord. Chem. Rev., 2024. 500.
204. Woodhouse, M.D. and McCusker, J.K., *Mechanistic Origin of Photoredox Catalysis Involving Iron(II) Polypyridyl Chromophores*. J. Am. Chem. Soc., 2020. 142(38): p. 16229-16233.
205. Gualandi, A., Marchini, M., Mengozzi, L., Natali, M., Lucarini, M., Ceroni, P., and Cozzi, P.G., *Organocatalytic Enantioselective Alkylation of Aldehydes with [Fe(bpy)₃]Br₂ Catalyst and Visible Light*. ACS Catal., 2015. 5(10): p. 5927-5931.
206. Parisien-Collette, S., Hernandez-Perez, A.C., and Collins, S.K., *Photochemical Synthesis of Carbazoles Using an [Fe(phen)₃](NTf₂)₂/O₂ Catalyst System: Catalysis toward Sustainability*. Org. Lett., 2016. 18(19): p. 4994-4997.
207. Lindroth, R., Ondrejko, A., and Wallentin, C.J., *Visible-Light Mediated Oxidative Fragmentation of Ethers and Acetals by Means of Fe(III) Catalysis*. Org. Lett., 2022. 24(8): p. 1662-1667.
208. Baslé, O., *Visible-light-induced 3d transition metal-catalysis: A focus on C-H bond functionalization*. Current Opinion in Green and Sustainable Chemistry, 2021. 32: p. 100539.

209. Abderrazak, Y., Bhattacharyya, A., and Reiser, O., *Visible-Light-Induced Homolysis of Earth-Abundant Metal-Substrate Complexes: A Complementary Activation Strategy in Photoredox Catalysis*. *Angew. Chem. Int. Ed.*, 2021. **60**(39): p. 21100-21115.
210. Yin, C., Wang, M., Cai, Z., Yuan, B., and Hu, P., *Visible-Light-Induced Iron Group Metal Catalysis: Recent Developments in Organic Synthesis*. *Synthesis*, 2022. **54**(22): p. 4864-4882.
211. Juliá, F., *Ligand-to-Metal Charge Transfer (LMCT) Photochemistry at 3d-Metal Complexes: An Emerging Tool for Sustainable Organic Synthesis*. *ChemCatChem*, 2022. **14**(19): p. e202200916.
212. Muñoz-Molina, J.M., Belderrain, T.R., and Pérez, P.J., *Atom Transfer Radical Reactions as a Tool for Olefin Functionalization – On the Way to Practical Applications*. *Eur. J. Inorg. Chem.*, 2011. **2011**(21): p. 3155-3164.
213. Nguyen, J.D., Tucker, J.W., Konieczynska, M.D., and Stephenson, C.R., *Intermolecular atom transfer radical addition to olefins mediated by oxidative quenching of photoredox catalysts*. *J. Am. Chem. Soc.*, 2011. **133**(12): p. 4160-3.
214. Wallentin, C.J., Nguyen, J.D., Finkbeiner, P., and Stephenson, C.R., *Visible light-mediated atom transfer radical addition via oxidative and reductive quenching of photocatalysts*. *J. Am. Chem. Soc.*, 2012. **134**(21): p. 8875-84.
215. Engl, S. and Reiser, O., *Making Copper Photocatalysis Even More Robust and Economic: Photoredox Catalysis with $[Cu^{II}(dmp)_2Cl]Cl$* . *Eur. J. Org. Chem.*, 2019. **2020**(10): p. 1523-1533.
216. Engl, S. and Reiser, O., *Copper Makes the Difference: Visible Light-Mediated Atom Transfer Radical Addition Reactions of Iodoform with Olefins*. *ACS Catal.*, 2020. **10**(17): p. 9899-9906.
217. Graml, A., Nevesely, T., Jan Kutta, R., Cibulka, R., and König, B., *Deazaflavin reductive photocatalysis involves excited semiquinone radicals*. *Nat. Commun.*, 2020. **11**(1): p. 3174.
218. Ghosh, I., Ghosh, T., Bardagi, J.I., and König, B., *Reduction of aryl halides by consecutive visible light-induced electron transfer processes*. *Science*, 2014. **346**(6210): p. 725-8.
219. Haimerl, J., Ghosh, I., König, B., Vogelsang, J., and Lupton, J.M., *Single-molecule photoredox catalysis*. *Chem. Sci.*, 2019. **10**(3): p. 681-687.
220. Brandl, F., Bergwinkl, S., Allacher, C., and Dick, B., *Consecutive Photoinduced Electron Transfer (conPET): The Mechanism of the Photocatalyst Rhodamine 6G*. *Chem. - Eur. J.*, 2020. **26**(35): p. 7946-7954.

221. Pitre, S.P., McTiernan, C.D., Vine, W., DiPucchio, R., Grenier, M., and Scaiano, J.C., *Visible-Light Actinometry and Intermittent Illumination as Convenient Tools to Study Ru(bpy)₃Cl₂ Mediated Photoredox Transformations*. Sci. Rep., 2015. 5: p. 16397.
222. Qiao, Y., Yang, Q., and Schelter, E.J., *Photoinduced Miyaura Borylation by a Rare-Earth-Metal Photoreductant: The Hexachloroacetate(III) Anion*. Angew. Chem. Int. Ed. Engl., 2018. 57(34): p. 10999-11003.
223. Giedyk, M., Narobe, R., Weiß, S., Touraud, D., Kunz, W., and König, B., *Photocatalytic activation of alkyl chlorides by assembly-promoted single electron transfer in microheterogeneous solutions*. Nat. Catal., 2019. 3(1): p. 40-47.
224. Miyake, Y., Ashida, Y., Nakajima, K., and Nishibayashi, Y., *Visible-light-mediated addition of α -aminoalkyl radicals generated from α -silylamines to α,β -unsaturated carbonyl compounds*. Chem. Commun., 2012. 48(55): p. 6966-8.
225. Miyake, Y., Nakajima, K., and Nishibayashi, Y., *Visible-light-mediated utilization of α -aminoalkyl radicals: addition to electron-deficient alkenes using photoredox catalysts*. J. Am. Chem. Soc., 2012. 134(7): p. 3338-41.
226. Fagnoni, M., Dondi, D., Ravelli, D., and Albini, A., *Photocatalysis for the formation of the C-C bond*. Chem. Rev., 2007. 107(6): p. 2725-56.
227. Luguera Ruiz, A., La Mantia, M., Merli, D., Protti, S., and Fagnoni, M., *Alkyl Radical Generation via C-C Bond Cleavage in 2-Substituted Oxazolidines*. ACS Catal., 2022. 12(19): p. 12469-12476.
228. Cooper, B.E. and Owen, W.J., *Silicon-carbon hyperconjugation in cation radicals I. Lowering of oxidation potentials of N-[(trimethylsilyl)methyl] aromatic amines*. J. Organomet. Chem., 1971. 29(1): p. 33-40.
229. Hasegawa, E., Xu, W., Mariano, P.S., Yoon, U.C., and Kim, J.U., *Electron-transfer-induced photoadditions of the silyl amine, Et₂NCH₂SiMe₃, to α,β -unsaturated cyclohexenones. Dual reaction pathways based on ion pair-selective cation-radical chemistry*. J. Am. Chem. Soc., 2002. 110(24): p. 8099-8111.
230. Thierry, T., Pfund, E., and Lequeux, T., *Metal-Free Aminomethylation of Aromatic Sulfones Promoted by Eosin Y*. Chem. - Eur. J., 2021. 27(60): p. 14826-14830.
231. Pandey, G., Kumaraswamy, G., and Bhalerao, U.T., *Photoinduced set generation of α -aminoradicals: A practical method for the synthesis of pyrrolidines and piperidines*. Tetrahedron Lett., 1989. 30(44): p. 6059-6062.
232. Pandey, G., Devi Reddy, G., and Kumaraswamy, G., *Photoinduced electron transfer (PET) promoted cyclisations of 1-[N-alkyl-N-(trimethylsilyl)methyl]amines tethered to proximate olefin: mechanistic and synthetic perspectives*. Tetrahedron, 1994. 50(27): p. 8185-8194.

233. Jeon, Y.T., Lee, C.P., and Mariano, P.S., *Radical cyclization reactions of α -silyl amine α,β -unsaturated ketone and ester systems promoted by single electron transfer photosensitization*. J. Am. Chem. Soc., 2002. **113**(23): p. 8847-8863.
234. Brumfield, M.A., Quillen, S.L., Yoon, U.C., and Mariano, P.S., *A novel method for heteroatom-substituted free radical generation by photochemical electron transfer induced desilylation of $RXCH_2SiMe_3$ systems*. J. Am. Chem. Soc., 2002. **106**(22): p. 6855-6856.
235. Xu, W., Jeon, Y.T., Hasegawa, E., Yoon, U.C., and Mariano, P.S., *Novel electron-transfer photocyclization reactions of α -silyl amine α,β -unsaturated ketone and ester systems*. J. Am. Chem. Soc., 2002. **111**(1): p. 406-408.
236. Nakajima, K., Kitagawa, M., Ashida, Y., Miyake, Y., and Nishibayashi, Y., *Synthesis of nitrogen heterocycles via α -aminoalkyl radicals generated from α -silyl secondary amines under visible light irradiation*. Chem. Commun., 2014. **50**(64): p. 8900-3.
237. Ruiz Espelt, L., McPherson, I.S., Wiensch, E.M., and Yoon, T.P., *Enantioselective conjugate additions of α -amino radicals via cooperative photoredox and Lewis acid catalysis*. J. Am. Chem. Soc., 2015. **137**(7): p. 2452-5.
238. Lenhart, D., Bauer, A., Pothig, A., and Bach, T., *Enantioselective Visible-Light-Induced Radical-Addition Reactions to 3-Alkylidene Indolin-2-ones*. Chem. - Eur. J., 2016. **22**(19): p. 6519-23.
239. Le Saux, E., Ma, D., Bonilla, P., Holden, C.M., Lustosa, D., and Melchiorre, P., *A General Organocatalytic System for Enantioselective Radical Conjugate Additions to Enals*. Angew. Chem. Int. Ed. Engl., 2021. **60**(10): p. 5357-5362.
240. McManus, J.B., Onuska, N.P.R., and Nicewicz, D.A., *Generation and Alkylation of α -Carbamyl Radicals via Organic Photoredox Catalysis*. J. Am. Chem. Soc., 2018. **140**(29): p. 9056-9060.
241. Neumann, S., Wenger, O.S., and Kerzig, C., *Controlling Spin-Correlated Radical Pairs with Donor-Acceptor Dyads: A New Concept to Generate Reduced Metal Complexes for More Efficient Photocatalysis*. Chem. - Eur. J., 2021. **27**(12): p. 4115-4123.
242. Kavarnos, G.J. and Turro, N.J., *Photosensitization by reversible electron transfer: theories, experimental evidence, and examples*. Chem. Rev., 1986. **86**(2): p. 401-449.
243. McLauchlan, K.A. and Steiner, U.E., *The spin-correlated radical pair as a reaction intermediate*. Mol. Phys., 1991. **73**(2): p. 241-263.
244. Glaser, F., Kerzig, C., and Wenger, O.S., *Multi-Photon Excitation in Photoredox Catalysis: Concepts, Applications, Methods*. Angew. Chem. Int. Ed. Engl., 2020. **59**(26): p. 10266-10284.

245. Braun, J.D., Lozada, I.B., Kolodziej, C., Burda, C., Newman, K.M.E., van Lierop, J., Davis, R.L., and Herbert, D.E., *Iron(II) coordination complexes with panchromatic absorption and nanosecond charge-transfer excited state lifetimes*. Nat. Chem., 2019. 11(12): p. 1144-1150.
246. Leis, W., Arguello Cordero, M.A., Lochbrunner, S., Schubert, H., and Berkefeld, A., *A Photoreactive Iron(II) Complex Luminophore*. J. Am. Chem. Soc., 2022. 144(3): p. 1169-1173.
247. Larsen, C.B., Braun, J.D., Lozada, I.B., Kunnus, K., Biasin, E., Kolodziej, C., Burda, C., Cordones, A.A., Gaffney, K.J., and Herbert, D.E., *Reduction of Electron Repulsion in Highly Covalent Fe-Amido Complexes Counteracts the Impact of a Weak Ligand Field on Excited-State Ordering*. J. Am. Chem. Soc., 2021. 143(49): p. 20645-20656.
248. Malme, J.T., Clendening, R.A., Ash, R., Curry, T., Ren, T., and Vura-Weis, J., *Nanosecond Metal-to-Ligand Charge-Transfer State in an Fe(II) Chromophore: Lifetime Enhancement via Nested Potentials*. J. Am. Chem. Soc., 2023. 145(11): p. 6029-6034.
249. Prakash, O., Lindh, L., Kaul, N., Rosemann, N.W., Losada, I.B., Johnson, C., Chábera, P., Ilic, A., Schwarz, J., Gupta, A.K., Uhlig, J., Ericsson, T., Häggström, L., Huang, P., Bendix, J., Strand, D., Yartsev, A., Lomoth, R., Persson, P., and Wärnmark, K., *Photophysical Integrity of the Iron(III) Scorpionate Framework in Iron(III)-NHC Complexes with Long-Lived 2LMCT Excited States*. Inorg. Chem., 2022. 61(44): p. 17515-17526.
250. Materna, K.L. and Hammarström, L., *Photoredox Catalysis Using Heterogenized Iridium Complexes**. Chem. - Eur. J., 2021. 27(68): p. 16966-16977.
251. Lindroth, R., Materna, K.L., Hammarström, L., and Wallentin, C.J., *Sustainable Ir-Photoredox Catalysis by Means of Heterogenization*. ACS Org. Inorg. Au, 2022. 2(5): p. 427-432.
252. Kaul, N. and Lomoth, R., *The Carbene Cannibal: Photoinduced Symmetry-Breaking Charge Separation in an Fe(III) N-Heterocyclic Carbene*. J. Am. Chem. Soc., 2021. 143(29): p. 10816-10821.
253. Zhang, M., Johnson, C.E., Ilic, A., Schwarz, J., Johansson, M.B., and Lomoth, R., *High-Efficiency Photoinduced Charge Separation in Fe(III)carbene Thin Films*. J. Am. Chem. Soc., 2023. 145(35): p. 19171-19176.
254. Worl, L.A., Duesing, R., Chen, P., Ciana, L.D., and Meyer, T.J., *Photophysical properties of polypyridyl carbonyl complexes of rhenium(I)*. J. Chem. Soc., Dalton Trans., 1991(S): p. 849-858.

